NONLINEAR SCATTERING OF BOSE-EINSTEIN CONDENSATES ON A FINITE BARRIER

by

Rachel Miller

A thesis submitted to the Faculty and the Board of Trustees of the Colorado School of Mines in partial fulfillment of the requirements for the degree of Master of Science (Mathematical and Computer Sciences).

Golden, Colorado

Date _____

Signed: _____
Rachel Miller

Approved: _____
Dr. Paul A. Martin
Professor of Mathematics
Thesis Advisor

Approved: _____
Dr. Lincoln D. Carr
Associate Professor of Physics
Thesis Co-Advisor

Golden, Colorado

Date _____

_____
Dr. Dinesh Mehta
Professor and Head,
Department of Mathematical & Computer Sciences

ABSTRACT

We consider the scattering of a Bose-Einstein condensate on a finite rectangular potential barrier. The nonlinear Schrödinger equation models the mean-field interactions of a Bose-Einstein condensate. The nonlinearity in this problem gives rise to several interesting physical and mathematical features which are not present in the well-known linear problem. In some strongly nonlinear systems, we observe the appearance of localized solitons in the condensate. Such solitons do not appear in the linear scattering case. Also, for given input parameters, the behavior of the condensate transmission across the barrier is split into two different regimes. Bifurcations in the transmission resonances occur in the transition region between these regimes.

In this work, we rigorously develop a completely general set of stationary-state solutions to the nonlinear Schrödinger equation. These solutions are used to numerically and analytically model the scattering of the Bose-Einstein condensate. In particular, we consider the transmission of the condensate across the potential barrier, with special focus on the resonances, where transmission is equal to unity. The nonlinearity requires that we use a different definition for transmission than the conventional definition of the linear scattering problem. As a result, the physical interpretation of the transmission changes and different behavior is observed. The character of the transmission plot depends on the size of the potential barrier and the strength of the nonlinearity.

We present density, transmission, and resonance plots for several physical cases.

We consider the new features and interpretations arising from nonlinearity and analyze the dependence of transmission and resonances on input parameters. Such new features provide many exciting possibilities for additional research. In addition, we discuss the connection between our methods and recent experiments. We conclude by noting future possibilities for extension and generalization of this project.

TABLE OF CONTENTS

LIST OF FIGURES

LIST OF TABLES

LIST OF ACRONYMS

BEC	Bose-Einstein condensate
NLS	Nonlinear Schrödinger equation
GPE	Gross-Pitaevskii equation
LSE	Linear Schrödinger equation

ACKNOWLEDGMENTS

One cannot travel the road of higher education alone. There are many who have supported, encouraged, and inspired me along what has been a long, sometimes tiring, but always exciting journey. I acknowledge them here, though these few pages are hardly space enough to express my gratitude.

First and foremost, I am grateful to God, and Jesus Christ my Savior. Without the Lord's divine hand of guidance, protection, and encouragement, I would have accomplished nothing.

Secondly, I must acknowledge my advisors, Drs. Lincoln Carr and Paul Martin. Dr. Carr graciously offered me the opportunity to do real research during my junior year, and this has provided much valuable experience and insight which would have otherwise been lost. I am also grateful to Dr. Carr for continually reminding me to look at research problems with *both* perspectives – the physicist's as well as the mathematician's.

It was Dr. Martin who taught me the fundamentals of PDEs, which provided much background and insight for this project. I am grateful to Dr. Martin for taking me on as an advisee, and also for his unique mathematical perspectives.

I thank my committee members, Dr. Willy Hereman and Dr. Luis Tenorio, for the time and effort they have put into teaching as well as the duties required of thesis committee members.

I am deeply indebted to Dr. Dan Sukle, my first physics teacher. His passion and enthusiasm were indeed contagious. Thank you also to Monica Geist, Robert Ream, Cathy Pellish, and Jim Voss for your encouragement and advice in my initial

mathematics studies.

I am grateful to David Flammer and Chris Kelso for the opportunity to be a TA, which was the first step toward an academic career. Thanks also to Gus Greivel and Drs. Anita Corn, Todd Ruskell, Vince Kuo, Pat Kohl, and Dinesh Mehta for allowing me to continue gaining experience in education, and for sharing their valuable wisdom. Dr. Corn was a wonderful role model for all of the women in the physics department. Her encouragement and unique insight continue to aid me in my journey.

Thank you to Dr. John DeSanto and Teri Woodington for encouraging me to pursue mathematics as a second degree, and to Dr. Jim Bernard for sharing the joy and wonder of quantum physics. Thank you to Matt Heller for initial collaboration and many beneficial physics discussions, to Dr. David Meskill, who reminded me that the world is bigger than just mathematics and physics, and to Dr. Alex Flournoy for his time and encouragement as a faculty mentor. His insight and expertise on teaching and graduate school have been extremely helpful.

I owe a debt to all of the instructors from whom I have had the privilege to learn, both at Front Range and CSM. Your enthusiasm is inspiring and encouraging.

I am also deeply grateful to my church family, who have never ceased to encourage and pray for me. Thank you to Pastor Rick for providing an additional scientific perspective (biology) which is not common at Mines.

And finally, I thank my parents for being generally supportive. Thanks, Mom, for helping me solve several difficult problems by just listening and nodding. And thanks to my stepfather, Greg, who helped me learn to communicate physics to a wide variety of people. Thank you also to Dad, Brandi, and Granny Betty for your encouragement.

In the middle of difficulty lies opportunity.

—Albert Einstein

Chapter 1

INTRODUCTION

The nonlinear Schrödinger equation (NLS), also known as the Gross-Pitaevskii equation, models the mean-field interactions of a Bose-Einstein condensate (BEC) at low temperatures [1, 2, 3, 4] in the presence of an external potential. The Gross-Pitaevskii equation may also be used to model ultracold mixtures of gaseous bosons and fermions [5, 6, 7], as well as superfluids more generally [8, 9].

1.1 Bose-Einstein Condensation

The condensation of a monatomic bosonic gas at ultracold temperatures, known today as the BEC, was predicted theoretically in 1925 by Einstein [10] and Bose [11]. However, BECs were not realized experimentally until 1995 [1]. BECs are formed experimentally by first cooling atoms in a magnetic trap produced by laser beams, then allowing the trapped atoms to cool further by evaporative methods [12, 13]. The hotter atoms escape the system, and at the end of the cooling process, a dilute, and therefore weakly-interacting, gas of ultracold atoms remains [1]. When the temperature of the atoms drops below the critical temperature obtained from the DeBroglie wavelength, they condense into the lowest-energy quantum state, resulting in a macroscopically observable occupation of this state [1]. Alkali metal atoms, such as rubidium, lithium, and sodium, are particularly useful for BEC experiments due to their internal energy-level structure, which enables the atoms to be manipulated with readily available lasers and cooled to very low temperatures [14, 12]. BECs may

also be observed in hydrogen [15]; however, the condensation process in this case is limited due to the recombination of atoms into H_2 molecules [12]. A variety of other elements have been Bose-condensed, including potassium [16], ytterbium [17], and metastable helium [18].

1.2 NLS Solution and Applications

In this work, we consider the steady-state transmission behavior of nonlinear waves of a BEC incident on a potential barrier. We assume that the BEC is confined in the transverse directions by a harmonic oscillator trap of frequency ω, and that its behavior is quasi-one-dimensional; that is, the longitudinal direction of the BEC is much larger than the transverse directions and the healing length ξ, and the chemical potential is much larger than the transverse excitation energy. The healing length ξ is given by

$$\xi^2 = \frac{1}{8\pi\bar{n}a_s}, \tag{1.1}$$

where a_s is the s-wave scattering length of atoms in the BEC, and $\bar{n}$ is the average linear number density. For ^{87}Rb, $a_s = 4.76$ nm [19].

Further, we assume that the width of the potential barrier is much less than the longitudinal dimension of the BEC, so that the system is effectively longitudinally infinite and far-field effects may be neglected. This physical situation can be experimentally produced; see, for example, Engels & Atherton [20]. In this experiment, a potential barrier was produced by an elliptical laser beam. The beam was then dragged through a quasi-one-dimensional ^{87}Rb BEC at various speeds. For intermediate drag speeds, Engels & Atherton observed the formation of dark solitons in the condensate. In the stationary frame of the laser, we can search for steady-state

solitons by our methods. Our study may also be applied to atom lasers [21, 22, 23, 24].

The one-dimensional NLS is

$$\left[-\frac{\hbar^2}{2m}\frac{\partial^2}{\partial x^2} + g\left|\Psi(x,t)\right|^2 + V(x)\right]\Psi(x,t) = i\hbar\frac{\partial}{\partial t}\Psi(x,t), \tag{1.2}$$

where $\hbar$ is the reduced Planck's constant, m is the atomic mass, and $\Psi(x,t)$ is the wave function. Also, g is the interaction strength or nonlinearity, and $V(x)$ is the potential. The nonlinearity is given by

$$g = \frac{4\pi\hbar^2 a_s}{m}, \tag{1.3}$$

where a_s is the s-wave scattering length for binary elastic collisions. This parameter may be negative or positive, corresponding to attractive or repulsive atomic interactions respectively. Our formal mathematics are applicable to both cases; however, in our numerical studies, we consider only repulsive interactions. Repulsive interactions are more common in experimental condensates, including the ^{87}Rb BEC used in the Engels & Atherton experiment [19, 20].

Nondimensionalizing (1.2) by scaling everything to harmonic oscillator units leads to the dimensionless or scaled NLS,

$$\left[-\frac{1}{2}\frac{\partial^2}{\partial \tilde{x}^2} + \tilde{g}\left|\tilde{\Psi}(\tilde{x},\tilde{t})\right|^2 + \tilde{V}(\tilde{x})\right]\tilde{\Psi}(\tilde{x},\tilde{t}) = i\frac{\partial}{\partial \tilde{t}}\tilde{\Psi}(\tilde{x},\tilde{t}), \tag{1.4}$$

where a tilde denotes a dimensionless quantity. In further discussion, we omit the tildes in the use of Eq. (1.4) except when we need to distinguish between dimension-

less quantities and quantities with units. The relationships between the dimensional quantities in Eq. (1.2) and the dimensionless quantities in Eq. (1.4) are given in Chapter 2.

In [25], the stationary-state solution to Eq. (1.4) is given for constant potential $V(x) = V_0$. The constant-potential solution is then applied to a potential step at the origin,

$$V(x) = V_0\Theta(x), \tag{1.5}$$

where $\Theta(x)$ is the Heaviside step function. The solution is also applied to a delta-function potential at the origin. Results are given for the density and phase of the BEC, and we discuss the relationship between phase and velocity.

In this work, we fully develop the stationary-state solutions, first for constant potentials, and then for piecewise-constant potentials. The derivations presented here are much more general and mathematically rigorous than those given in previous studies. We develop the stationary-state solutions as generally as possible, considering the possible domain of each parameter appearing in the final solution. In addition, we maintain mathematical rigor, making as few assumptions as are reasonable. In this way, we are able to state the most general set of stationary-state solutions.

As an application of our general solution, we treat a piecewise-constant potential barrier of the form

$$V(x) = \begin{cases} 0, & x < x_1, \\ V_0, & x_1 < x < x_2, \\ 0, & x_2 < x, \end{cases} \tag{1.6}$$

where $V_0 \in \mathbb{R}$. The barrier can have any width and height, with the boundaries x_1 and x_2 located at any positions along the x-axis. We apply this fully general solution to a numerical study of the transmission of the BEC across the barrier. The solution and code are easily generalized to arbitrary piecewise-constant potentials with a finite number of jump discontinuities. We consider only the barrier (1.6) in this work.

In cases when the potential $V(x)$ is constant or piecewise-constant, Eq. (1.4) can be solved analytically for stationary states of the form [25]

$$\Psi(x,t) = \sqrt{\rho(x)}\, e^{i[\phi(x)-\mu t]}, \tag{1.7}$$

where ρ is the linear number density of particles in the BEC, ϕ is the phase, and μ is the eigenvalue or chemical potential. In Eq. (1.7), we have written the complex wave function Ψ in polar form. Thus $\rho(x)$ and $\phi(x)$ may be taken to be real, with $\rho(x) \geq 0$, without loss of generality; see Section 2.2.1 for formal discussion. In this interpretation, $\rho \geq 0$ is also a physical necessity, since ρ represents the particle density. We will show in Section 2.2.3 that μ must also be a real number.

We consider a rectangular potential barrier of height $V_0 \geq 0$, with boundaries at x_1 and x_2, as shown in Fig. 1.1. Our methods are also applicable to a potential well, $V_0 < 0$; however, we restrict ourselves to the study of scattering from a positive barrier in this work.

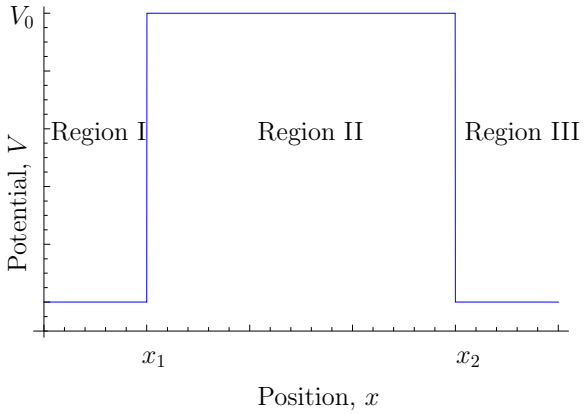

Figure 1.1: Potential barrier.

In each region, the potential $V(x)$ is constant, and we can show that the density has the form

$$\rho(x) = A\,\mathrm{sn}^2(bx + \delta_0|m) + B, \tag{1.8}$$

where A is the density scaling, b is the translational scaling, m is the elliptic parameter, and δ_0 and B are offsets [25, 26]. The function sn is one of twelve Jacobi elliptic functions, which are discussed further in Appendix A. By making certain constraints on A, B, and δ_0, we can restrict ourselves to physically relevant solutions, as we discuss in Section 2.3.2.

When the parameter m is between 0 and 1, the Jacobi elliptic functions can be interpreted geometrically as the elliptical analog of the trigonometric functions [27]. In this interpretation, the square root of the elliptic parameter m represents the eccentricity of an ellipse. In the limit that $m \to 0$, the Jacobi elliptic functions become the trigonometric functions; in the limit $m \to 1$, they become the hyperbolic functions. For $m \notin [0, 1]$, transformations exist which can be used to write the Jacobi

elliptic functions in terms of functions whose parameter lies in $[0, 1]$. Therefore, we need not consider parameter values outside $[0, 1]$. These transformations are given in Appendix A. We will also show in Section 2.3.1 that $m \in \mathbb{R}$.

If a subset of parameter values is known for the potential-barrier solution, then boundary conditions can be used to find the values of all other parameters. Therefore, we can obtain a complete analytical solution for the particle density over the entire domain. For instance, if we completely characterize an atom laser on such a barrier, the steady-state physical solution is uniquely determined.

In particular, by fixing the parameters in one region of Fig. 1.1, we may find the values of all parameters in the other two regions [25]. Here, we take all parameters in Region I as known values and use these to find values in regions II and III. An atom laser beam originates on one side of the barrier, and impinges on the barrier from this same side. In this sense, the left-hand side of the barrier can be considered as the "incident" side; however, see the discussions of superposition below and in Section 3.1. By fixing the input parameters on one side of the barrier, we break the right-left symmetry of the problem.

Due to the nonlinear nature of Eq. (1.4), the superposition principle does not apply. The wave function cannot be expressed as separate left-traveling and right-traveling waves. We cannot define an "incident" side of the barrier, and we cannot distinguish between "incident" and "reflected" waves. Therefore, the transmission coefficient must be defined differently than the usual convention taken in the case of the linear Schrödinger equation, when $g = 0$ in (1.4). This leads to a different physi-

cal interpretation of the transmission coefficient, and also very different behavior as compared to the linear case. These considerations are discussed in more detail in Chapter 3.

We also consider the transmission resonances; that is, parameter values for which $T = 1$. We find that the resonances exhibit several different regimes of interesting behavior, depending on the width of the potential barrier and the magnitude of the chemical potential of the condensate.

1.3 Previous Work

The solution to the one-dimensional NLS, Eq. (1.4), with constant potential and repulsive interactions has been explored numerically [28] and analytically [28, 29, 30] by Carr *et al.* Attractive interactions, corresponding to negative nonlinearity g, have also been analytically treated by Carr *et al.* [31].

A later paper by Seaman *et al.* [25] extends the constant-potential solution to a discontinuous potential step at the origin, $V = V_0\Theta(x)$, and to a delta-function potential, $V = V_0\delta(x)$. The delta-function case is found to be similar to the step case, except that there is a discontinuity in $d\rho/dx$ of $4V_0\rho(0)$ at the origin. The delta-function potential has also been studied by Witthaut *et al.*, along with the delta shell potential

$$V(x) = \begin{cases} +\infty, & x < 0, \\ \lambda\delta(x-a), & x \geq 0, \end{cases} \tag{1.9}$$

where $a > 0$ [26]. The delta potential is useful for the study of bound and scattering states, while the delta shell is popular for decay studies.

The potential well, i.e. $V_0 < 0$, has been studied analytically by Carr *et al.* [32], for bound states only. Such states take the form of Jacobi elliptic functions, as in the scattering case; however, the bound states are localized or partially localized. In this case, experimental parameters may be tuned to achieve different regimes of tunneling.

Ishkhanyan & Krainov have analytically considered reflection from a rectangular barrier in the limit of very small nonlinearity, $g \ll \mu$ [33]. In this limit, perturbation theory is used to expand the NLS, and a multi-scale method is applied to find the solutions. The reflection coefficient R can then be determined by the usual methods of linear quantum mechanics, decomposing the wave functions in each region into left- and right-traveling waves via the superposition principle. By extension, the transmission coefficient T may also be determined via $T = 1 - R$, though this is not considered in [33].

Engels & Atherton experimentally studied the behavior of a BEC in the presence of a barrier [20]. In this experiment, the barrier was produced by an elliptical laser beam, then dragged through the BEC. For intermediate drag speeds, a train of dark solitons was observed in the presence of the barrier. Such solitons have been produced by other experimental methods, for example, by merging two coherent BECs [34]. An experiment by Weller *et al.* at Heidelberg studied the dynamical behavior and interactions of such solitons [35]. Solitons are localized, persistent, robust nonlinear structures which appear often in BEC experiments [36, 37]. A key feature of solitons is that they interact elastically and do not dissipate. In the absence of external effects, solitons may collide with or pass through one another without changing their shape

or amplitude [38, 39]. Such behavior was observed in the Heidelberg experiment, and was found to agree with numerical simulations of NLS solution dynamics [35].

In this work, we generalize and extend the NLS solution for the potential barrier. We rigorously develop the full set of stationary-state solutions of the form (1.7), with no assumptions on the relative magnitudes of physical parameters. In particular, we do not assume g to be small. Therefore, the superposition principle is not valid, or even approximately valid, except in the linear limit $g = 0$. We do not use perturbation theory; rather, we solve the NLS analytically through very general methods. Therefore our solution set represents the most general set of physically valid stationary-state solutions, and is applicable to arbitrary piecewise-constant potentials. We determine the necessary conditions on all parameters in Eqs. (1.4) and (1.8) to yield physically relevant solutions, though we note that other, mathematically valid solutions exist outside this parameter space. In our numerical results, we do not consider the subset of solutions which are mathematically valid, but not relevant to real physical systems. We determine the transmission coefficient T by numerical integration of the densities on either side of the barrier, and we analyze the behavior of T and its resonances for several physical cases. We also present soliton results such as those seen in the Weller [35] and Engels [20] experiments.

Chapter 2

FORMAL DERIVATIONS

We begin with the canonical NLS, including units:

$$\left[-\frac{\hbar^2}{2m}\frac{\partial^2}{\partial x^2} + g\left|\Psi(x,t)\right|^2 + V(x)\right]\Psi(x,t) = i\hbar\frac{\partial}{\partial t}\Psi(x,t). \tag{2.1}$$

Assuming that the BEC is confined by a harmonic oscillator trap of frequency ω in the transverse directions [20, 25], we rescale Eq. (2.1) according to the harmonic oscillator length

$$\ell = \sqrt{\frac{\hbar}{m\omega}}\,. \tag{2.2}$$

Make the following definitions of unitless quantities:

$$\tilde{x} = \frac{x}{\ell}, \tag{2.3}$$

$$\tilde{t} = \omega t, \tag{2.4}$$

$$\tilde{g} = \frac{g}{\hbar\omega\ell}, \tag{2.5}$$

$$\tilde{V} = \frac{V}{\hbar\omega,} \tag{2.6}$$

$$\tilde{\Psi} = \Psi\ell^{1/2}. \tag{2.7}$$

Multiplying Eq. (2.1) by $\frac{1}{\hbar\omega}$ and replacing partial derivative operators by their equivalents in terms of the dimensionless quantities defined in Eqs. (2.3)–(2.7), we obtain

$$\left[-\frac{1}{2}\frac{\partial^2}{\partial\tilde{x}^2}+\frac{g}{\hbar\omega}\left|\Psi\right|^2+\tilde{V}\right]\Psi=i\frac{\partial}{\partial\tilde{t}}\Psi. \tag{2.8}$$

Multiply Eq. (2.8) by judicious forms of 1 where units remain:

$$\left[-\frac{1}{2}\frac{\partial^2}{\partial\tilde{x}^2}+\frac{g}{\hbar\omega}\frac{\ell}{\ell}\left|\Psi\right|^2+\tilde{V}\right]\Psi\frac{\ell^{1/2}}{\ell^{1/2}}=i\frac{\partial}{\partial\tilde{t}}\Psi\frac{\ell^{1/2}}{\ell^{1/2}} \tag{2.9}$$

$$\Rightarrow\left[-\frac{1}{2}\frac{\partial^2}{\partial\tilde{x}^2}+\tilde{g}\left|\tilde{\Psi}\right|^2+\tilde{V}\right]\tilde{\Psi}=i\frac{\partial}{\partial\tilde{t}}\tilde{\Psi}. \tag{2.10}$$

Equation (2.10) is the scaled form of the one-dimensional nonlinear Schrödinger equation.

2.1 Solution of NLS for Constant Potential

In Eq. (1.4), assume that the potential is constant; that is, $V=V_0$. We seek stationary state solutions of the form (1.7). In the analysis that follows, we assume that $\mu\in\mathbb{R}$, $g\in\mathbb{R}$, and $\phi\in\mathbb{R}$. The possibility of complex values will be discussed in Section 2.2.

Let $R(x):=\sqrt{\rho(x)}$ and substitute this into Eq. (1.4):

$$-\frac{1}{2}\,\frac{d^2R}{dx^2}+\frac{1}{2}\,\left(\frac{d\phi}{dx}\right)^2R-\frac{1}{2}\,i\left[2\left(\frac{dR}{dx}\right)\left(\frac{d\phi}{dx}\right)+R\frac{d^2\phi}{dx^2}\right]+gR^3+V_0R=\mu R. \tag{2.11}$$

In Eq. (2.11), we must have $R\in\mathbb{R}$ and $R\geq 0$, since $\rho(x)$ is real and non-negative. Sign changes are absorbed into the phase, $\phi(x)$, in the solution given by Eq. (1.7).

Equate real and imaginary parts of Eq. (2.11). The real part is

$$-\frac{1}{2}\,\frac{d^2R}{dx^2}+\frac{1}{2}\,\left(\frac{d\phi}{dx}\right)^2 R+gR^3+V_0R=\mu R, \tag{2.12}$$

and the imaginary part is

$$2\left(\frac{dR}{dx}\right)\left(\frac{d\phi}{dx}\right)+R\frac{d^2\phi}{dx^2}=0. \tag{2.13}$$

Rearranging and integrating Eq. (2.13) yields

$$\frac{d\phi}{dx}=\alpha R^{-2} \tag{2.14}$$

$$=\frac{\alpha}{\rho(x)}, \tag{2.15}$$

provided that $d\phi/dx$ does not vanish, where α is a constant of integration.

Substitute (2.14) into (2.12) and rearrange. This yields

$$-\frac{1}{2}\,\left(\frac{dR}{dx}\right)\left(\frac{d^2R}{dx^2}\right)=\left[-\frac{1}{2}\,\alpha^2R^{-3}-gR^3+(\mu-V_0)R\right]\frac{dR}{dx}. \tag{2.16}$$

We observe that the left-hand side of Eq. (2.16) can be written as an exact derivative:

$$-\frac{1}{4}\,\frac{d}{dx}\left[\left(\frac{dR}{dx}\right)^2\right]=\left(-\frac{1}{2}\,\alpha^2R^{-3}-gR^3+(\mu-V_0)R\right)\frac{dR}{dx}. \tag{2.17}$$

Integrating Eq. (2.17), rearranging, and substituting for R, we obtain

$$\frac{d\rho}{dx}=\pm2\sqrt{g\rho^3-2(\mu-V_0)\rho^2+C\rho-\alpha^2}\,, \tag{2.18}$$

where C is another constant of integration and we have the constraint that the radi-

cand must be non-negative, since $\rho \in \mathbb{R} \Rightarrow d\rho/dx \in \mathbb{R}$.

Rearrange and integrate Eq. (2.18). We obtain

$$2x + \delta_0 = \pm \int \frac{d\rho}{\sqrt{g\rho^3 - 2(\mu - V_0)\rho^2 + C\rho - \alpha^2}}, \tag{2.19}$$

where δ_0 is a constant of integration. The right-hand side of Eq. (2.19) is a Jacobi elliptic integral of the first kind [40, 25], which can be inverted to obtain expressions for ρ in terms of the Jacobi elliptic functions. There are twelve such functions. However, since the square of one Jacobi elliptic function may be related linearly to the square of any other Jacobi elliptic function, among other identities [40], we need only consider solutions of the form

$$\rho(x) = A\,\mathrm{sn}^2(bx + \delta_0|m) + B, \tag{2.20}$$

where we have absorbed the sign ambiguity into the parameters, keeping in mind that physical reality requires $\rho(x) \geq 0,\ \forall x \in \mathbb{R}$. However, this is also mathematically general, since the sign can be incorporated into the phase $\phi(x)$.

Differentiating Eq. (2.20), we find that

$$\frac{d\rho}{dx} = 2Ab\,\mathrm{sn}(bx + \delta_0|m)\,\mathrm{cn}(bx + \delta_0|m)\,\mathrm{dn}(bx + \delta_0|m). \tag{2.21}$$

Let $u := bx + \delta_0$. Substitute Eqs. (2.20) and (2.21) into Eq. (2.18) and square

both sides. This yields

$$\begin{aligned} Ab\,\mathrm{sn}^2(u|m)\,\mathrm{cn}^2(u|m)\,\mathrm{dn}^2(u|m) = \\ g[A^3\,\mathrm{sn}^6(u|m) + 3AB^2\,\mathrm{sn}^4(u|m) + 3AB^2\,\mathrm{sn}^2(u|m) + B^3] \\ - 2(\mu - V_0)[A^2\,\mathrm{sn}^4(u|m) + 2AB\,\mathrm{sn}^2(u|m) + B^2] \\ + C[A\,\mathrm{sn}^2(u|m) + B] - \alpha^2. \end{aligned} \tag{2.22}$$

When using Eq. (2.22), we must keep in mind that the act of squaring both sides has introduced extraneous results. These are filtered out by the code.

Using the identities

$$\mathrm{sn}^2(u|m) = 1 - \mathrm{cn}^2(u|m), \tag{2.23}$$

$$\mathrm{dn}^2(u|m) = 1 - m\,\mathrm{sn}^2(u|m), \tag{2.24}$$

we can rewrite the left-hand side of Eq. (2.22) as

$$Ab\,\mathrm{sn}^2(u|m) \cdot [1 - m\,\mathrm{sn}^2(u|m)] \cdot [1 - \mathrm{sn}^2(u|m)]. \tag{2.25}$$

Equate (2.25) with the right-hand side of Eq. (2.22) and rearrange. This leads to a sixth-order equation in $\mathrm{sn}(u|m)$. Since distinct powers of sn are linearly independent, as shown in Appendix B, we may equate coefficients of like powers of $\mathrm{sn}(u|m)$ when $A \neq 0$. We obtain four relationships. From $\mathrm{sn}^6(u|m)$, we get

$$m = \frac{A}{b^2} g, \tag{2.26}$$

from $\mathrm{sn}^4(u|m)$ and Eq. (2.26), we obtain

$$\mu = \frac{1}{2}\left[b^2 + (A+3B)g\right] + V_0, \tag{2.27}$$

from $\mathrm{sn}^2(u|m)^2$ we find that

$$C = -3B^2 g + 4(\mu - V_0)B + Ab^2, \tag{2.28}$$

and from $\mathrm{sn}^0(u|m)$ with Eqs. (2.26)–(2.28),

$$\alpha^2 = B(A+B)(b^2 + Bg). \tag{2.29}$$

Since α appears only as α^2, and $\rho(x)$ does not depend on α, all solutions with $\alpha \neq 0$ are doubly degenerate. That is, $\pm\alpha$ result in solutions with the same density $\rho(x)$ and eigenvalue μ, but opposite phases. The solution with $\alpha = 0$ corresponds to the linear limit.

The degeneracy of solutions is very interesting physically. Phase is related to the BEC flow by

$$v(x) = \frac{\hbar}{m}\frac{d\phi}{dx}, \tag{2.30}$$

where v is the velocity of the BEC; we term this the *supercurrent*. Thus, for a given $|\alpha|$, we see two solutions which are identical in every respect except for the sign of the phase. There are two relevant flows in this system: the background flow of the aggregate BEC, i.e., the supercurrent, and the flow of solitons on that background. One solution corresponds to soliton flow toward the barrier with supercurrent flow away from the barrier, and the corresponding solution with $\alpha \to -\alpha$ corresponds to

the opposite flow situation, where the solitons stream towards the barrier and the supercurrent flows away from it.

Equations (2.26), (2.27), and (2.29) will be useful in calculations for determining parameter values.

2.2 Complex Physical Parameters in NLS

In the NLS, Eq. (1.4), some or all of the parameters may be complex. We develop here the physical and mathematical conditions for the domains of all NLS parameters.

2.2.1 Complex phase

Suppose the wave function $\Psi(x,t)$ in the NLS (1.4) is complex. We can write the wave function as

$$\Psi(x,t) = f(x,t) + ig(x,t), \tag{2.31}$$

where f and g are real-valued functions. Alternatively, we can write $\Psi(x,t)$ in polar form as

$$\Psi(x,t) = h(x,t)e^{i\theta(x,t)}, \tag{2.32}$$

where h and θ are real-valued functions.

Using Euler's formula to rewrite Eq. (2.32), we obtain

$$\Psi(x,t) = h(x,t)\{\cos[\theta(x,t)] + i\sin[\theta(x,t)]\}. \tag{2.33}$$

The signs of the real and imaginary parts of Ψ may be absorbed into the trigonometric functions. Therefore, we may assume without loss of generality that $h(x,t) \geq 0$.

By writing $\Psi(x,t)$ in the form of Eq. (1.7), we have expressed it in polar form as in Eq. (2.32). Therefore, the phase $\phi(x)$ in Eq. (1.7) may be taken to be a real-valued function without loss of generality. Since $\phi(x) \in \mathbb{R}$, we must also have $\partial\phi/\partial x \in \mathbb{R}$, and therefore Eq. (2.15) implies that $\alpha \in \mathbb{R}$.

2.2.2 Complex nonlinearity

In interacting physical systems, the nonlinearity g may be a complex number. The imaginary part corresponds to a 2-body loss of energy, this energy being carried away by loss processes having a variety of physical origins. In the case of BECs, we have a dilute system of alkali atoms interacting via s-wave processes [12]. These alkali atoms have no accessible internal degrees of freedom, and thus energy cannot be lost in this manner. Therefore, for our physical system, the nonlinearity g is purely real.

In addition, it must be noted that the BEC system is dilute enough that only two-body interactions are relevant. Thus, three-body losses in the BEC, which lead to higher-order nonlinearity in the governing equation, may be neglected.

2.2.3 Complex eigenvalue

Consider again Eq. (1.4), with constant potential $V = V_0$. We again seek solutions of the form (1.7), but this time we allow $\mu \in \mathbb{C}$. Let

$$\mu = \mu_r + i\mu_i, \tag{2.34}$$

where $\mu_r, \mu_i \in \mathbb{R}$. Substitute (2.34) in (1.7) and the result into Eq. (1.4). This yields

$$\frac{1}{8}\,\rho^{-3/2}\left(\frac{d\rho}{dx}\right)^2 - \frac{1}{4}\,\rho^{-1/2}\left(\frac{d^2\rho}{dx^2}\right) + \frac{1}{2}\,\rho^{1/2}\left(\frac{d\phi}{dx}\right)^2 - \frac{1}{2}\;i\left[\rho^{-1/2}\left(\frac{d\rho}{dx}\right)\left(\frac{d\phi}{dx}\right) + \rho^{1/2}\left(\frac{d^2\phi}{dx^2}\right)\right] + g\rho e^{2\mu_i t} + V_0\rho^{1/2} = \rho^{1/2}(\mu_r + i\mu_i). \tag{2.35}$$

Equate real and imaginary parts of Eq. (2.35). We find that the real parts yield

$$\frac{1}{8}\,\rho^{-3/2}\left(\frac{d\rho}{dx}\right)^2 - \frac{1}{4}\,\rho^{-1/2}\left(\frac{d^2\rho}{dx^2}\right) + \frac{1}{2}\,\rho^{1/2}\left(\frac{d\phi}{dx}\right)^2 + g\rho e^{2\mu_i t} + V_0\rho^{1/2} = \rho^{1/2}\mu_r, \tag{2.36}$$

and the imaginary parts yield

$$-\frac{1}{2}\;\left[\rho^{-1/2}\left(\frac{d\rho}{dx}\right)\left(\frac{d\phi}{dx}\right) + \rho^{1/2}\left(\frac{d^2\phi}{dx^2}\right)\right] = \rho^{1/2}\mu_i. \tag{2.37}$$

Multiply Eq. (2.37) by $4\rho^{3/2}$ and rearrange:

$$\rho\left(\frac{d^2\phi}{dx^2}\right) + \left(\frac{d\rho}{dx}\right)\left(\frac{d\phi}{dx}\right) = -2\rho\mu_i. \tag{2.38}$$

The left-hand side of Eq. (2.38) is an exact derivative. Integrating, we find that

$$\frac{d\phi}{dx} = \frac{\alpha}{\rho(x)} - \frac{2\mu_i}{\rho(x)}\int^x \rho(x')\,dx', \tag{2.39}$$

where α is a constant of integration. Note that when $\mu \in \mathbb{R}$; that is, when $\mu_i = 0$, Eq. (2.39) reduces to the previously obtained result, Eq. (2.15).

Substitute (2.39) into Eq. (2.36) to obtain

$$\frac{1}{8}\,\rho^{-3/2}\left(\frac{d\rho}{dx}\right)^2-\frac{1}{4}\,\rho^{-1/2}\left(\frac{d^2\rho}{dx^2}\right)+\frac{1}{2}\,\rho^{1/2}\left\{\alpha^2\rho^{-2}+4\mu_i^2\rho^{-2}\left[\int^x\rho(x')\,dx'\right]^2 -4\mu_i\rho^{-1}\int^x\rho(x')\,dx'\right\}+V_0\rho^{1/2}+g\rho e^{2\mu_i t}=\rho^{1/2}\mu_r. \quad (2.40)$$

Equation (2.40) is an ordinary differential equation for $\rho = \rho(x)$. However, the last term on the left-hand side, $g\rho e^{2\mu_i t}$, is time-dependent. Since ρ is assumed to be independent of time, and the parameters g, V, μ, and α are constant, this is a contradiction. That is, there are no solutions of Eq. (2.40). We conclude that the ansatz (1.7) is not a valid solution for this problem when $\mathrm{Im}(\mu) \neq 0$.

2.3 Complex Parameters in Density

In the density (2.20), some of the parameters may be complex. We can use the requirement that $\rho(x) \in \mathbb{R},\ \forall x \in \mathbb{R}$, to determine which parameters may take complex values.

2.3.1 Complex m

We will show that when the elliptic parameter m has nonzero imaginary part, $\mathrm{sn}^2(u|m)$ is a complex-valued function for all u. In this case, the density (2.20) cannot be made to be a real-valued function for any values of the other parameters. Therefore, m must be real.

Theorem 1. *$sn(u|m)$ is a complex-valued function for $Im(m) \neq 0$.*

Proof. Since $\mathrm{sn}(u|m)$ is an odd function of u [40], it has a Maclaurin expansion of

the form [41]

$$\begin{aligned}\mathrm{sn}(u|m) &= \sum_{n=0}^{\infty} s_n u^{2n+1} \\ &= u \sum_{n=0}^{\infty} s_n u^{2n}.\end{aligned} \tag{2.41}$$

In Eq. (2.41), the coefficient s_n is in general dependent on m, and may be complex. We show that $\mathrm{Im}(s_n) \neq 0$ when $\mathrm{Im}(m) \neq 0$.

The first several terms of the series (2.41) are given in several reference books, including [40] and [42]. To find the general term, we turn to the differential equation [43, 44]:

$$\left[\frac{d}{du}\,\mathrm{sn}(u|m)\right]^2 = [1 - \mathrm{sn}^2(u|m)][1 - m\,\mathrm{sn}^2(u|m)]. \tag{2.42}$$

Substituting Eq. (2.41) into Eq. (2.42) gives

$$\left[\sum_{n=0}^{\infty}(2n+1)s_n u^{2n}\right]^2 = \left\{1 - u^2\left[\sum_{n=0}^{\infty} s_n u^{2n}\right]^2\right\} \cdot \left\{1 - mu^2\left[\sum_{n=0}^{\infty} s_n u^{2n}\right]^2\right\}. \tag{2.43}$$

Rearrange Eq. (2.43), using the property that

$$\left[\sum_{n=0}^{\infty} f_n u^{2n}\right]^2 = \sum_{n=0}^{\infty} g_n u^{2n}, \tag{2.44}$$

where

$$g_n = \sum_{\ell=0}^{n} f_\ell f_{n-\ell}. \tag{2.45}$$

We obtain

$$\sum_{n=0}^{\infty} k_n u^{2n} = 1 - (m+1)u^2 \sum_{n=0}^{\infty} p_n u^{2n} + u^4 \sum_{n=0}^{\infty} h_n u^{2n}, \tag{2.46}$$

where

$$k_n = \sum_{\ell=0}^{n} (2\ell+1) s_\ell (2n-2\ell+1) s_{n-\ell}, \tag{2.47}$$

$$p_n = \sum_{\ell=0}^{n} s_\ell s_{n-\ell}, \tag{2.48}$$

$$h_n = \sum_{q=0}^{n} p_q p_{n-q}. \tag{2.49}$$

Since distinct powers of u are linearly independent, we can equate coefficients of like powers of u. We find

$$k_0 = 1 = s_0^2, \tag{2.50}$$

$$p_0 = s_0^2 = 1, \tag{2.51}$$

$$k_1 = -(1+m) p_0, \tag{2.52}$$

$$h_0 = p_0^2 = 1. \tag{2.53}$$

Substituting Eq. (2.52) into the definition of the k_n, (2.47), we find that

$$s_1 = -\frac{1+m}{6}. \tag{2.54}$$

From Eqs. (2.48) and (2.54),

$$p_1 = 2s_1 = -\frac{1+m}{3}, \tag{2.55}$$

and from (2.49),

$$h_1 = \frac{-2(1+m)}{3}. \tag{2.56}$$

We can continue to apply these formulas recursively. For the ℓth coefficient, we find

$$-(1+m)p_{\ell-1} + h_{\ell-2} = 2(2\ell+1)s_\ell + \sum_{q=1}^{\ell-1}(2q+1)s_q(2\ell-2q-1)s_{\ell-q}. \tag{2.57}$$

Equation (2.57) may be solved for any given s_ℓ once $s_{\ell-1}$ has been found using the methods above. From the 0th and 1st terms found above, and the recursive nature of the algorithm, it is clear that all coefficients s_ℓ will be polynomials in m.

Let $m = a + b\,i$. Then each coefficient s_ℓ has the form

$$s_\ell = (a + b\,i)^n, \tag{2.58}$$

for some integer n, which will, in general, be different for each ℓ. Expand Eq. (2.58) using the binomial theorem:

$$s_\ell = \sum_{k=0}^{n} \binom{n}{k} a^k (\,ib)^{n-k}. \tag{2.59}$$

We require $\mathrm{sn}(u|m) \in \mathbb{R}\ \forall u$; thus the imaginary part of the Maclaurin series must vanish. The only way that this can occur for *all* u is that the imaginary parts of all of the coefficients s_ℓ must vanish. For $\ell = 1$,

$$\mathrm{Im}(s_1) = b = 0. \tag{2.60}$$

That is, $b = 0$ is the only solution to $\mathrm{Im}(s_1) = 0$. It remains to prove that $b = 0$ is a solution to $\mathrm{Im}(s_\ell) = 0,\ \forall \ell \in \mathbb{Z}$. If this is not the case, then it follows that $\mathrm{Im}[\,\mathrm{sn}(u|m)] \neq 0\ \forall u$; that is, $\mathrm{sn}(u|m)$ is complex for all parameters m, including real

values, and Eq. (1.8) is not a valid solution of the NLS.

With Eq. (2.59), we find

$$\mathrm{Im}(s_\ell) = \sum_{\{k:n-k \text{ odd}\}} \binom{n}{k} a^k (\, ib)^{n-k} = 0, \tag{2.61}$$

and $b = 0$ is indeed a solution for all ℓ. In fact, $b = 0$ is the only solution that satisfies Eq. (2.61) for *all* integers ℓ, as shown by Eq. (2.60). That is, we may have $\mathrm{sn}(u|m) \in \mathbb{R}, \forall u$, if and only if $m \in \mathbb{R}$.

Therefore, we have proven that $\mathrm{Im}(m) \neq 0 \Rightarrow \mathrm{Im}[\,\mathrm{sn}(u|m)] \neq 0$. QED.

2.3.2 Other complex density parameters

We begin by assuming that all other parameters in (2.20) may be complex. Write real and imaginary parts as follows:

$$A = A_r + \, iA_i, \tag{2.62}$$

$$B = B_r + \, iB_i, \tag{2.63}$$

$$b = b_r + \, ib_i, \tag{2.64}$$

$$\delta_0 = \delta_{0r} + \, i\delta_{0i}. \tag{2.65}$$

The argument of the Jacobi function in (2.20) is $bx + \delta_0$. Substituting Eqs.

(2.62)–(2.65) and writing real and imaginary parts, we find that

$$a := \mathrm{Re}(bx + \delta_0) = b_r x + \delta_{0r}, \tag{2.66}$$

$$y := \mathrm{Im}(bx + \delta_0) = b_i x + \delta_{0i}. \tag{2.67}$$

Using complex-argument transformations [40], we find that

$$\begin{aligned}\mathrm{sn}(a + iy|m) = \frac{1}{\mathrm{cn}^2(y|1-m) + m\,\mathrm{sn}^2(a|m)\,\mathrm{sn}^2(y|1-m)} \,[\,&\mathrm{sn}(a|m)\,\mathrm{dn}(y|1-m) \\ +\; i\,&\mathrm{cn}(a|m)\,\mathrm{dn}(a|m)\,\mathrm{sn}(y|1-m)\,\mathrm{cn}(y|1-m)]\,.\end{aligned} \tag{2.68}$$

For convenience, define

$$\zeta := \frac{1}{\mathrm{cn}^2(y|1-m) + m\,\mathrm{sn}^2(a|m)\,\mathrm{sn}^2(y|1-m)}. \tag{2.69}$$

Note that $\zeta \in \mathbb{R}$. Substitute Eqs. (2.69) and (2.68) into (2.20). We find

$$\begin{aligned}\mathrm{Re}[\rho(x)] = \zeta^2 \{ A_r [\,&\mathrm{sn}^2(a|m)\,\mathrm{dn}^2(y|1-m) \\ &- \mathrm{cn}^2(a|m)\,\mathrm{dn}^2(a|m)\,\mathrm{sn}^2(y|1-m)\,\mathrm{cn}^2(y|1-m)] \\ -2A_i\,&\mathrm{sn}(a|m)\,\mathrm{cn}(a|m)\,\mathrm{dn}(a|m)\,\mathrm{sn}(y|1-m)\,\mathrm{cn}(y|1-m)\,\mathrm{dn}(y|1-m)\} \\ &+ B_r,\end{aligned} \tag{2.70}$$

$$\begin{aligned}\mathrm{Im}[\rho(x)] = \zeta^2 \big\{ A_i \big[&\mathrm{sn}^2(a|m)\,\mathrm{dn}^2(y|1-m) \\ &- \mathrm{cn}^2(a|m)\,\mathrm{dn}^2(a|m)\,\mathrm{sn}^2(y|1-m)\,\mathrm{cn}^2(y|1-m)\big] \\ &+2A_r\,\mathrm{sn}(a|m)\,\mathrm{cn}(a|m)\,\mathrm{dn}(a|m)\,\mathrm{sn}(y|1-m)\,\mathrm{cn}(y|1-m)\,\mathrm{dn}(y|1-m)\big\} \\ &+ B_i. \quad (2.71)\end{aligned}$$

We must have $\rho(x) \in \mathbb{R}$; thus (2.71) must vanish for all x. Therefore

$$\begin{aligned}A_i \big[&\mathrm{sn}^2(a|m)\,\mathrm{dn}^2(y|1-m) - \mathrm{cn}^2(a|m)\,\mathrm{dn}^2(a|m)\,\mathrm{sn}^2(y|1-m)\,\mathrm{cn}^2(y|1-m)\big] \\ &+ 2A_r\,\mathrm{sn}(a|m)\,\mathrm{cn}(a|m)\,\mathrm{dn}(a|m)\,\mathrm{sn}(y|1-m)\,\mathrm{cn}(y|1-m)\,\mathrm{dn}(y|1-m) \\ &= -B_i[\,\mathrm{cn}^2(y|1-m) + m\,\mathrm{sn}^2(a|m)\,\mathrm{sn}^2(y|1-m)]^2. \quad (2.72)\end{aligned}$$

Rearrange, and use Eqs. (2.23) and (2.24):

$$\begin{aligned}A_i \big\{ &\mathrm{sn}^2(a|m)\,\big[1-(1-m)\,\mathrm{sn}^2(y|1-m)\big] \\ &- \big[1-\mathrm{sn}^2(a|m)\big]\cdot\big[1-m\,\mathrm{sn}^2(a|m)\big]\,\mathrm{sn}^2(y|1-m)\,\big[1-\mathrm{sn}^2(y|1-m)\big]\big\} \\ &+ B_i\,\big[1-\mathrm{sn}^2(y|1-m)+m\,\mathrm{sn}^2(a|m)\,\mathrm{sn}^2(y|1-m)\big]^2 \\ &= 2A_r\,\mathrm{sn}(a|m)\,\mathrm{cn}(a|m)\,\mathrm{dn}(a|m)\,\mathrm{sn}(y|1-m)\,\mathrm{cn}(y|1-m)\,\mathrm{dn}(y|1-m). \quad (2.73)\end{aligned}$$

Now, square both sides of Eq. (2.73) and use the identities (2.23) and (2.24) on the right-hand side. For convenience, define

$$X := \mathrm{sn}(a|m) \quad (2.74)$$

and

$$Y := \mathrm{sn}(y|1-m). \quad (2.75)$$

Rearranging, simplifying, and collecting terms in Eq. (2.73), we are left with

$$
\begin{aligned}
&B_i^2 + (-2A_iB_i - 4B_i^2)Y^2 + (A_i^2 + 6A_iB_i + 6B_i^2)Y^4 - (2A_i^2 + 6A_iB_i + 4B_i^2)Y^6 \\
&\quad + (A_i^2 + 2A_iB_i + B_i^2)Y^8 + X^2[2A_iB_i + (-2A_i^2 - 4A_iB_i + 4A_iB_im + 4B_i^2m)Y^2 \\
&+(2A_i^2 - 4A_i^2m - 14A_iB_im - 12B_i^2m)Y^4 + (2A_i^2 + 4A_iB_i + 6A_i^2m + 16A_iB_im + 12B_i^2m)Y^6 \\
&\quad - (2A_i^2 + 2A_iB_i + 2A_i^2m + 6A_iB_im + 4B_i^2m)Y^8] + X^4[A_i^2 + (4A_i^2m + 2A_iB_im)Y^2 \\
&+ (-2A_i^2 + 2A_iB_im + 4A_i^2m^2 + 8A_iB_im^2 + 6B_i^2m^2)Y^4 - (8A_i^2m + 10A_iB_im + 4A_i^2m^2 \\
&+ 14A_iB_im^2 + 12B_i^2m^2)Y^6 + (A_i^2 + 4A_i^2m + 6A_iB_im + A_i^2m^2 + 6A_iB_im^2 + 6B_i^2m^2)Y^8] \\
&\quad + X^6[-2A_i^2mY^2 + (2A_i^2m - 4A_i^2m^2 - 2A_iB_im^2)Y^4 + (2A_i^2m + 6A_i^2m^2 + 8A_iB_im^2 \\
&\quad + 4A_iB_im^3 + 4B_i^2m^3)Y^6 - (2A_i^2m + 2A_i^2m^2 + 6A_iB_im^2 + 2A_iB_im^3 + 4B_i^2m^3)Y^8] \\
&\quad + X^8[A_i^2m^2Y^4 - (2A_i^2m^2 + 2A_iB_im^3)Y^6 + (A_i^2m^2 + 2A_iB_im^3 + B_i^2m^4)Y^8] \\
&= X^2[4A_r^2Y^2 + 4A_r^2(m-2)Y^4 + 4A_r^2(1-m)Y^6] + X^6[4A_r^2mY^2 + 4A_r^2m(-2+m)Y^4 \\
&+ 4A_r^2m(1-m)Y^6] + X^4[-4A_r^2(1+m)Y^2 + 4A_r^2(2+m-m^2)Y^4 + 4A_r^2(m^2-1)Y^6].
\end{aligned}
\tag{2.76}
$$

It can be shown that products of the form $X^pY^q = \mathrm{sn}^p(a|m)\,\mathrm{sn}^q(y|1-m)$ and $X^rY^s = \mathrm{sn}^r(a|m)\,\mathrm{sn}^s(y|1-m)$ are linearly independent when $p = r$ and $q = s$ are not simultaneously true. The proof is given in Appendix B. If neither $\mathrm{sn}(a|m)$ nor $\mathrm{sn}(y|1-m)$ is everywhere constant, we can equate coefficients of such products on either side of Eq. (2.76). This process leads to 22 equations, which are not all independent. From the constants, we find

$$B_i = 0, \tag{2.77}$$

from coefficients of $\mathrm{sn}^4(y|1-m)$ and Eq. (2.77),

$$A_i = 0, \tag{2.78}$$

and from coefficients of $\mathrm{sn}^2(a|m)\,\mathrm{sn}^2(y|1-m)$ and Eqs. (2.78), (2.77), we obtain

$$A_r = 0. \tag{2.79}$$

Substituting Eqs. (2.77)–(2.79) into the remaining 19 coefficient equations does not yield any new information. Therefore in this case we have

$$\rho(x) = B_r = \text{constant}. \tag{2.80}$$

Equating coefficients in Eq. (2.76) as above will not yield correct results if a or y are such that one of the Jacobi functions is constant for all x.

We have shown that $g,\ m \in \mathbb{R}$. From Eq. (2.26), it follows that either $A = b^2$ or $A \in \mathbb{R}$ and $b^2 \in \mathbb{R}$. By (2.27), $b^2 \neq A$ in general. Therefore, we must have $A_i = 0$ and either $b_r = 0$ or $b_i = 0$; that is, b may be pure real or pure imaginary, but not complex. These cases correspond to one of $\mathrm{sn}(a|m)$ or $\mathrm{sn}^2(y|1-m)$ being constant.

If $b_r = 0$ and $b_i \neq 0$, then $a = \delta_{0r}$ and $\mathrm{sn}(a|m)$ is constant $\forall x$, but $\mathrm{sn}(y|1-m)$ varies. In this case, Eq. (2.77) still holds, and so $B_i = 0$.

If $b_i = 0$ and $b_r \neq 0$, then $y = \delta_{0i}$ and $\mathrm{sn}(y|1-m)$ is constant $\forall x$, but $\mathrm{sn}(a|m)$ varies. In this case, we may equate coefficients of like powers of $\mathrm{sn}(a|m)$ in Eq. (2.76).

Equating coefficients of $\mathrm{sn}^0(a|m)$, that is, constants, we find

$$B_i^2 + Y^2(-2A_iB_i - 4B_i^2) + Y^4(A_i^2 + 6A_iB_i + 6B_i^2) \\ + Y^6(2A_i^2 + 6A_iB_i + 4B_i^2) + Y^8(A_i + B_i)^2 = 0, \quad (2.81)$$

where $Y := \mathrm{sn}(y|1-m)$, as before. We have $A_i = 0$ from the requirement that $m \in \mathbb{R}$, above. Putting $A_i = 0$ in Eq. (2.81), we find that either $B_i = 0$ or else

$$Y^8 + 4Y^6 + 6Y^4 - 4Y^2 + 1 = 0. \quad (2.82)$$

However, we note that since $\mathrm{sn}(a|m)$ varies with x, so does $A\,\mathrm{sn}^2(bx+\delta_0)$, and therefore any imaginary part resulting from this term will also be dependent on x. Since $A_i = 0$, the imaginary part would have to come from the Jacobi function. Since it depends on x, there is no possible way for an imaginary term resulting from $A\,\mathrm{sn}^2(bx+\delta_0)$ to cancel B_i, which is constant. Therefore, in order to have $\rho(x) \in \mathbb{R}, \forall x$, we must have $B_i = 0$.

If $b_i = b_r = 0$, so that both $\mathrm{sn}(a|m)$ and $\mathrm{sn}(y|1-m)$ are constant, then the density $\rho(x)$ is also constant. In this case $\rho = A \in \mathbb{R}$, and we need not consider dependence on other parameters.

Thus, we have determined the constraints on imaginary parts of all parameters for all cases. A summary of the parameter conditions is given in Table 2.1.

Table 2.1: Conditions on physical & mathematical parameters.

Parameter	Condition
A	Real
B	Real
b	Either $\mathrm{Re}(b) = 0$ or $\mathrm{Im}(b) = 0$
δ_0	No constraints
m	Real
g	Real
μ	Real
α	Real

For a given physically determined nonlinear parameter g, our choice of A, B, δ_0, and μ determines the complete solution.

2.4 Potential Barrier – Boundary Conditions

For the nonlinear scattering problem, we have a piecewise-constant potential barrier as in Fig. 1.1. The constant-potential density solution (2.20) may be applied in each region of constant potential. We need boundary conditions in order to match the densities on either side of the boundaries x_1 and x_2.

Consider the stationary-state solution of the NLS, Eq. (1.7). Let $x = a$ be a boundary of the potential barrier. The wave function $\Psi(x,t)$ must be continuous for all x. If $\Psi(x,t)$ is discontinuous, then in the NLS, Eq. (1.4), $\nabla^2\Psi \to \infty$ at the discontinuity. This is non-physical. In particular, $\Psi(x,t)$ must be continuous at the

boundary $x = a$. Thus (1.7) yields

$$\sqrt{\rho^+(a)}e^{\,i[\phi^+(a)-\mu^+t]} = \sqrt{\rho^-(a)}e^{\,i[\phi^-(a)-\mu^-t]}, \tag{2.83}$$

where superscripts + and − denote the value of a quantity on the right or left-hand side of $x = a$, respectively. Replace exponentials in Eq. (2.83) using Euler's formula, and equate real and imaginary parts. The real parts yield

$$\sqrt{\rho^+(a)}\cos[\phi^+(a) - \mu^+t] = \sqrt{\rho^-(a)}\cos[\phi^-(a) - \mu^-t], \tag{2.84}$$

and the imaginary parts yield

$$\sqrt{\rho^+(a)}\sin[\phi^+(a) - \mu^+t] = \sqrt{\rho^-(a)}\sin[\phi^-(a) - \mu^-t]. \tag{2.85}$$

Equations (2.84) and (2.85) must be satisfied for all time t. Choose $t = 0$. This yields

$$\sqrt{\rho^+(a)}\cos[\phi^+(a)] = \sqrt{\rho^-(a)}\cos[\phi^-(a)], \tag{2.86}$$

$$\sqrt{\rho^+(a)}\sin[\phi^+(a)] = \sqrt{\rho^-(a)}\sin[\phi^-(a)]. \tag{2.87}$$

It can be shown that the first spatial derivative of the wave function must also be continuous for all x. The proof is given in Appendix B. Differentiating (1.7) with respect to x, and enforcing continuity at $x = a$, yields

$$\left\{\frac{1}{2}\,[\rho^+(a)]^{-1/2}\frac{d\rho^+}{dx}\bigg|_a + i\sqrt{\rho^+(a)}\,\frac{d\phi^+}{dx}\bigg|_a\right\}e^{\,i\phi^+(a)} = \left\{\frac{1}{2}\,[\rho^-(a)]^{-1/2}\frac{d\rho^-}{dx}\bigg|_a + i\sqrt{\rho^-(a)}\,\frac{d\phi^-}{dx}\bigg|_a\right\}e^{\,i\phi^-(a)}. \tag{2.88}$$

Substitute (2.15) in Eq. (2.88), replace exponentials by Euler's formula, and equate real and imaginary parts. The real parts yield

$$\begin{aligned}&[\rho^+(a)]^{-1/2}\left\{\frac{1}{2}\left.\frac{d\rho^+}{dx}\right|_a\cos[\phi^+(a)-\mu^+t]-\alpha^+\sin[\phi^+(a)-\mu^+t]\right\}\\&\quad=[\rho^-(a)]^{-1/2}\left\{\frac{1}{2}\left.\frac{d\rho^-}{dx}\right|_a\cos[\phi^-(a)-\mu^-t]-\alpha^-\sin[\phi^-(a)-\mu^-t]\right\},\end{aligned}\tag{2.89}$$

and the imaginary parts yield

$$\begin{aligned}&[\rho^+(a)]^{-1/2}\left\{\alpha^+\cos[\phi^+(a)-\mu^+t]+\frac{1}{2}\left.\frac{d\rho^+}{dx}\right|_a\sin[\phi^+(a)-\mu^+t]\right\}\\&\quad=[\rho^-(a)]^{-1/2}\left\{\alpha^-\cos[\phi^-(a)-\mu^-t]+\frac{1}{2}\left.\frac{d\rho^-}{dx}\right|_a\sin[\phi^-(a)-\mu^-t]\right\}.\end{aligned}\tag{2.90}$$

Equations (2.89) and (2.90) must be satisfied for all time. Choose $t=0$. This yields

$$\begin{aligned}&[\rho^+(a)]^{-1/2}\left\{\frac{1}{2}\left.\frac{d\rho^+}{dx}\right|_a\cos[\phi^+(a)]-\alpha^+\sin[\phi^+(a)]\right\}\\&\quad=[\rho^-(a)]^{-1/2}\left\{\frac{1}{2}\left.\frac{d\rho^-}{dx}\right|_a\cos[\phi^-(a)]-\alpha^-\sin[\phi^-(a)]\right\},\end{aligned}\tag{2.91}$$

$$\begin{aligned}&[\rho^+(a)]^{-1/2}\left\{\alpha^+\cos[\phi^+(a)]+\frac{1}{2}\left.\frac{d\rho^+}{dx}\right|_a\sin[\phi^+(a)]\right\}\\&\quad=[\rho^-(a)]^{-1/2}\left\{\alpha^-\cos[\phi^-(a)]+\frac{1}{2}\left.\frac{d\rho^-}{dx}\right|_a\sin[\phi^-(a)]\right\}.\end{aligned}\tag{2.92}$$

Multiply Eq. (2.91) by Eq. (2.86) to obtain

$$\begin{aligned}&\frac{1}{2}\left.\frac{d\rho^+}{dx}\right|_a\cos^2[\phi^+(a)]-\alpha^+\sin[\phi^+(a)]\cos[\phi^+(a)]\\&\qquad=\frac{1}{2}\left.\frac{d\rho^-}{dx}\right|_a\cos^2[\phi^-(a)]-\alpha^-\sin[\phi^-(a)]\cos[\phi^-(a)].\end{aligned}\tag{2.93}$$

Multiply Eq. (2.92) by Eq. (2.87) to get

$$\alpha^+ \sin[\phi^+(a)] \cos[\phi^+(a)] + \frac{1}{2} \left. \frac{d\rho^+}{dx} \right|_a \sin^2[\phi^+(a)] = \alpha^- \sin[\phi^-(a)] \cos[\phi^-(a)] + \frac{1}{2} \left. \frac{d\rho^-}{dx} \right|_a \sin^2[\phi^-(a)]. \quad (2.94)$$

Now add (2.93) to (2.94). After simplification, we find that

$$\left. \frac{d\rho^+}{dx} \right|_a = \left. \frac{d\rho^-}{dx} \right|_a, \quad (2.95)$$

that is, the first derivative of the density must be continuous at the boundary.

Multiply Eq. (2.91) by Eq. (2.87), which yields

$$\frac{1}{2} \left. \frac{d\rho^+}{dx} \right|_a \sin[\phi^+(a)] \cos[\phi^+(a)] - \alpha^+ \sin^2[\phi^+(a)] = \frac{1}{2} \left. \frac{d\rho^-}{dx} \right|_a \sin[\phi^-(a)] \cos[\phi^-(a)] - \alpha^- \sin^2[\phi^-(a)]. \quad (2.96)$$

Multiply Eq. (2.92) by Eq. (2.86). We find

$$\alpha^+ \cos^2[\phi^+(a)] + \frac{1}{2} \left. \frac{d\rho^+}{dx} \right|_a \sin[\phi^+(a)] \cos[\phi^+(a)] = \alpha^- \cos^2[\phi^-(a)] + \frac{1}{2} \left. \frac{d\rho^-}{dx} \right|_a \sin[\phi^-(a)] \cos[\phi^-(a)]. \quad (2.97)$$

Now subtract (2.96) from (2.97). Simplifying, we obtain

$$\alpha^+ = \alpha^-. \quad (2.98)$$

The phase parameter α must also be continuous across the boundary. Thus, α has a constant value for all x, since it is constant in each region as found in the process of solving Eq. (1.4) for constant potential.

We now return to the original wave function continuity equation, (2.83). Take the modulus of both sides of (2.83):

$$\sqrt{\rho^+(a)} = \sqrt{\rho^-(a)} \tag{2.99}$$

$$\Rightarrow \rho^+(a) = \rho^-(a), \tag{2.100}$$

since $\rho \geq 0$. Thus, the linear particle density of the BEC must be continuous at the boundary.

Substitute Eq. (2.100) into Eqs. (2.86) and (2.87) to obtain

$$\sqrt{\rho(a)}\{\cos[\phi^+(a)] - \cos[\phi^-(a)]\} = 0, \tag{2.101}$$

$$\sqrt{\rho(a)}\{\sin[\phi^+(a)] - \sin[\phi^-(a)]\} = 0, \tag{2.102}$$

where we now use $\rho(a)$ to replace $\rho^{\pm}(a)$ for the density at the boundary, since it is continuous. By Eqs. (2.101) and (2.102), it follows that either the density vanishes at the boundary, or else we have the system

$$\cos[\phi^+(a)] = \cos[\phi^-(a)], \tag{2.103}$$

$$\sin[\phi^+(a)] = \sin[\phi^-(a)]. \tag{2.104}$$

Equations (2.103) and (2.104) can be satisfied simultaneously only when

$$\phi^+(a) = \phi^-(a) + 2n\pi,\ n \in \mathbb{Z}. \tag{2.105}$$

From Eq. (2.105), it follows that the full wave function solutions (1.7) have denumerably infinite degeneracy.

Substitute Eqs. (2.100) and (2.105) into (2.83):

$$\sqrt{\rho(a)}e^{i[\phi^-(a)+2n\pi]}e^{-i\mu^+t} = \sqrt{\rho(a)}e^{i\phi^-(a)}e^{-i\mu^-t}. \tag{2.106}$$

If $\rho(a) \neq 0$, Eq. (2.106) can be simplified to

$$e^{-i\mu^+t} = e^{-i\mu^-t}. \tag{2.107}$$

Equation (2.107) must be satisfied for all time, and so we conclude that

$$\mu^+ = \mu^-, \tag{2.108}$$

except possibly when $\rho(x)$ vanishes at the boundary. If Eq. (2.108) is not satisfied in this case, then we have a jump discontinuity in μ at the boundary. It can be shown that this case is not physically relevant via a perturbation argument.

The density ρ is nonvanishing for all x, except when $B = 0$. Therefore, ρ may vanish at the boundary only when $B = 0$ and the boundary is at the location of a root of $\mathrm{sn}(bx + \delta_0|m)$. A slight boost of the BEC velocity leads to a slight perturbation of B off of zero, and in this case μ must be continuous across the boundary. That is,

a small perturbation of a solution with a jump discontinuity in μ leads to a violation of the boundary conditions. Therefore, Eq. (2.108) must be satisfied in all cases, including the case in which $\rho(x)$ vanishes at the boundary.

The methods described above can be used at any boundary; that is, at any location of a jump discontinuity in $V(x)$. Thus, if we know the values of all parameters in one region of constant potential, we can apply the boundary conditions derived in this section at every boundary, thereby determining the parameters in all other regions.

2.5 Determination of Parameters in Regions II and III

Assume that A, b, δ_0, and B are known in Region I of Fig. 1.1. These parameters are denoted with an "I" subscript in the analysis that follows. Also assume that the physical parameters g, μ, and V_0 are known. From these, we may determine b_I, α_I, and m_I from Eqs. (2.27), (2.29), and (2.26), respectively. Therefore, the solution is completely known in Region I. Note that g is a physical characteristic of the condensate, and is therefore constant for all x [25, 19].

We use the known values in Region I to determine values in Region II, which are denoted with a "II" subscript. The boundary, a, is x_1 in this case.

Substitute Eq. (2.100) into the density, (2.20), to obtain

$$\rho_I(x_1) = A_{II}\,\mathrm{sn}^2(b_{II}x_1 + \delta_{0,II}|m_{II}) + B_{II} \tag{2.109}$$

$$\Rightarrow\ \mathrm{sn}^2(b_{II}x_1 + \delta_{0,II}|m_{II}) = \frac{\rho_I(x_1) - B_{II}}{A_{II}} \tag{2.110}$$

$$\Rightarrow \delta_{0,II} = \ \mathrm{sn}^{-1}\left(\pm\sqrt{\frac{\rho_I(x_1) - B_{II}}{A_{II}}}\left|\frac{A_{II}}{(b_{II})^2}g\right.\right) - b_{II}x_1, \tag{2.111}$$

where we have used Eq. (2.26) to replace m_{II} in the inverse sn.

Using Eqs. (2.27) and (2.108), we can obtain the scaling:

$$(b_{II})^2 = 2(\mu - V_{II}) - (A_{II} + 3B_{II})g. \tag{2.112}$$

From Eqs. (2.111) and (2.112) we can determine the horizontal scaling and offset if we know A_{II} and B_{II}.

Substitute Eqs. (2.98) and (2.112) into Eq. (2.29) to get

$$\alpha_I^2 = B_{II}(A_{II} + B_{II})[2(\mu - V_{II}) - (A_{II} + 3B_{II})g + B_{II}g]. \tag{2.113}$$

From Eqs. (2.22), (2.23), and (2.24), we find

$$\left(\frac{d\rho}{dx}\right)^2 = 4A^2b^2\,\mathrm{sn}^2(bx + \delta_0|m)[1 - \ \mathrm{sn}^2(bx + \delta_0|m)][1 - m\,\mathrm{sn}^2(bx + \delta_0|m)]. \tag{2.114}$$

Substitute Eqs. (2.95) and (2.110) into (2.114). We obtain

$$\left(\left.\frac{d\rho_I}{dx}\right|_{x_1}\right)^2 = 4A_{II}^2 b_{II}^2 \left(\frac{\rho_I(x_1) - B_{II}}{A_{II}}\right)\left(\frac{A_{II} - \rho_I(x_1) + B_{II}}{A_{II}}\right) \times \left(\frac{A_{II} - m_{II}\rho_I(x_1) + m_{II}B_{II}}{A_{II}}\right). \quad (2.115)$$

Substitute Eqs. (2.26) and (2.112) into Eq. (2.115) and simplify, which yields

$$\left(\left.\frac{d\rho_I}{dx}\right|_{x_1}\right)^2 = -4[B_{II}-\rho_I(x_1)]\cdot[A_{II}+B_{II}-\rho_I(x_1)]\cdot\{2(\mu-V_{II})-[A_{II}+2B_{II}+\rho_I(x_1)]g\}. \quad (2.116)$$

In deriving Eq. (2.116) we assumed that $A_{II} \neq 0$; that is, the density in Region II is not constant. If the density in Region I is also non-constant, this is a valid assumption.

Equations (2.113) and (2.116) are quadratic in A_{II} and cubic in B_{II}. These equations can be solved for A_{II} and B_{II}, and the solution can be substituted into Eqs. (2.112) and (2.111) to find the remaining parameter values in Region II. Therefore, given all values in Region I as described above, we can obtain the complete solution for Region II.

To find the density on the right-hand side of the barrier, Region III, we apply the above process at x_2, this time taking Region II parameters as those on the left, i. e. values with a "-" subscript in the boundary conditions. The process may be extended to an arbitrary number of boundaries in a similar manner.

2.6 Linear Limit

When $g \to 0$ in Eq. (1.4), our solution reduces to the well-known barrier scattering solution of linear quantum mechanics (see, for example, [45, 46]). In this case, we find that B must be zero.

Proof. In the linear case, $g \to 0$, the Schrödinger equation is

$$\left[-\frac{1}{2}\,\frac{\partial^2}{\partial x^2} + V(x)\right]\Psi(x,t) = i\frac{\partial}{\partial t}\Psi(x,t). \tag{2.117}$$

Taking $V(x) = V_0$ constant, and a stationary-state solution of the form (1.7), the density (2.20) becomes

$$\rho(x) = A\sin^2(bx + \delta_0) + B. \tag{2.118}$$

Substituting the stationary-state solution (1.7) into Eq. (2.117), we find

$$\begin{aligned}\frac{1}{8}\,\rho^{-3/2}\left(\frac{d\rho}{dx}\right)^2 - \frac{1}{4}\,\rho^{-1/2}\frac{d^2\rho}{dx^2} - \frac{3}{4}\,i\rho^{-1/2}\left(\frac{d\rho}{dx}\right)\left(\frac{d\phi}{dx}\right)\\ - \frac{1}{2}\;i\rho^{1/2}\frac{d^2\phi}{dx^2} + \frac{1}{2}\,\rho^{1/2}\left(\frac{d\phi}{dx}\right)^2 + V_0\rho^{1/2} = \mu\rho^{1/2}.\end{aligned} \tag{2.119}$$

Equate real and imaginary parts. The real part is

$$\frac{1}{8}\,\rho^{-3/2}\left(\frac{d\rho}{dx}\right)^2 - \frac{1}{4}\,\rho^{-1/2}\frac{d^2\rho}{dx^2} + \frac{1}{2}\,\rho^{1/2}\left(\frac{d\phi}{dx}\right)^2 + V_0\rho^{1/2} = \mu\rho^{1/2}, \tag{2.120}$$

and the imaginary part is

$$-\frac{3}{4}\left(\frac{d\rho}{dx}\right)\left(\frac{d\phi}{dx}\right) - \frac{1}{2}\,\rho^{1/2}\frac{d^2\phi}{dx^2} = 0. \tag{2.121}$$

Integrating Eq. (2.121) yields

$$\frac{d\phi}{dx} = \frac{\alpha}{\rho(x)}, \tag{2.122}$$

where α is a constant of integration, provided that $\rho(x)$ is not everywhere zero. Substitute (2.122) into Eq. (2.120) and rearrange to obtain

$$-\frac{1}{4}\left(\frac{d\rho}{dx}\right)^2 + \frac{1}{2}\,\rho\frac{d^2\rho}{dx^2} - \alpha^2 = -2(\mu - V_0)\rho^2. \tag{2.123}$$

Finally, substitute the density (2.118) into Eq. (2.123). Using the trigonometric identity $\sin^2(\theta) + \cos^2(\theta) = 1$, we find

$$\begin{aligned} &- A^2b^2\sin^4(bx+\delta_0) + ABb^2[1 - 2\sin^2(bx+\delta_0)] \\ &\qquad = -2(\mu - V_0)[A^2\sin^4(bx+\delta_0) + 2AB\sin^2(bx+\delta_0) + B^2]. \end{aligned} \tag{2.124}$$

Equation (2.124) must be true for all x. Therefore, if $b \neq 0$, the coefficients of like powers of $\sin(bx + \delta_0)$ on either side of Eq. (2.124) must be equal. We find

$$-A^2b^2 = -2(\mu - V_0)A^2, \tag{2.125}$$

$$-2ABb^2 = -4AB(\mu - v_0), \tag{2.126}$$

$$ABb^2 = -2(\mu - V_0)B^2. \tag{2.127}$$

From Eq. (2.125), we must have either $A = 0$ or

$$b^2 = 2(\mu - V_0). \tag{2.128}$$

From Eq. (2.126), we must have either $A = 0$ or $B = 0$ or

$$b^2 = 2(\mu - V_0). \tag{2.129}$$

Finally, Eq. (2.127) implies that either $B = 0$ or

$$b^2 = -2(\mu - V_0)\frac{A}{B}. \tag{2.130}$$

If $A \neq 0$, then Eq. (2.128) must hold. Therefore, we must have either $B = 0$ or $B = -A$, by (2.127) and (2.130). Substituting $B = -A$ into the density (2.118), we find

$$\rho(x) = A[\sin^2(bx + \delta_0) - 1] \tag{2.131}$$

$$= -A\cos^2(bx + \delta_0) \tag{2.132}$$

$$= -A\sin^2(\pi/2 - bx - \delta_0) \tag{2.133}$$

$$= A'\sin^2(b'x + \delta_0') + B', \tag{2.134}$$

where, in relation to (2.118),

$$A' := -A, \tag{2.135}$$

$$b' := -b, \tag{2.136}$$

$$\delta_0' := -\delta_0 + \pi/2, \tag{2.137}$$

$$B' = 0. \tag{2.138}$$

Therefore this case is equivalent to $B = 0$. We have thus shown that in the linear limit, B is always equal to 0. QED.

Chapter 3

NONLINEAR SCATTERING

We consider a BEC in the presence of a potential barrier as in Fig. 1.1. The effective potential experienced by the BEC is

$$V_{\text{eff}} := V_0 + g\rho(x). \tag{3.1}$$

In the regime $\mu > \max(V_{\text{eff}})$, transmission over the barrier is classically allowed. For $\mu < \max(V_{\text{eff}})$, transmission is classically forbidden. In both regimes, our scattering displays quantum or wave-like effects, modified by the nonlinearity.

3.1 Calculation of Transmission

In the linear case, the wave function in each region can be split into a sum of two terms representing left- and right-traveling waves, using superposition [46]. We assume that the direction of travel is from left to right, so that the left-hand side of the barrier is the incident side. On this side, the solution contains both right- and left-traveling waves, i.e., incident & reflected waves. We choose only the right-traveling waves on the transmission side of the barrier. In this case, we may define the transmission coefficient as

$$T = \frac{\langle|\Psi_{\text{trans}}|^2\rangle}{\langle|\Psi_{\text{inc}}|^2\rangle}, \tag{3.2}$$

where Ψ_{trans} is the transmitted wave function and Ψ_{inc} is the incident wave function [45]. The angle brackets, $\langle \cdot \rangle$, denote an average value over one period of the function. The definition given by Eq. (3.2) is standard in linear quantum mechanics. In this interpretation, $T \leq 1$ over the entire domain of the system, and T represents the probability that a given particle will be transmitted across the barrier.

However, in the nonlinear case superposition does not apply. We cannot define separate left- and right-traveling waves in this case, and thus the transmission coefficient is defined simply as

$$T = \frac{\langle |\Psi_{III}|^2 \rangle}{\langle |\Psi_I|^2 \rangle}, \tag{3.3}$$

where Ψ_I and Ψ_{III} are the total wave functions in regions I and III, as defined in Fig. 1.1, respectively. Note that since neither region can be said to be the incident side of the barrier in this case, we could just as easily have defined the transmission coefficient inversely. We use the definition in Eq. (3.3) for consistency with the physical case of an atom laser. In the atom laser, particles are emitted from the laser and impinge on the barrier from one side, which we take to be the left-hand side. In this sense, we can think of the left-hand side of the barrier as the "incident" side for our problem, even though there is no superposition principle.

Thus, in the nonlinear case, we find that T may exceed unity. Physically, output cannot exceed input, and we conclude that the "transmission" coefficient as we define it contains information for atom lasers incident on either side of the barrier. Since we cannot choose only right- or left-traveling waves in the solution, due to the nonlinearity, we cannot define T to restrict incidence to only one side of the barrier, and must consider both circumstances in the same solution set.

Since $|\Psi|^2 = \rho$ in this case, we have

$$T = \frac{\langle \rho_{III} \rangle}{\langle \rho_I \rangle}. \tag{3.4}$$

The period of $\mathrm{sn}^2(bx+\delta_0|m)$ is $2K(m)/b$, where $K(m)$ is the complete elliptic integral of the first kind [40]. Thus we obtain the average density by

$$\langle \rho \rangle = \frac{b}{2K(m)} \int \rho(x)\, dx, \tag{3.5}$$

where the integral is taken over one period of $\rho(x)$.

Using the properties of Jacobi functions and elliptic integrals, we can show that if $0 \leq m \leq 1$,

$$\langle \rho \rangle = B + A \left[\frac{1}{m} - \frac{E(m)}{mK(m)} \right], \tag{3.6}$$

where $E(m)$ is the complete elliptic integral of the second kind, as follows. The average density is given by Eq. (3.5), with $\rho(x)$ as in Eq. (1.8). The period of the density is $2K(m)/b$. We can show that integrating from 0 to $2K(m)/b$ is equivalent to integrating over a general integral of length $2K(m)/b$. We first consider the integral of the Jacobi elliptic function,

$$\int_0^{2K(m)/b} \mathrm{sn}^2(bx + \delta_0|m)\, dx = \frac{1}{b} \int_{\delta_0}^{2K(m)+\delta_0} \mathrm{sn}^2(u|m)\, du, \tag{3.7}$$

where we have used the substitution $u = bx + \delta_0$. Using the relationships [40]

$$\int_0^w \mathrm{sn}^2(u|m)\, du = \frac{w - E(w|m)}{m}, \quad 0 \leq m \leq 1, \tag{3.8}$$

where $E(u|m)$ is the incomplete elliptic integral of the second kind, and

$$E[w + 2K(m)|m] = E(w|m) + 2E(m), \quad 0 \leq m \leq 1, \tag{3.9}$$

we may simplify Eq. (3.7). Write

$$\begin{aligned}
&\frac{1}{b}\int_{\delta_0}^{2K(m)+\delta_0} \mathrm{sn}^2(u|m)\,du \\
&\qquad = \frac{1}{b}\left[\int_0^{2K(m)+\delta_0} \mathrm{sn}^2(u|m)\,du - \int_0^{\delta_0} \mathrm{sn}^2(u|m)\,du\right] &(3.10)\\
&\qquad = \frac{1}{b}\left[\frac{2K(m)+\delta_0 - E[2K(m)+\delta_0|m]}{m} - \frac{\delta_0 - E(\delta_0|m)}{m}\right] &(3.11)\\
&\qquad = \frac{1}{b}\left[\frac{2K(m)+\delta_0 - E(\delta_0|m) - 2E(m)}{m} - \frac{\delta_0 - E(\delta_0|m)}{m}\right] &(3.12)\\
&\qquad = \frac{2K(m) - 2E(m)}{bm}. &(3.13)
\end{aligned}$$

Substituting this result into Eq. (3.5), using Eq. (1.8), leads to

$$\langle\rho\rangle = A\left[\frac{1}{m} - \frac{E(m)}{mK(m)}\right] + B. \tag{3.14}$$

If $m \notin [0, 1]$, we must first apply a transformation to write the density in terms of Jacobi elliptic functions which depend on a parameter $m' \in [0, 1]$, then use the methods above to simplify the integral. The relevant transformations are given in Appendix A.

3.2 Results

The density and transmission of the BEC are considered for several regimes.

3.2.1 Wide barrier

We consider a barrier whose width is much larger than its height. In this case, we have a barrier of width 20 and height 1. Density and phase plots for this barrier are given in Figs. 3.1 and 3.2. The corresponding transmission plots are shown in Figs. 3.3–3.5.

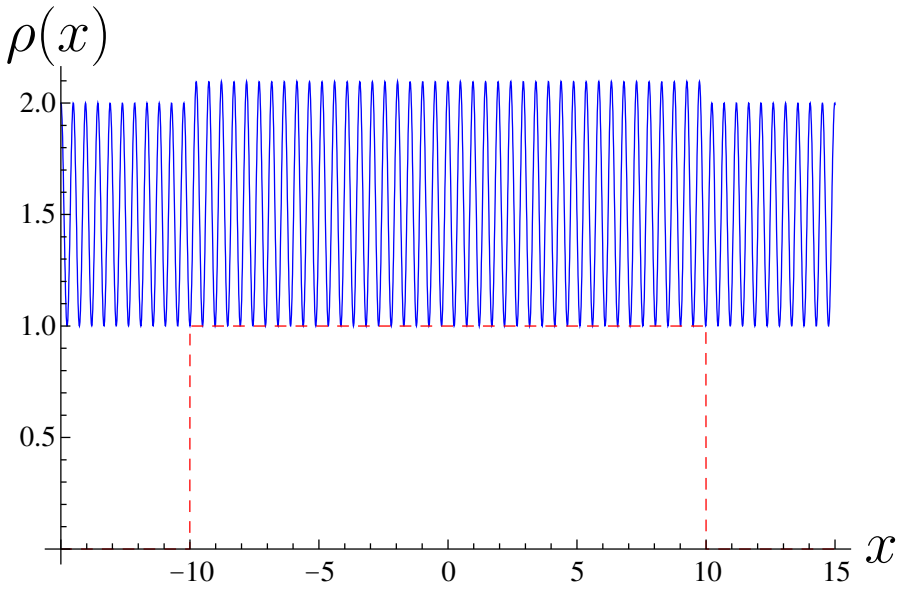

Figure 3.1: Density plot for wide barrier.

The potential barrier is shown as a dashed line in Figs. 3.1 and 3.2 for reference. The nonlinearity for these plots is $g = 0.1$. We note that the phase in each region is determined up to an arbitrary offset and that the phase parameter α may take either sign. We have chosen the positive sign for α, with an offset of zero.

The phase consists of small oscillations on a linear background. The background

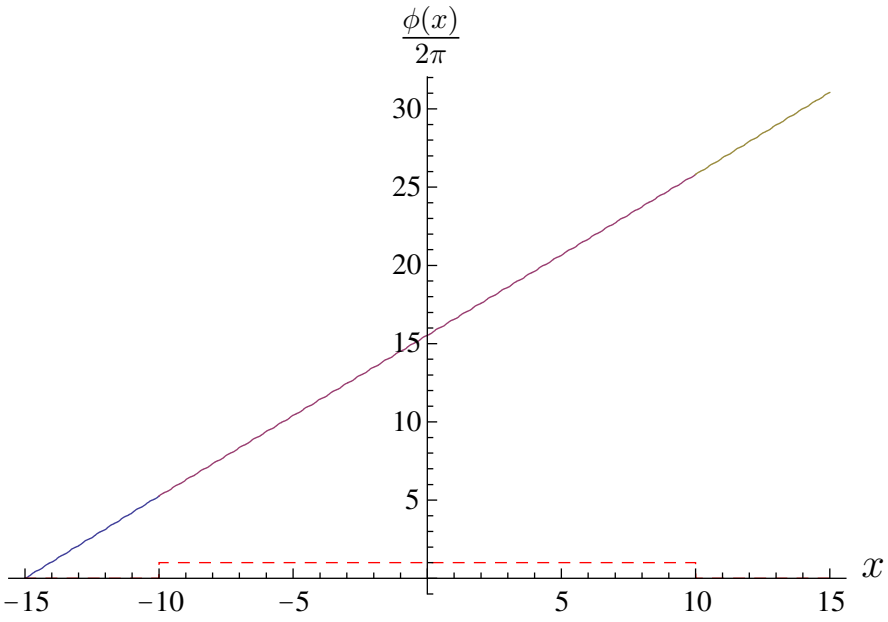

Figure 3.2: Phase plot for wide barrier.

slopes are the same on either side of the barrier. This means that the velocity profile of the BEC remains the same on either side of the barrier. This need not be true in general, as we will see in Section 3.2.6. The velocity profile is given by Eq. (2.30).

In Fig. 3.3, five transmission plots are shown on the same set of horizontal axes. The dashed line denotes $T = 1$, and the solid curve is the transmission coefficient. The nonlinearity g increases in steps of 0.01 as we move upward on the plot. Each transmission plot is at a convenient vertical offset for illustration, but the plots are not otherwise scaled or shifted. The nonlinearity is shown next to each curve for reference.

Note that the transmission coefficient may be greater than 1. This is not a novel physical feature; it arises due to the redefinition of transmission as in Eq. (3.3) and the invalidity of superposition in this problem, as discussed in Section 3.1. However, the

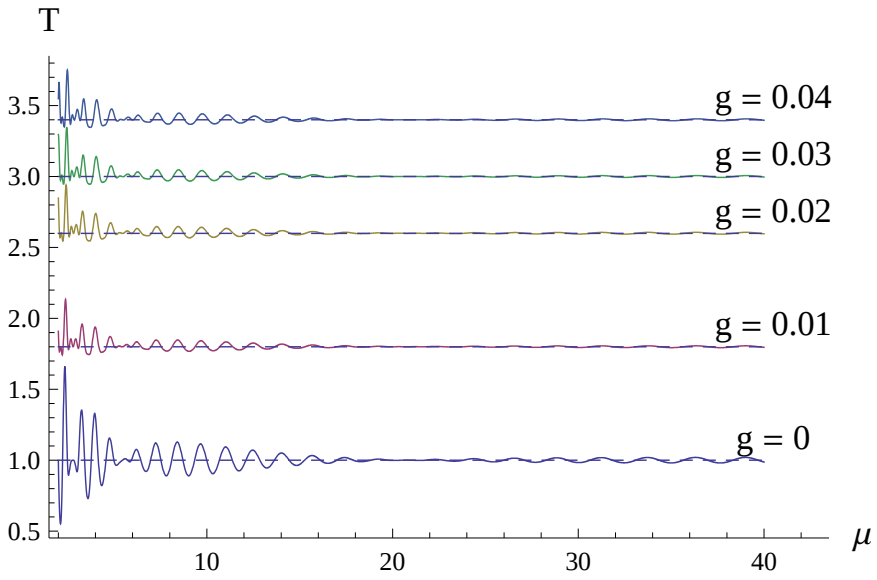

Figure 3.3: Transmission for wide barrier with small nonlinearity.

physical interpretation is different: since we cannot separate right- and left-traveling waves, the transmission coefficient no longer represents a probability for some particle to be transmitted through the barrier.

Comparing the linear, i.e $g = 0$, transmission curve in Fig. 3.3 with the other transmission plots in the same figure, we see that there is a significant change in transmission behavior when we enter the nonlinear regime, even for small $[\mathcal{O}(10^{-2})]$ nonlinearity. The most significant change occurs when μ is small, meaning that the potential barrier has a greater overall effect on the condensate. In the linear case, T oscillates on either side of 1, and the amplitude of oscillations is similar in either direction. In the nonlinear case, we see that while transmission can still be less than 1, it does not drop as far below 1 as in the linear case. This suggests that in the case of repulsive nonlinearity, $g > 0$, atomic interactions tend to cause more parti-

cles to be transmitted through the barrier than for the case of noninteracting particles.

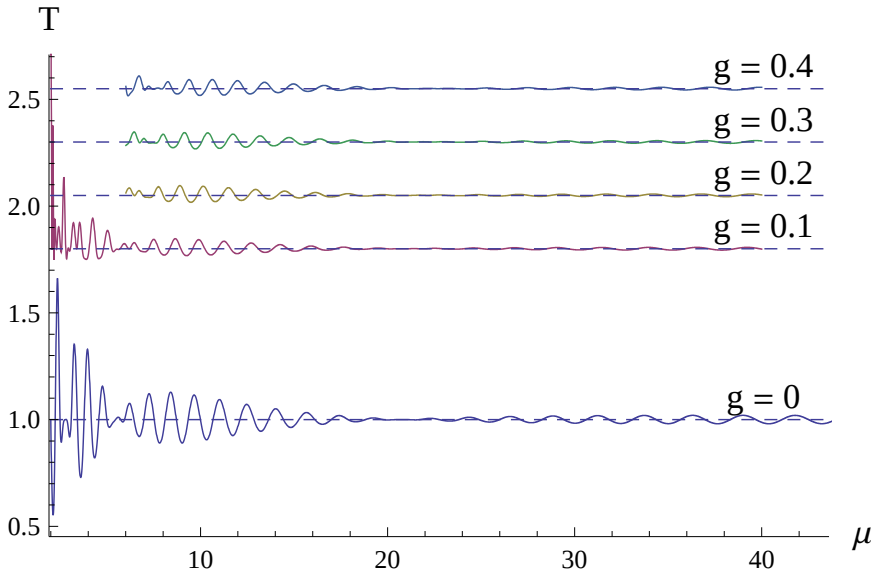

Figure 3.4: Transmission for wide barrier with medium nonlinearity I.

In Figs. 3.4 and 3.5, several transmission plots are shown on the same set of horizontal axes. The dashed lines correspond to $T = 1$. Individual transmission curves have been shifted by convenient vertical offsets for illustration, but the plots are not otherwise scaled or shifted. The nonlinearity g, shown next to each curve for reference, increases in steps of 0.1 as we move upward on the plot.

As g increases, new peaks appear in the small-μ regime, and the behavior of T changes significantly for smaller μ. This regime does not appear for $g \geq 0.2$. The reason is that g and μ are not completely independent. For a given chemical potential μ, when the nonlinearity g becomes larger than a certain cut-off value, solutions are generated that have $\rho(x) \in \mathbb{C}$. This is invalid because, when we solved the NLS, we

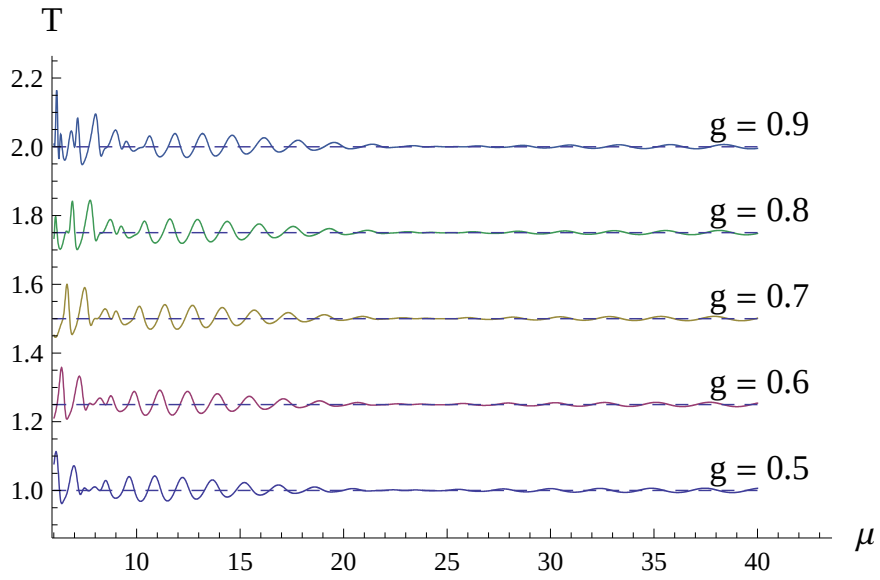

Figure 3.5: Transmission for wide barrier with medium nonlinearity II.

assumed $\rho(x) \in \mathbb{R}$. We may take $\rho(x) \in \mathbb{R}$ without loss of generality, as discussed in Section 2.2.1.

The appearance of complex $\rho(x)$ means that one or more of our assumptions are breaking down in this regime. A complete analysis of this situation is a matter for future study. We hypothesize that this regime occurs because the chemical potential μ is becoming complex. This case is not allowed, as we showed in Section 2.2.3. Thus, in this regime, the solution to the NLS, Eq. (1.4), has a different form than the one we postulated in (1.7). We do not consider such alternate solutions in this work. The cut-off for valid solutions is discussed further in Section 3.3.

For larger values of μ, the overall behavior of the transmission does not change significantly between each plot. However, we do see a shift in the transmission curve.

For higher μ, the transmission plot retains its shape and shifts to the right as g increases. This feature is especially apparent when a computer is used to animate the transmission plots for increasing g. In Figs. 3.4–3.5, this regime occurs when $\mu \gtrsim 6$.

Another feature of note is that with the definition (3.3) of transmission, the amplitude of oscillations in T does not decrease monotonically as in the usual linear interpretation. In all of the transmission plots of Figs. 3.3–3.5, we see significant oscillations on either side of a transition region between $\mu = 20$ and $\mu = 26$. In this region, we have almost perfect resonance, i.e. $T = 1$. For a discussion of transmission resonances, see Section 3.2.4.

3.2.2 Narrow barrier

We consider a barrier with width a factor of 10 smaller than its height. In this case, we expect the barrier to have less of an effect on the behavior of the BEC. Density and phase plots are given in Figs. 3.6 and 3.7. The corresponding transmission plots are given in Figs. 3.9–3.13.

We use a potential barrier of height 1 and width 0.1. The barrier is shown as a dashed line in Figs. 3.6 and 3.7 for reference. The nonlinearity for this solution is $g = 1.99$. Since the barrier is small relative to the healing length of the BEC, the change in amplitude of the density across the barrier is not as significant as for the wide-barrier case.

We have again chosen the positive sign for α, with a phase offset of zero in each region. We observe that in this case, the phase is not linear. The velocity profile of

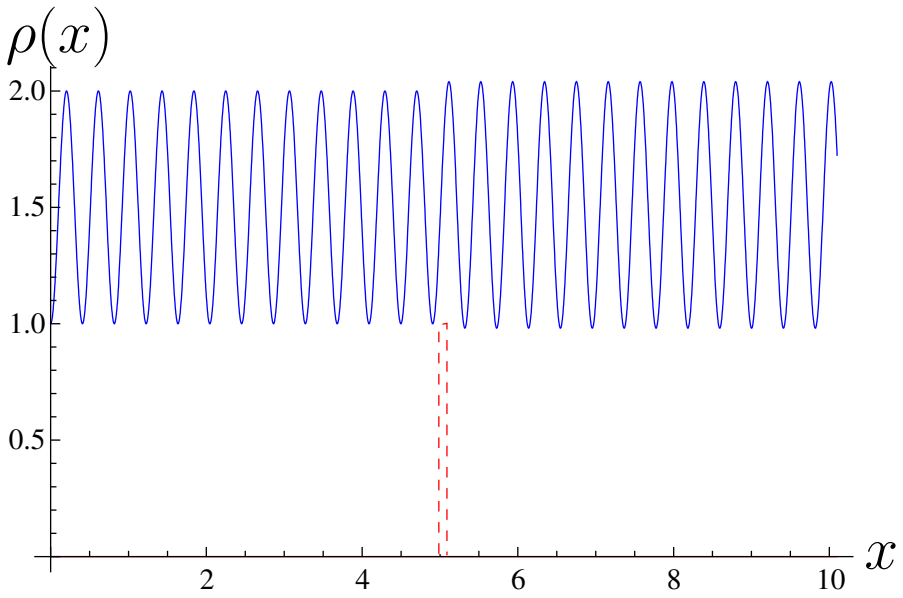

Figure 3.6: Density plot for narrow barrier.

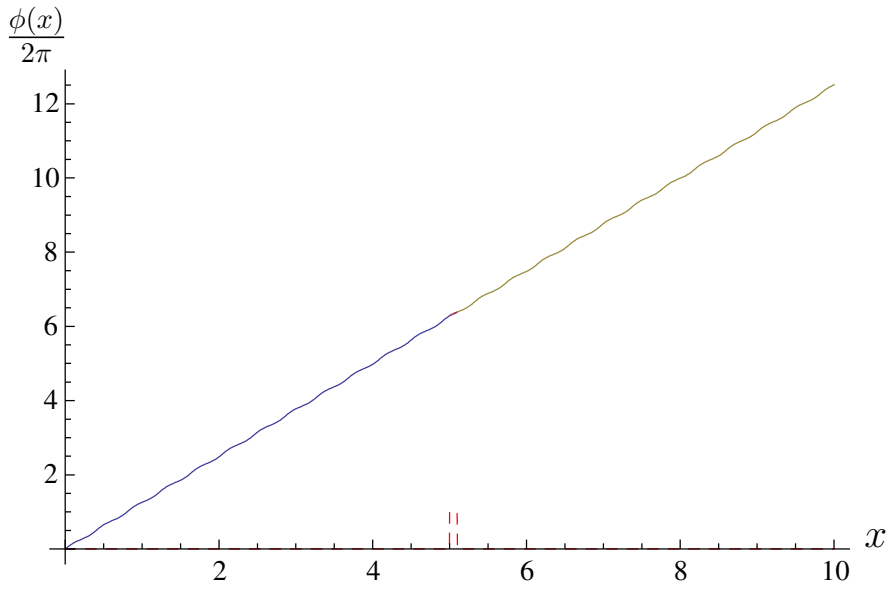

Figure 3.7: Phase plot for narrow barrier.

the BEC, i.e., the slope of the phase, changes smoothly as we move from one side of the barrier to the other.

The phase consists of small oscillations on a linear background. A zoomed-in view of the phase is given in Fig. 3.8. This plot clearly shows the oscillation over the barrier. For illustrative purposes, the height of the potential barrier in Fig. 3.8 is scaled to 21% of its true size. The barrier width is not scaled.

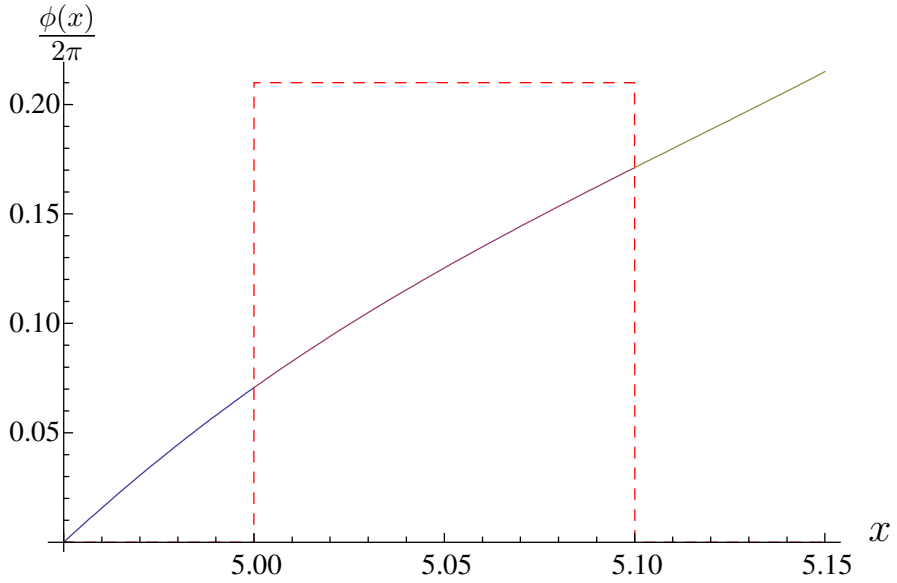

Figure 3.8: Phase oscillations over narrow barrier, zoom view.

Again, the background slopes are the same on either side of the barrier. The slope over the barrier, however, is smaller by a factor of 0.2. This shows that the barrier is not completely invisible to the BEC.

In Fig. 3.9, five transmission plots are shown on the same set of horizontal axes,

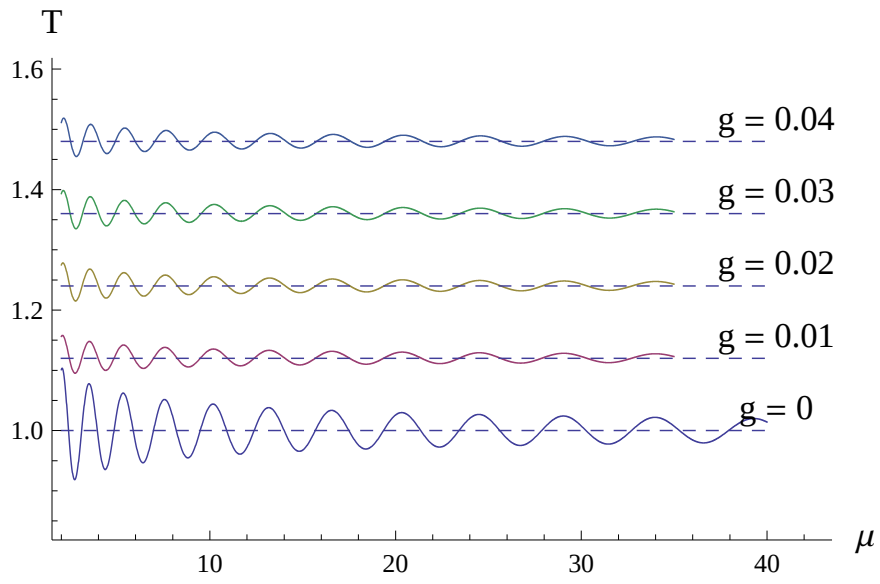

Figure 3.9: Transmission for narrow barrier with small nonlinearity.

with vertical offsets in T for illustration. The plots are not otherwise shifted or scaled. The dashed line denotes $T = 1$, and the solid curve is the transmission coefficient. The nonlinearity g increases in steps of 0.01 as we move upward on the plot. The nonlinearity is shown next to each curve for reference.

Comparing the linear, i.e. $g = 0$, transmission curve in Fig. 3.9 with the other transmission plots in the same figure, we again see a significant drop in the amplitude of oscillations as we go from the linear to the nonlinear regime. Again, the nonlinear transmission tends to stay further above 1 than below 1, although the difference in amplitudes above and below 1 is smaller than in the wide-barrier case.

In each of Figs. 3.10–3.13, five transmission plots are shown on the same set of horizontal axes. The transmission curves are offset vertically for illustration, but are

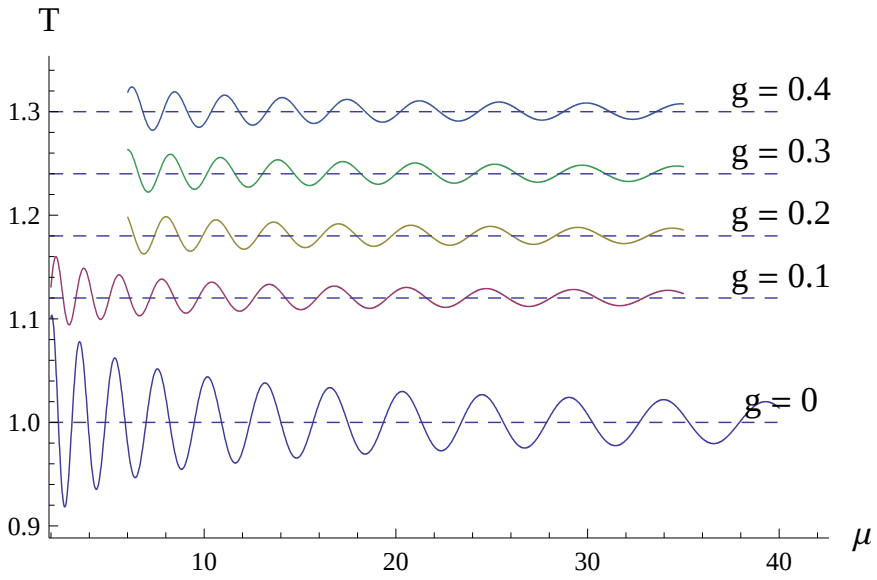

Figure 3.10: Transmission for narrow barrier with medium nonlinearity I.

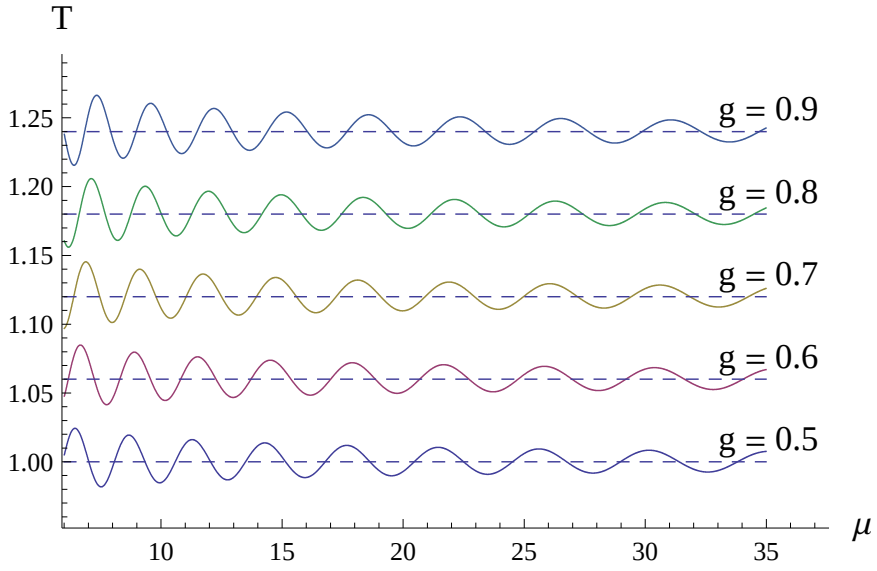

Figure 3.11: Transmission for narrow barrier with medium nonlinearity II.

not otherwise shifted or scaled. The dashed line denotes $T = 1$, and g increases in steps of 0.1 as we move upward on the plot. The nonlinearity is shown next to each

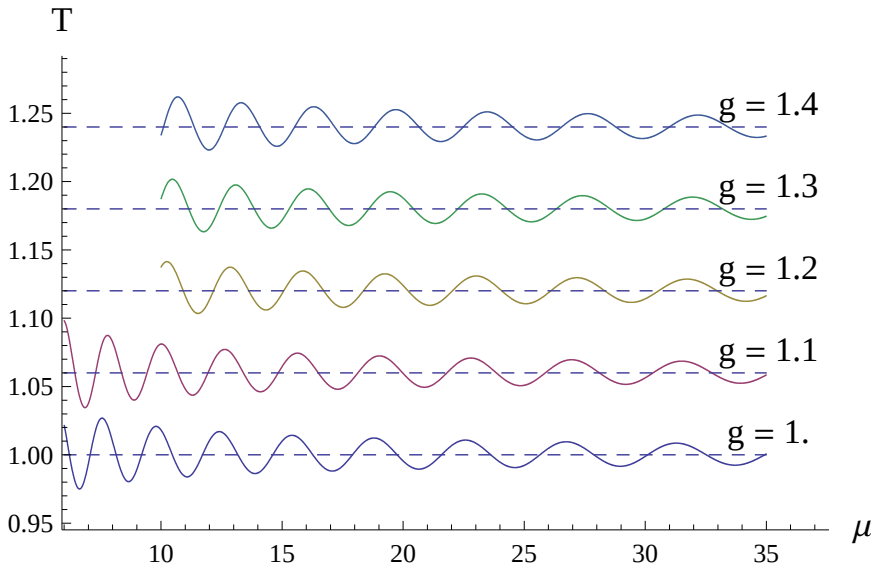

Figure 3.12: Transmission for narrow barrier with medium nonlinearity III.

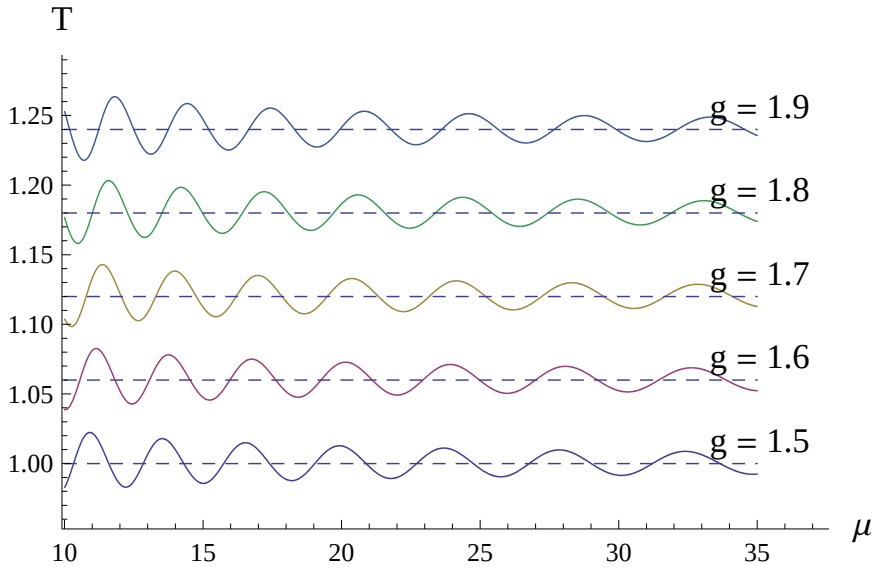

Figure 3.13: Transmission for narrow barrier with medium nonlinearity IV.

curve for reference.

The amplitude of oscillations decreases smoothly in this case. We also see that there is no region of near-perfect resonance as in the wide-barrier case: T oscillates quasi-periodically about $T = 1$. Again, the transmission curve shifts to the right as the nonlinearity g increases. The narrowness of the barrier also has the effect of smoothing the oscillations as compared to the wide-barrier case.

3.2.3 Strong nonlinearity

We consider a barrier of width 5 and height 1. Density and phase plots are given in Figs. 3.14 and 3.15. The corresponding transmission plots are given in Figs. 3.16 and 3.17.

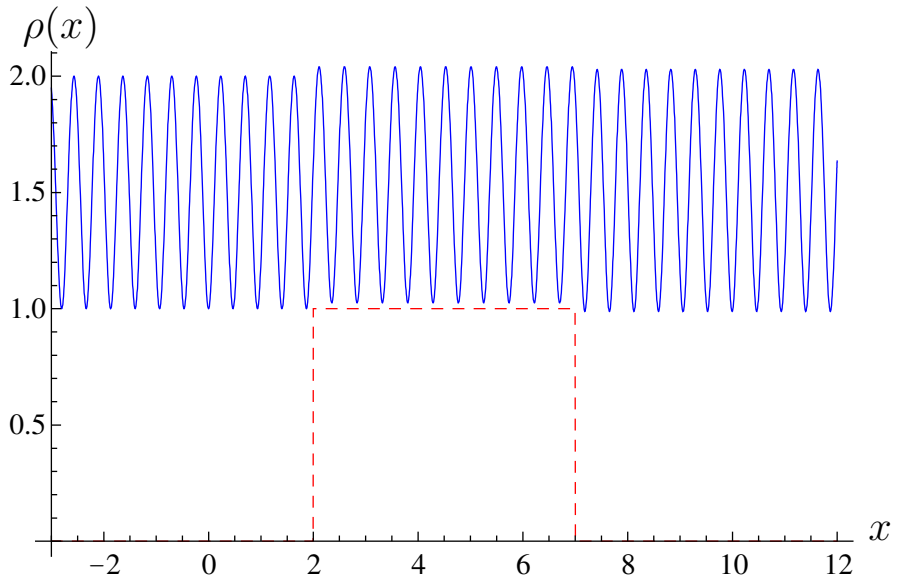

Figure 3.14: Density plot with strong nonlinearity.

The potential barrier is shown as a dashed line in Figs. 3.14 and 3.15 for reference. The nonlinearity is $g = 9.9$ for these plots. We have again chosen the positive

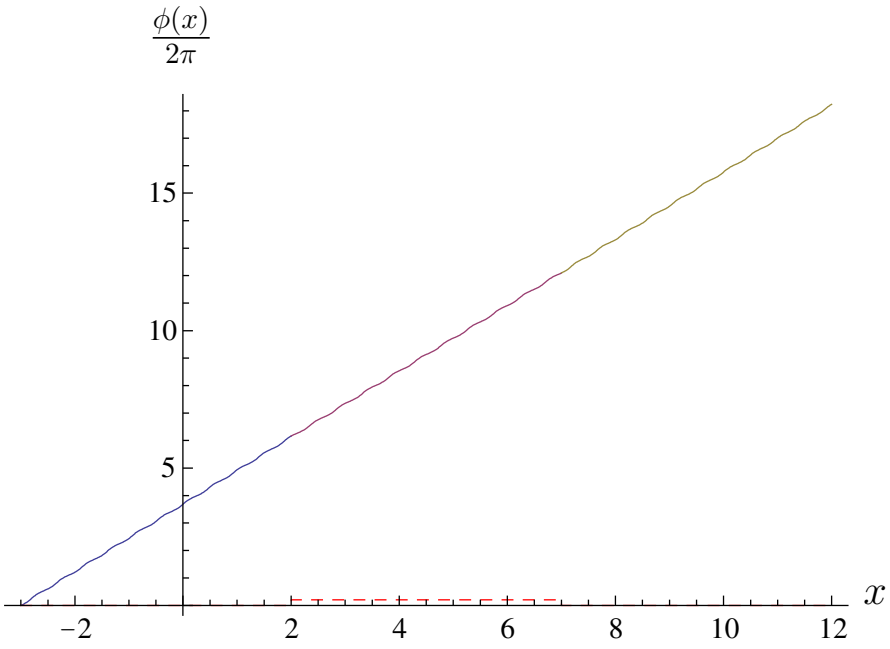

Figure 3.15: Phase plot with strong nonlinearity.

sign for α, with no phase offset.

The phase is nearly linear in this case, though slight variations are clearly visible. Again, the velocity profile of the BEC changes smoothly across the barrier, and the background slopes are the same on either side.

In Figs. 3.16 and 3.17, several transmission plots are shown on the same horizontal axes. The transmission curves are offset for illustrative purposes, but are not otherwise shifted or scaled. The nonlinearity is shown next to each curve for reference.

In this case we see two oscillations – the transmission coefficient itself oscillates up and down within an envelope of oscillations above and below 1. Again there is no

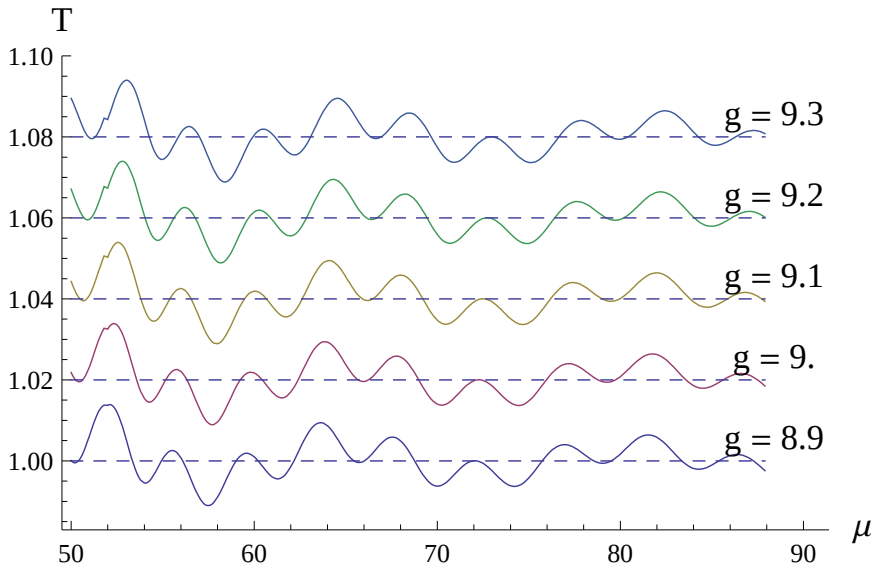

Figure 3.16: Transmission for medium-width barrier with strong nonlinearity I.

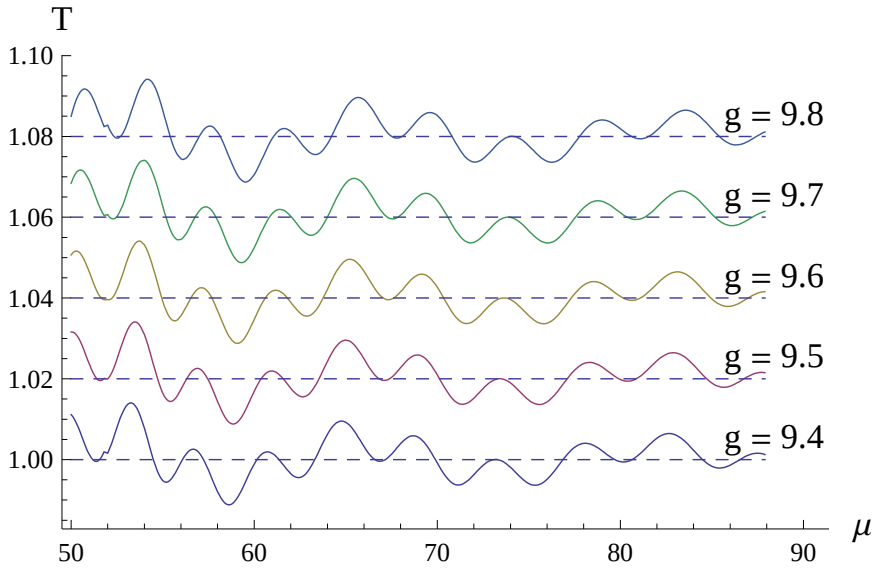

Figure 3.17: Transmission for medium-width barrier with strong nonlinearity II.

region of near-constant resonance.

3.2.4 Transmission resonances

We consider the behavior of the transmission resonances; that is, the points at which $T = 1$. Resonance plots are given in Figs. 3.18, 3.19, and 3.20. The resonance plots are "cut off" at low g-values for small values of μ; this is due to the relationship between g and μ discussed in Section 3.2.1. The cut-off is explored further in Section 3.3.

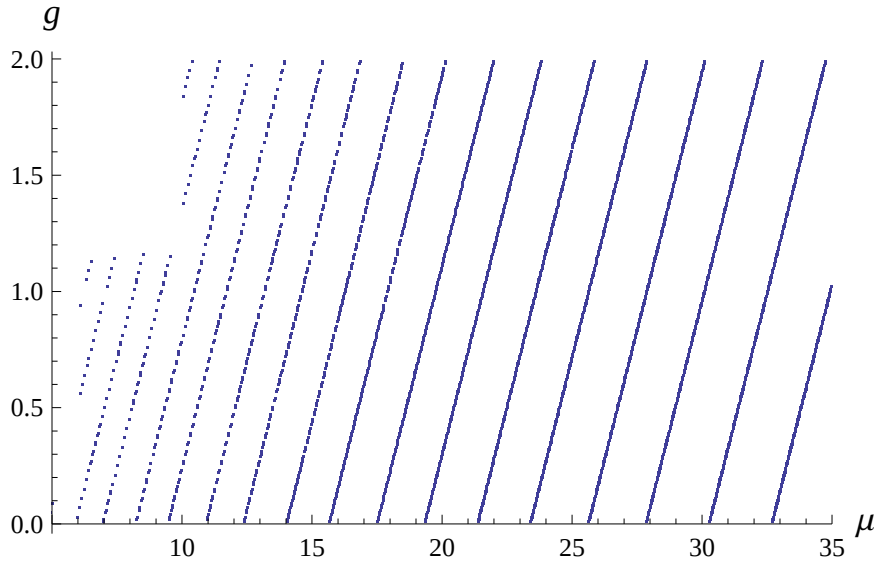

Figure 3.18: Transmission resonances for narrow barrier.

Figure 3.18 corresponds to the transmission plots in Section 3.2.2. The barrier is narrow compared to its height. A barrier of width 0.1 and height 1 was used. The sampling sizes used for g and μ are consistent throughout the entire plot. The resonances shift slightly to the right as g increases, as observed in the transmission plots. We see lines of resonance whose slope $\Delta g/\Delta\mu$ are all the same. The spacing between these lines increases as μ increases.

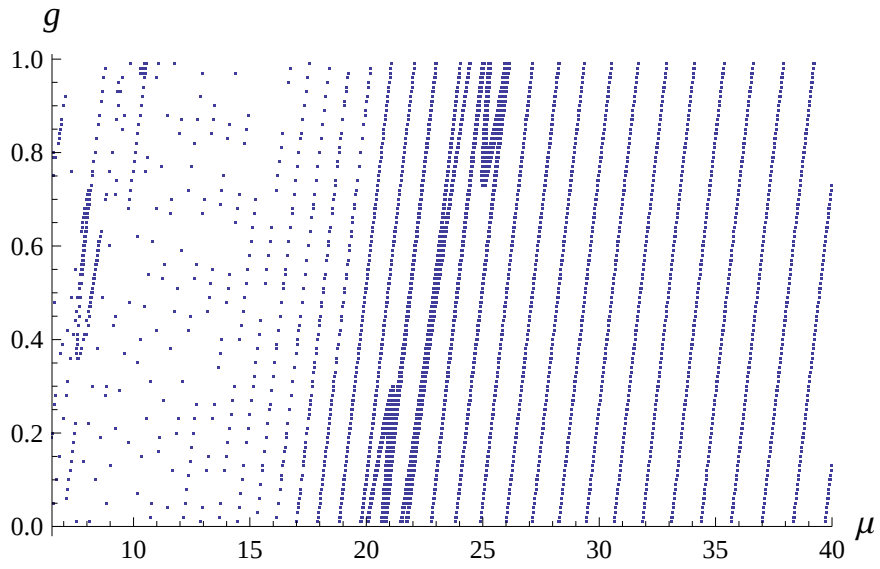

Figure 3.19: Transmission resonances for wide barrier, displaying bifurcations.

Figure 3.19 corresponds to the transmission plots in Section 3.2.1. The barrier is wide compared to its height. A barrier of width 20 and height 1 was used. The sampling sizes used for g and μ are consistent throughout the entire plot. Here, the resonances are sparse for lower values of μ and more uniform for higher values of μ. For mid-range μ, we see very different behavior. There are three regions between $\mu = 20$ and $\mu = 26$ where the resonances are extremely dense. These correspond to the region of near-constant resonance seen in the transmission plots. It shifts to the right as g increases, as observed in the transmission plots. Also, three bifurcations are present in this region. This is a novel feature arising from the strongly nonlinear character of the system, and presents exciting possibilities for future research.

In the regions where lines of resonance appear, the spacing between these lines

is smaller than in Fig. 3.18. The spacing increases as μ increases, though not as fast as in the narrow-barrier case.

Thus, we can see that this case corresponds to a very different physical regime than that of Fig. 3.18.

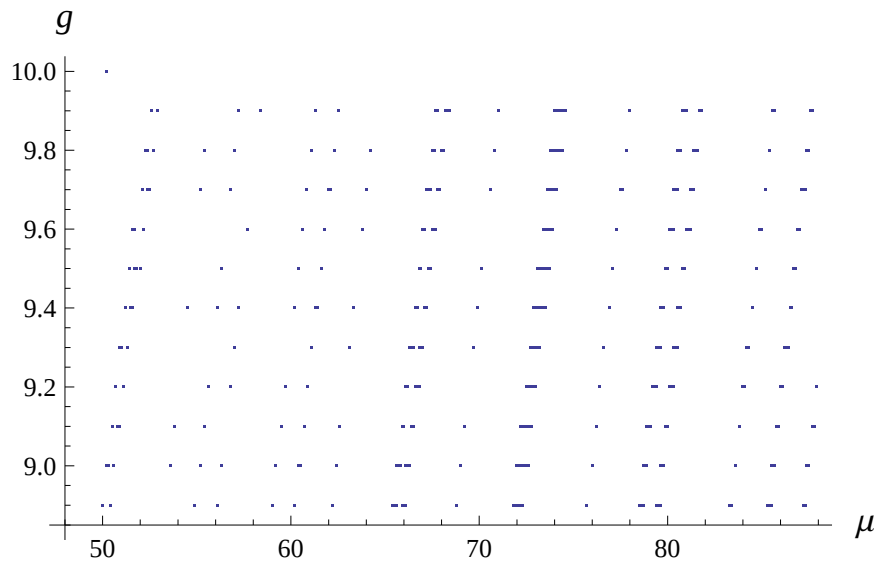

Figure 3.20: Transmission resonances for barrier with strong nonlinearity; discrete sampling.

Figure 3.20 corresponds to the transmission plots in Section 3.2.3, with a barrier of width 5 and height 1. In Fig. 3.20, the sampling increments for g and μ are larger than those used in Figs. 3.18 and 3.19. This accounts for the more sparse appearance of the plot. In this case, we again see constant-slope lines of resonance for low and high values of μ. In the region $54 \leq \mu \leq 64$, the resonances are more sparsely distributed. Also, clusters of two or more resonance lines are apparent. The spacing

between lines does not change monotonically in this case.

We conclude that the behavior of transmission resonances is strongly dependent on the width of the barrier and the strength of the nonlinearity, with all other parameters held constant. Wider barriers are more "visible" to the condensate, so the most novel behavior appears for wider barriers. For large values of the chemical potential μ, the effective potential of the barrier has less of an effect on the condensate.

3.2.5 Resonance slopes

The resonances in Fig. 3.19 lie along parallel straight lines. We consider the slope of these resonance lines as a function of the input parameters A_I and B_I. Slope plots are shown in Fig. 3.21.

In Fig. 3.21, several slope plots are shown on the same set of horizontal axes. The slope curves are vertically offset for illustration, but are not otherwise scaled or shifted. In these plots, we used a potential barrier of width 0.1 and height 1, as in Fig. 3.19.

For a given A_I, we observe identical slopes for each value of B_I. Therefore we conclude that the density offset B_I and the transmission coefficient T are not related over the range of parameters we considered. The density offset is primarily related to the barrier height; that is, B adjusts the height of the density relative to the potential barrier, but not its amplitude or wavelength. We note that the elliptic parameter m, which is strongly governed by the nonlinearity of the system, depends on both amplitude A and wavelength $1/b$, but does not depend on the offset B, as shown in

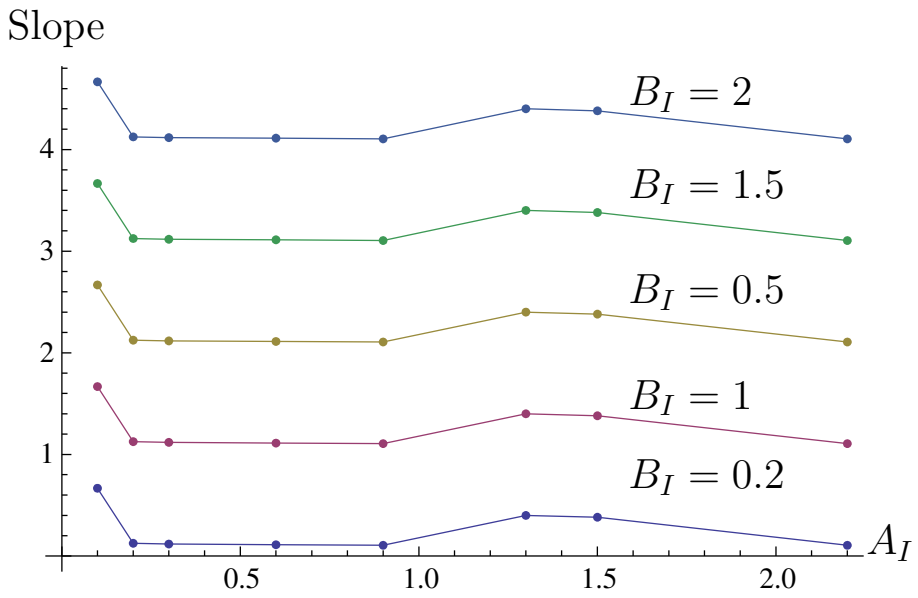

Figure 3.21: Slope of resonance lines as a function of input parameters. Curves are a guide to the eye.

Eq. (2.26). As we will see in Section 3.2.6, the strength of nonlinearity governs the character of the density profile, i.e., the broadening of the peaks in the Jacobi elliptic function. This affects the average density, and thus the transmission coefficient.

Thus we conclude that the slopes of the resonance lines are governed primarily by the amplitude and wavelength of the input BEC density, and that a constant density offset B does not have a significant effect on the transmission coefficient.

3.2.6 Localized solutions

A density plot showing a highly nonlinear system is shown in Fig. 3.22. A well-localized solution can be seen above the potential barrier. The corresponding phase plot is given in Fig. 3.23.

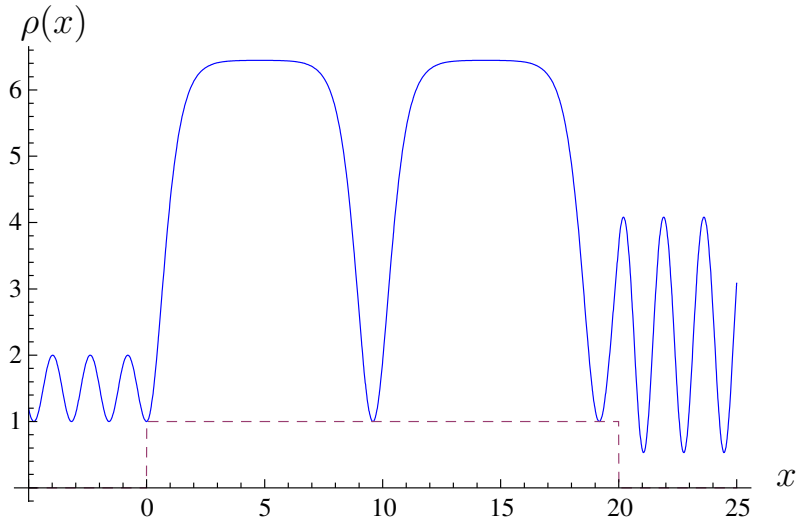

Figure 3.22: Localized density over wide barrier.

In Figs. 3.22 and 3.23, the potential barrier is shown as a dashed line, for reference. The barrier has height $V_0 = 1$ and width 20. The nonlinearity is $g = 2.02$. Over the barrier, the peaks of the sn^2 function broaden significantly. This is indicative of elliptic parameter m near 1. The local minimum of the density over the barrier is a dark soliton, a very well-localized solution. It has been generally shown that dark solitons appear in the limit that the elliptic parameter m, which is proportional to the strength of the nonlinearity, approaches unity from below [28]. This is a fascinating effect. Unlike the density plots seen previously, in this nonlinear system, the wave function transitions from a wave with small parameter m, which is nearly linear and similar to a sine wave, in Region I, to a well-localized dark soliton in Region II, and back to a nearly linear wave in Region III. The localization is a result of the strongly nonlinear character of this system. Such systems are experimentally accessible [28].

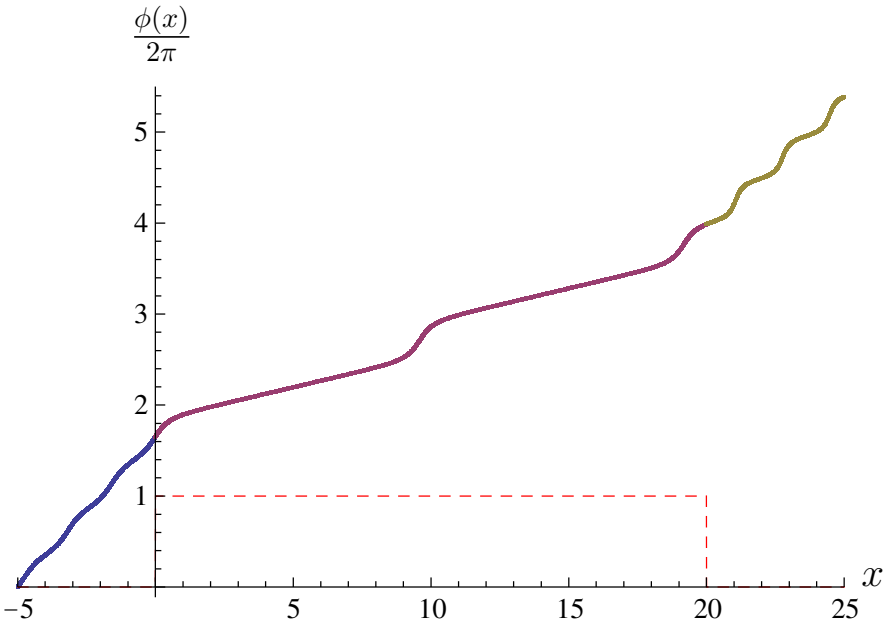

Figure 3.23: Phase plot for localized solution.

The oscillatory waves on either side of the barrier are slightly deformed standing waves which are close to the linear solution.

The phase has an overall linear envelope on either side of the barrier, with clearly visible oscillations on this background. The sudden increase in phase seen near $x = 10$ corresponds to the position of the soliton. Thus, the BEC flows more quickly at this position than elsewhere.

In this case, the background slopes differ slightly on either side, and the slope over the barrier is smaller by a factor of 3. This shows that the velocity profile of the BEC need not be the same on either side of the barrier.

Soliton trains may also be observed in some highly nonlinear systems [47, 20]. An example is shown in Fig. 3.24. The corresponding phase plot is shown in Fig. 3.25.

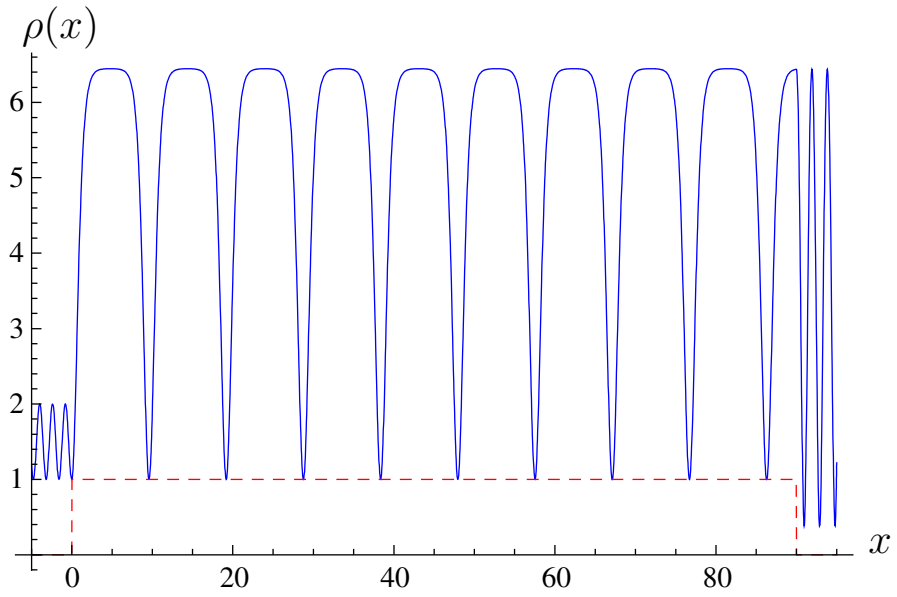

Figure 3.24: Density showing train of localized dark solitons.

The potential barrier is shown as a dashed line in Figs. 3.24 and 3.25 for reference. The barrier has height $V_0 = 1$ and width 90. The nonlinearity is $g = 2.02$. The density notches above the potential barrier are dark solitons. Since the amplitude of the wave function $\Psi(x,t)$ in (1.7) is independent of time, the density does not dissipate. If no barriers are present, these solitons will travel through time while maintaining their shape. In the Engels experiment [20], the BEC is viewed in the frame of a moving potential barrier.

Again, the phase profile shows oscillations on a linear background. On either side of the barrier, the background slope is different. The velocity profile of the BEC

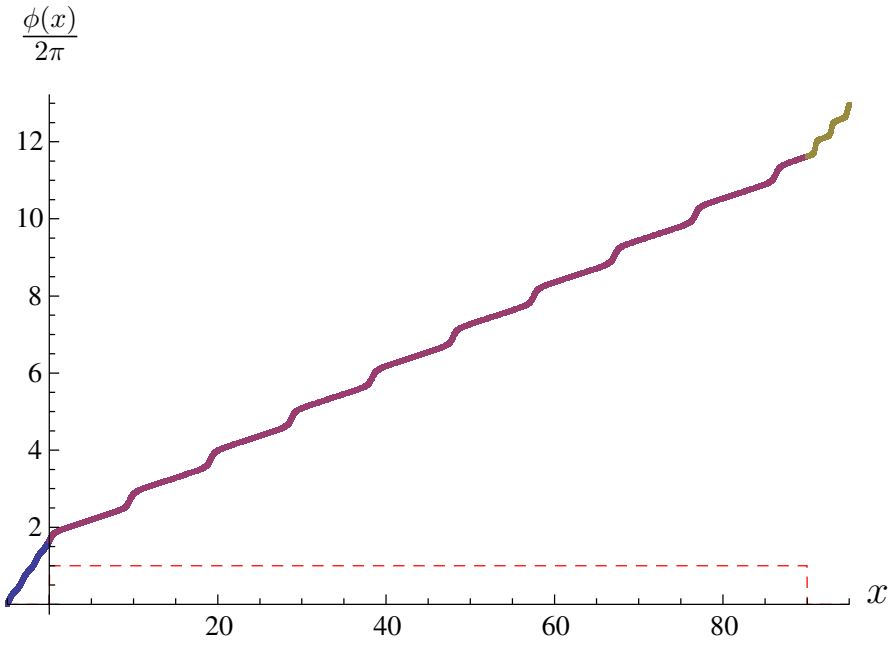

Figure 3.25: Phase plot for soliton train.

is thus different in each region. There is a steep increase in phase at the location of each soliton, just as we observed in Fig. 3.23.

3.3 Valid-Solution Nonlinearity Cut-Off

For a given chemical potential μ, the density $\rho(x)$ becomes complex when the nonlinearity g increases above a cut-off value. This cut-off is seen at small values of μ in the transmission plots. The reasons for the occurrence of the cut-off were discussed in Section 3.2.1.

A plot of the cut-off for the wide-barrier case is shown in Fig. 3.26. The plot shows, for a given value of μ, the lowest g-value at which non-real density is first encountered, to two decimal places.

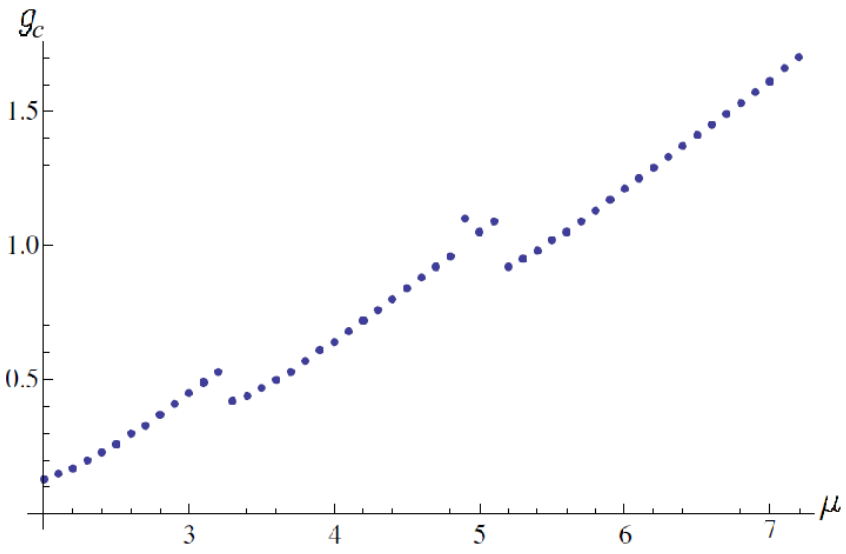

Figure 3.26: Real density cut-off g_c as a function of μ.

We observe that in general, the cut-off nonlinearity g_c increases as μ increases. However, there are jump discontinuities at which the cut-off value decreases slightly. The graph becomes more nearly linear for larger values of μ. We postulate that the graph will become completely linear at very large chemical potential μ, except for isolated jump discontinuities like those seen in Fig. 3.26.

Thus we see that certain combinations of nonlinearity g and chemical potential μ, i.e., those which lie above the cut-off curve in Fig. 3.26, are not allowed. These parameter combinations correspond to regimes in which our assumptions break down. In these regimes, Eq. (1.7) is not a solution to the NLS, and we must seek solutions of a different form.

3.4 Numerical Verifications

We compute the transmission coefficient of the BEC numerically via Eqs. (3.4) and (3.5). Numerical integration of the density is performed using Simpson's 3/8 Rule, which can be found in many reference texts, including [48]. Our algorithm is as follows. Divide the region of integration into N equally-spaced subregions $[x_i, x_{i+1}]$. Then divide each subregion into 4 smaller, equally-spaced regions of width $h = \frac{x_{i+1}-x_i}{4}$. For each of the N subregions, the integral of the density is approximated numerically by

$$\int_{x_i}^{x_{i+1}} \rho(x)\,dx = \frac{3}{8}h[\rho(x_i) + 3\rho(x_i+h) + 3\rho(x_i+2h) + \rho(x_{i+1})] + \mathcal{O}\big(h^5\big)\,. \qquad (3.15)$$

The *Mathematica* code for the transmission computation is given in Appendix C.

3.4.1 Convergence

We divide the integration region into 25 subregions for application of Simpson's Rule. Convergence was analyzed by performing the same calculation with 50 and 100 integration subregions and computing the errors

$$\varepsilon_{n_1,n_2} = \ln\left(\frac{|T_{n_2} - T_{n_1}|}{T_{\text{avg}}}\right), \qquad (3.16)$$

where T_{n_i} denotes the transmission computed with n_i integration subregions, with $n_1, n_2 \in \{25, 50, 100\}$. In Eq. (3.16), T_{avg} denotes the average value of transmission over the plot interval. These errors are $\mathcal{O}(10^{-76})$ or smaller, so we conclude that the method is well-converged. Log plots of the errors are given in Figs. 3.27, 3.28, and 3.29.

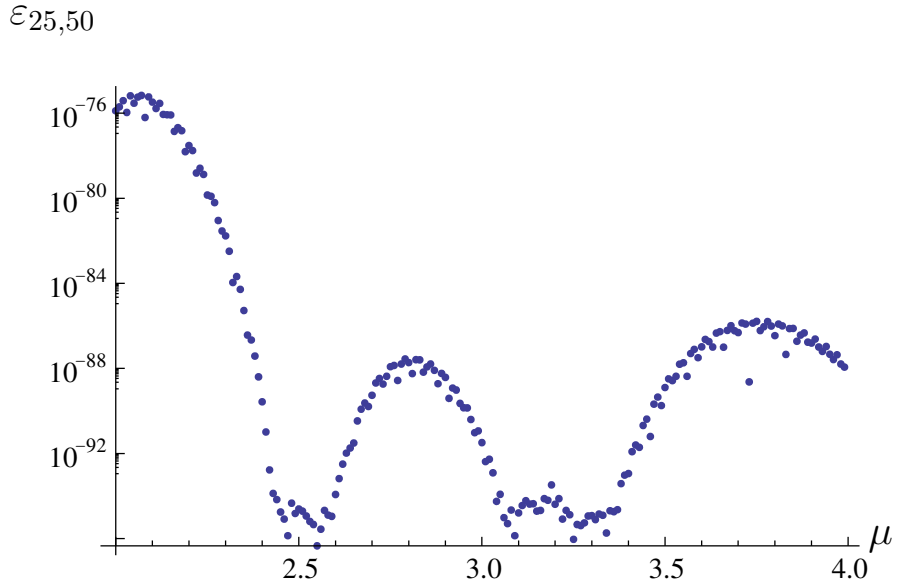

Figure 3.27: Error for numerical integration, 25 and 50 subregions.

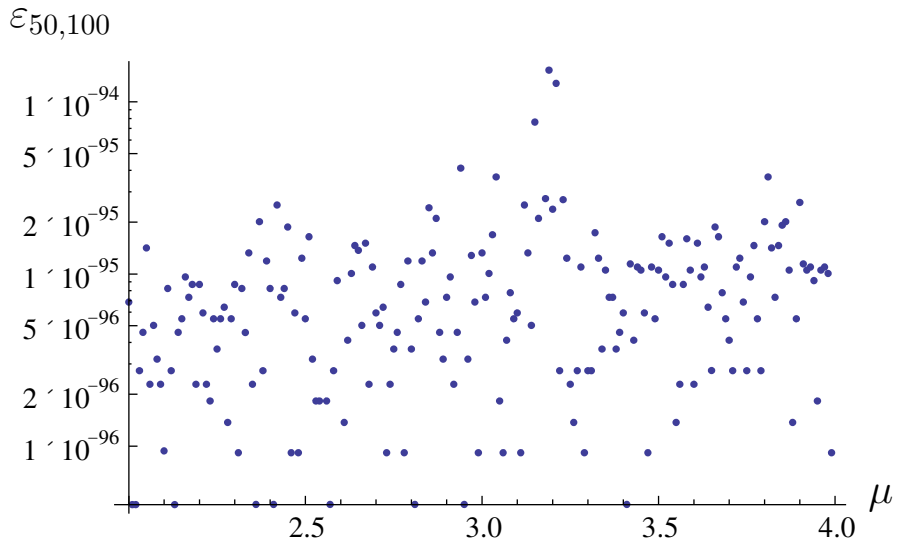

Figure 3.28: Error for numerical integration, 50 and 100 subregions.

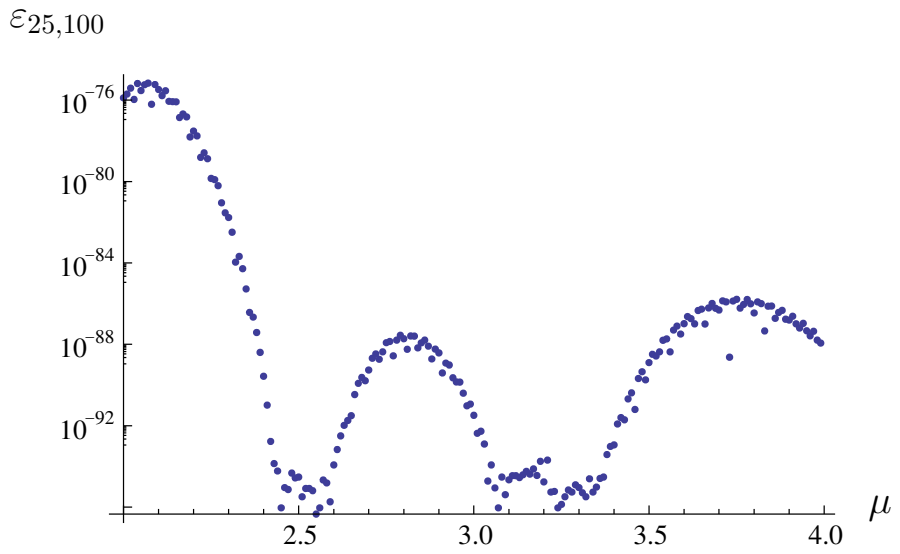

Figure 3.29: Error for numerical integration, 25 and 100 subregions.

3.4.2 Translational invariance

If we shift the potential barrier, keeping the width fixed, so that

$$x_1 \to x_1 + \Delta x,$$
$$x_2 \to x_2 + \Delta x,$$

we expect no change in the solution. This provides another check on the validity of the code. We shift the barrier by Δx and introduce a coordinate transformation in the input density, so that the density in region I becomes

$$\rho_I(x) = A_I \,\mathrm{sn}^2[b_I(x + \Delta x)|m_I] + B_I. \tag{3.17}$$

We keep all input parameters the same and compute the error

$$\varepsilon = \ln\left(\frac{|T - T_s|}{T_{\text{avg}}}\right), \tag{3.18}$$

where T_s is the transmission obtained for the shifted barrier and T_{avg} denotes the average value of transmission over the plot interval. A log plot of the error is given in Fig. 3.30. The maximum error is $\mathcal{O}(10^{-5})$, which is within the chosen numerical tolerance for the code.

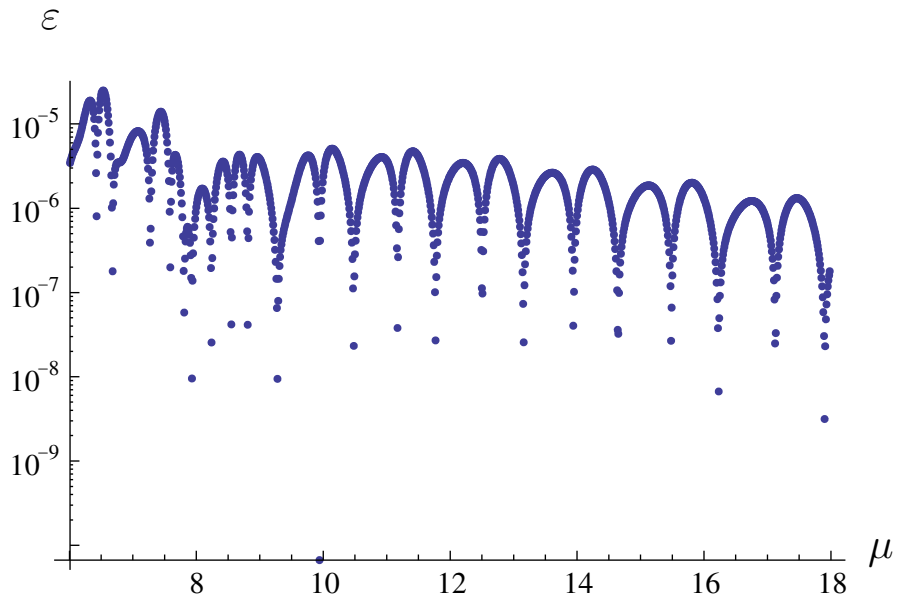

Figure 3.30: Error in transmission due to translational barrier shift.

3.4.3 Limits

Linear limit: We consider the NLS, Eq. (1.4), in the limit that $g \to 0$. In this limit, the solution should reduce to the well-known linear scattering solution, which

is analyzed in many quantum mechanics texts, including [45]. In the linear limit, by Eq. (2.26), we find that $m \to 0$, so that the linear density is

$$\rho(x) = A\sin^2(bx + \delta_0), \tag{3.19}$$

since $B = 0$ in the linear case, as found in Section 2.6. For comparison with the nonlinear case, we define transmission as $\langle\rho_{III}\rangle/\langle\rho_I\rangle$. The integral for $\langle\rho\rangle$ can be evaluated exactly in this case:

$$\langle\rho\rangle = \int_0^{2\pi/b} A\sin^2(bx + \delta_0)\,dx \tag{3.20}$$

$$= \tfrac{1}{2}A. \tag{3.21}$$

Therefore, the transmission is

$$T_\ell = \frac{A_{III}}{A_I}. \tag{3.22}$$

We can compare the value given by Eq. (3.22) to the value T obtained numerically by the code. Transmission plots are shown in Figs. 3.31 and 3.32. A log plot of the error,

$$\varepsilon = \frac{|T - T_\ell|}{T_{\text{avg}}}, \tag{3.23}$$

is given in Fig. 3.33. The maximum value of the error is $\mathcal{O}(10^{-7})$, which is within the numerical tolerance of the code.

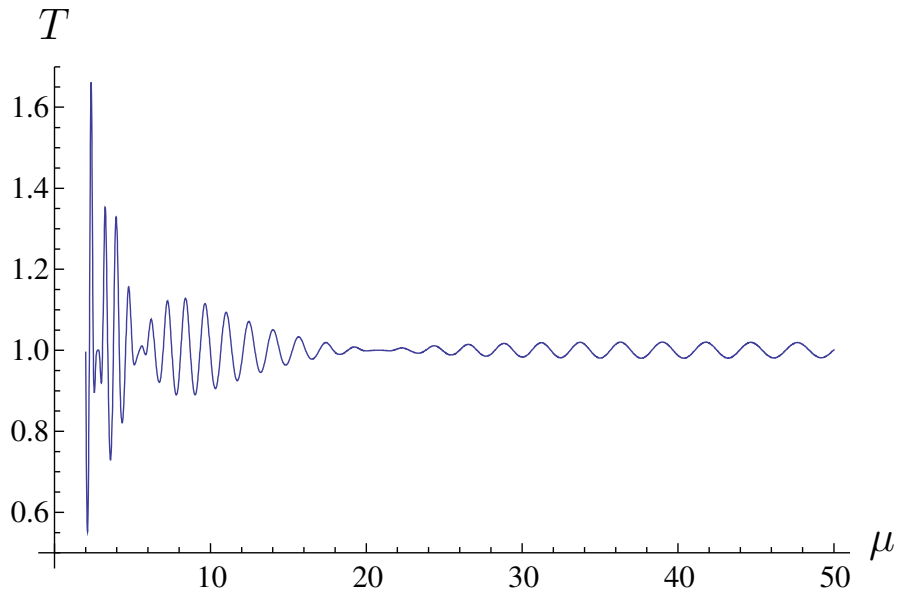

Figure 3.31: Numerically computed transmission for linear limit.

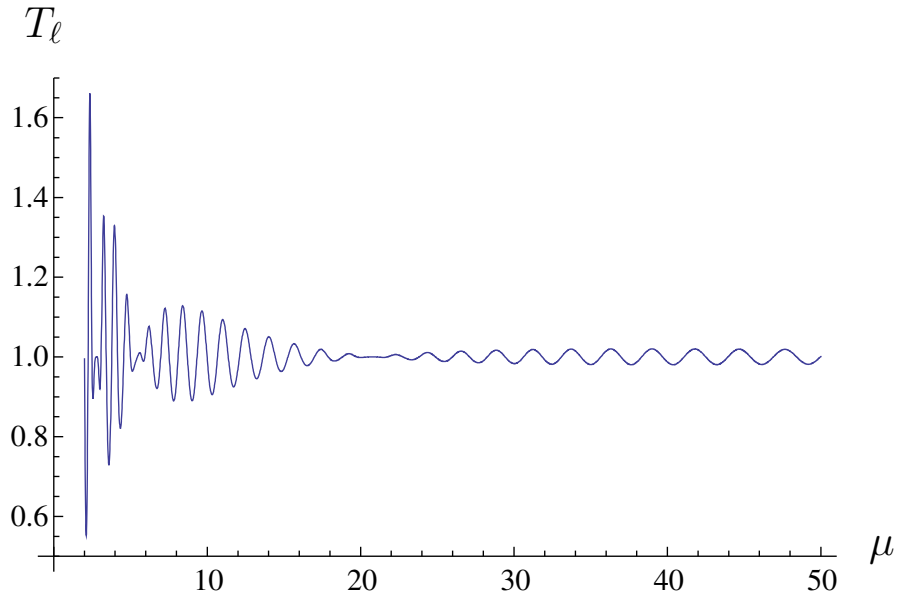

Figure 3.32: Exact linear value of transmission.

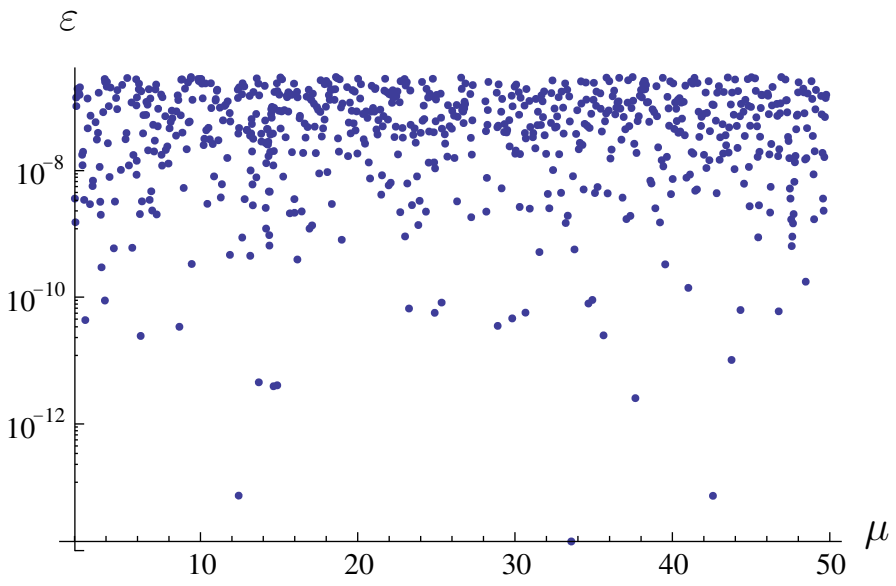

Figure 3.33: Error in transmission for linear limit.

Constant potential limit: Consider the NLS, Eq. (1.4), with potential barrier (1.6), in the limit that $V_0 \to 0$. In this case, boundary conditions are redundant and we expect all parameters to be constant $\forall x$. By setting a "barrier" of $V_0 = 0$ in the code, we can verify that the code gives the correct solution; namely, the amplitude, period, and shifts in the density should not change at the "boundary" locations. Indeed this is the case, providing an additional verification of correctness for the code. A density plot for this case, with a "barrier" of width 5 and height 1, is shown in Fig. 3.34.

Since the density parameters do not change over space, we expect to find a transmission coefficient of 1. We compute and plot the error

$$\varepsilon = \ln\left(\frac{|T-1|}{T_{\text{avg}}}\right), \tag{3.24}$$

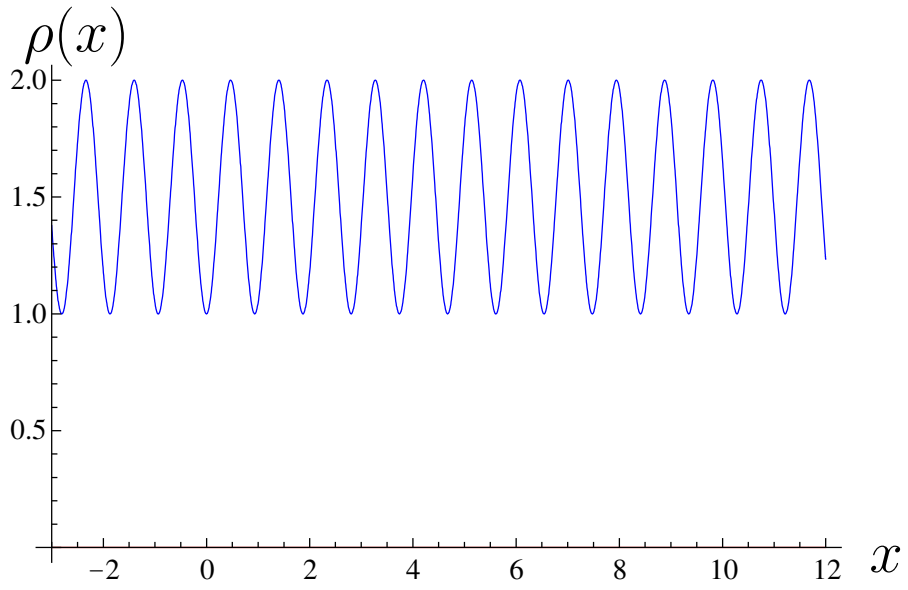

Figure 3.34: Density plot for zero barrier.

where T_{avg} denotes the average value of transmission over the plot interval. A log plot of the error is given in Fig. 3.35.

Alternatively, we can consider a constant nonzero potential: $V(x) = V_c$, $\forall x$ in Eq. (1.4). Again we expect all parameters to be constant $\forall x$. We set a "barrier" of $V_I = V_{II} = V_{III} = 2$ and width 5 in the code and plot the density. The plot is shown in Fig. 3.36.

Again, since the density parameters do not change over space, we expect to find a transmission coefficient of 1. We compute and plot the error

$$\varepsilon = \ln\left(\frac{|T-1|}{T_{\text{avg}}}\right), \tag{3.25}$$

where T_{avg} denotes the average value of transmission over the plot interval. A log

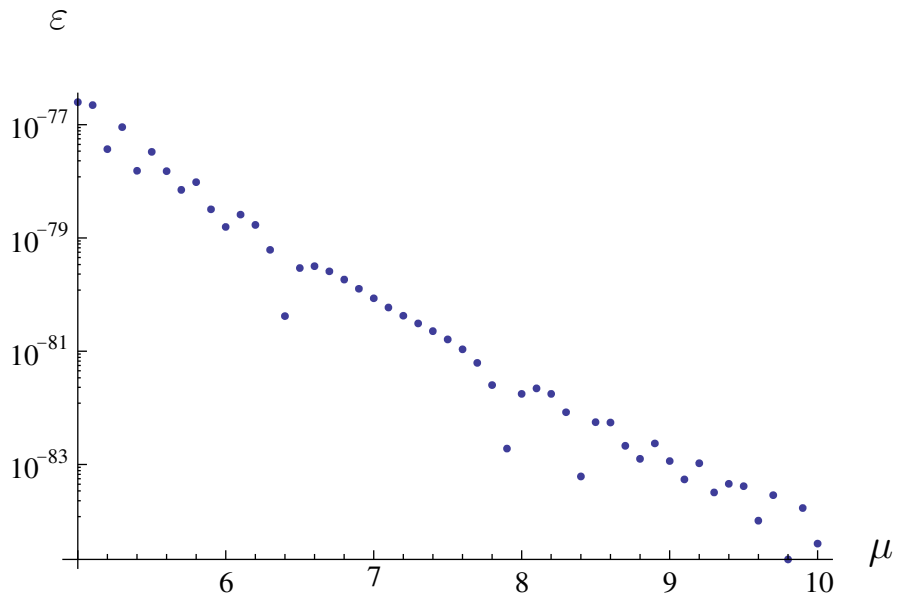

Figure 3.35: Error in transmission for zero barrier.

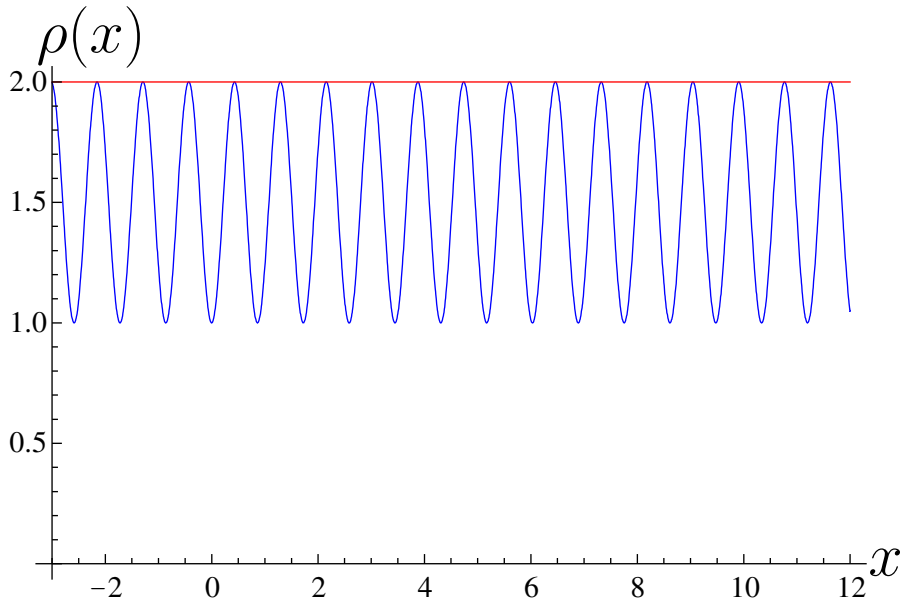

Figure 3.36: Density plot for nonzero flat barrier.

plot of the error is given in Fig. 3.37.

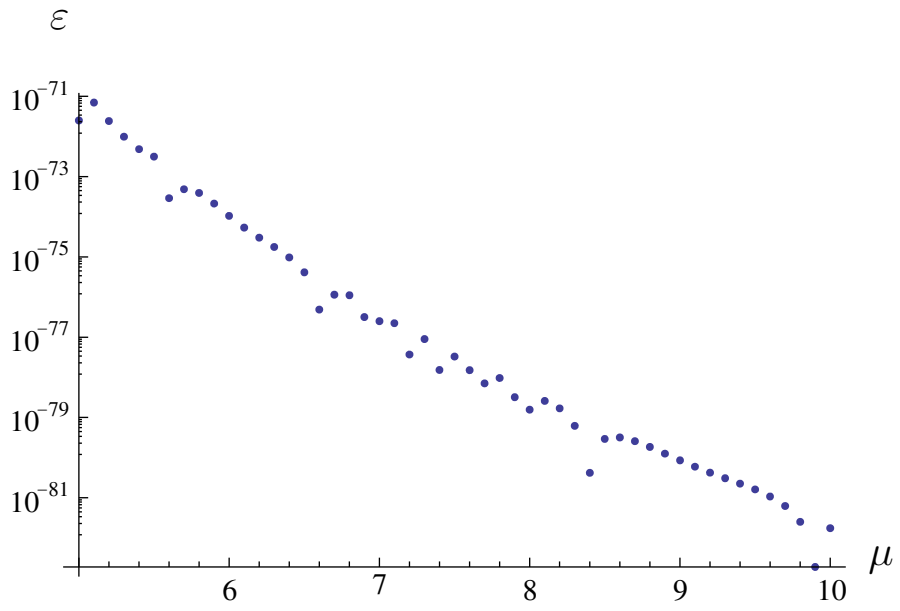

Figure 3.37: Error in transmission for nonzero flat barrier.

Therefore the code gives the expected results for density and transmission in the constant-potential limits.

Thomas-Fermi limit: We consider the limit that $\hbar\partial^2\Psi/\partial x^2 \to 0$ in the unscaled NLS, Eq. (2.1). In this limit, the unscaled NLS becomes

$$\left[g\left|\Psi(x,t)\right|^2 + V(x)\right]\Psi(x,t) = i\hbar\frac{\partial}{\partial t}\Psi(x,t). \tag{3.26}$$

Substituting Eq. (1.7) for the wave function Ψ in (3.26) and rearranging, we obtain

$$g\rho^{3/2} + [V(x) - \hbar\mu]\rho^{1/2} = 0, \tag{3.27}$$

so that either $\rho(x) \equiv 0$, the trivial case, or else

$$\rho(x) = \frac{\hbar\mu - V(x)}{g}, \tag{3.28}$$

when $g \neq 0$. Note that Eq. (3.28) works for any spatially-dependent potential $V(x)$.

Equation (3.28) is the well-known Thomas-Fermi limit [12]. It is relevant when the curvature of Ψ is nearly zero. This can be accomplished either by taking the limit $A/B \to 0$, so that the amplitude of oscillations is small, or by taking the limit $1/b \to \infty$, so that the wavelength of oscillations is large.

Chapter 4

CONCLUSION

We have developed, in full mathematical generality, the complete stationary-state solution set for the nonlinear Schrödinger equation (1.4) when the potential $V(x)$ is piecewise-constant. These solutions were used to numerically compute the transmission coefficient of the BEC. The behavior of the transmission, as well as the transmission resonances, were analyzed in Section 3.2. We found that the nonlinearity inherent in this problem introduces many new features, which are not present in the well-understood linear case. Due to nonlinearity, we cannot break the solution into right- and left-traveling waves and incident and reflected parts, and we cannot say which side of the barrier is the "incident" side. The physical interpretation must therefore be changed for the nonlinear case, and we find that transmission may be greater than unity. Under the new definition, Eq. (3.3), the transmission coefficient no longer represents a probability for some particle to be transmitted through the barrier. Nevertheless, the behavior of this transmission coefficient still presents interesting physics. We defined transmission in Eq. (3.3) to be consistent with an atom laser which impinges on the left side of the barrier. Due to the nonlinearity, we cannot distinguish between input and output parts of the wave function; that is, right- vs. left-traveling waves, and thus the transmission coefficient incorporates both.

We have considered three kinds of plots in our results: density/phase, transmission/resonance, and the slope behavior of the transmission resonances. We found that

in some highly nonlinear cases, localized dark soliton solutions are observed above the potential barrier. We also found that the density solutions are doubly degenerate: there are pairs of solutions which are identical in every respect except for the sign of the phase. The two signs of phase correspond to two different flows in the BEC. We found that the velocity profile of the BEC, which is proportional to $d\phi/dx$, exhibits different behavior for localized and non-localized solutions.

We analyzed the transmission and resonances in detail for several physical regimes. We found that the behavior of transmission for $g \neq 0$ is very different than that observed in the linear case. Also, the behavior of the transmission curve is strongly dependent on the barrier width and the strength of the nonlinearity. A wider barrier is more visible to the BEC, and this leads to very different transmission properties than those observed for narrower barriers. The barrier height V_0 mainly offsets the value of μ for a given g at which the strongly oscillatory behavior of T, seen in the left side of the transmission plots of Section 3.2.1, switches over to the smoother behavior seen in the right-hand regions of the transmission plots. The oscillatory region changes shape as g changes, while the smoother region shifts to the right as g increases. The barrier height determines where this transition occurs.

Bifurcations appear in a transition region in the resonance plot for the wide barrier. The resonances are also more densely packed in this region, which corresponds to a region of near-perfect resonance in the transmission plot. In this region, T is nearly flat at unity, which indicates that the barrier is almost perfectly invisible to the BEC.

A complete characterization of these bifurcations is a problem open for further study. We hypothesize that the three bifurcation points seen in Fig. 3.19 may be used to predict the locations of additional bifurcation points which lie outside the regime displayed in our results.

Numerical analysis was performed to verify the correctness of our code. Convergence was verified for the numerical integration. Several well-known limits were checked, and in all cases, the code yielded the theoretically expected results. Therefore, we can be confident that the code given in Appendix C produces physically and mathematically valid results.

Finally, the theoretical data obtained from our code was connected to the experiment of Engels & Atherton [20]. For certain physical parameters, the BEC exhibits well-localized soliton solutions over the potential barrier. Comparison of the theory with experiment, using the physical parameter values relevant to the experiment, is a matter for future study.

This work represents one step on the long journey toward a completely general theory of nonlinear scattering. The methods discussed in this thesis may be extended to more general piecewise-constant potentials. In addition, the constant-potential solution may possibly, by way of some sophisticated mathematics, be extended to spatially dependent potentials. The BEC scattering problem is a treasure trove of new physical insights waiting to be mined, and many more research opportunities have yet to be explored.

REFERENCES

[1] M. H. Anderson, J. R. Ensher, M. R. Matthews, C. E. Wieman, and E. A. Cornell. Observation of Bose-Einstein condensation in a dilute atomic vapor. *Science*, 269:198–201, 1995.

[2] K. B. Davis, M. O. Mewes, M. R. Andrews, N. J. van Druten, D. S. Durfee, D. M. Kurn, and W. Ketterle. Bose-Einstein condensation in a gas of sodium atoms. *Phys. Rev. Lett.*, 75(22):3969–3973, Nov 1995.

[3] C. C. Bradley, C. A. Sackett, J. J. Tollett, and R. G. Hulet. Evidence of Bose-Einstein condensation in an atomic gas with attractive interactions. *Phys. Rev. Lett.*, 75(9):1687–1690, Aug 1995.

[4] C. C. Bradley, C. A. Sackett, and R. G. Hulet. Analysis of in situ images of Bose-Einstein condensates of lithium. *Phys. Rev. A*, 55(5):3951–3953, May 1997.

[5] T. Maruyama and H. Yabu. Quadrupole oscillations in Bose-Fermi mixtures of ultracold atomic gases made of Yb atoms in the time-dependent Gross-Pitaevskii and Vlasov equations. *Phys. Rev. A*, 80(4):043615, Oct 2009.

[6] F. Schreck, L. Khaykovich, K. L. Corwin, G. Ferrari, T. Bourdel, J. Cubizolles, and C. Salomon. Quasipure Bose-Einstein condensate immersed in a Fermi sea. *Phys. Rev. Lett.*, 87:080403–1–4, 2001.

[7] A. G. Truscott, K. E. Strecker, W. I. McAlexander, G. Partridge, and R. G. Hulet. Observation of Fermi pressure in a gas of trapped atoms. *Science*, 291:2570, 2001.

[8] R. J. Donnelly. *Quantized Vortices in Helium II.* Cambridge University Press, New York, 1991.

[9] M. A. Hoefer and B. Ilan. Theory of two-dimensional oblique dispersive shock waves in supersonic flow of a superfluid. *Phys. Rev. A*, 80(6):061601, Dec 2009.

[10] A. Einstein. Quantentheorie des einatomigen idealen gases. *Sitzungsberichte der Preussischen Akademie der Wissenschaften*, 1:3, 1925.

[11] S. N. Bose. Plancks gesetz und lichtquantenhypothese. *Z. Phys.*, 26:178–181, 1924.

[12] F. Dalfovo, S. Giorgini, L. P. Pitaevskii, and S. Stringari. Theory of Bose-Einstein condensation in trapped gases. *Rev. Mod. Phys.*, 71:463–512, 1999.

[13] W. Ketterle and N. J. van Druten. Bose-Einstein condensation of a finite number of particles trapped in one or three dimensions. *Physical Review A*, 54:656–659, 1996.

[14] A. J. Leggett. Bose-Einstein condensation in the alkali gases: Some fundamental concepts. *Rev. Mod. Phys.*, 73:307–356, 2001.

[15] D. G. Fried, T. C. Killian, L. Willmann, D. Landhuis, S. C. Moss, D. Kleppner, and T. J. Greytak. Bose-Einstein condensation of atomic hydrogen. *Phys. Rev. Lett.*, 81(18):3811–3814, Nov 1998.

[16] G. Modugno, G. Ferrari, G. Roati, R. J. Brecha, A. Simoni, and M. Inguscio. Bose-Einstein condensation of potassium atoms by sympathetic cooling. *Science*, 294(5545):1320–1322, 2001.

[17] Y. Takasu, K. Maki, K. Komori, T. Takano, K. Honda, M. Kumakura, T. Yabuzaki, and Y. Takahashi. Spin-singlet Bose-Einstein condensation of two-electron atoms. *Phys. Rev. Lett.*, 91:040404, 2003.

[18] A. Robert, O. Sirjean, A. Browaeys, J. Poupard, S. Nowak, D. Boiron, C. I. Westbrook, and A. Aspect. A Bose-Einstein condensate of metastable atoms. *Science*, 292(5516):461–464, 2001.

[19] E. G. M. van Kempen, S. J. J. M. F. Kokkelmans, D. J. Heinzen, and B. J. Verhaar. Interisotope determination of ultracold rubidium interactions from three high-precision experiments. *Phys. Rev. Lett.*, 88(9):093201, Feb. 2002.

[20] P. Engels and C. Atherton. Stationary and nonstationary fluid flow of a Bose-Einstein condensate through a penetrable barrier. *Phys. Rev. Lett.*, 99:160405, 2007.

[21] K. Helmerson, D. Hutchinson, K. Burnett, and W. D. Phillips. Atom lasers. *Phys. World*, 12:31–35, 1999.

[22] I Bloch, T. W. Hänsch, and T. Esslinger. Atom laser with a cw output coupler. *Phys. Rev. Lett.*, 82:3008–3011, 2000.

[23] E. W. Hagley, L. Deng, M. Kozuma, J. Wen, K. Helemerson, S. L. Rolston, and W. D. Phillips. A well-collimated quasi-continuous atom laser. *Science*, 283:1706–1709, 1999.

[24] N. Pavloff. Breakdown of superfluidity of an atom laser past an obstacle. *Phys. Rev. A*, 66:013610, 2002.

[25] B. T. Seaman, L. D. Carr, and M. J. Holland. Effect of a potential step or impurity on the Bose-Einstein condensate mean field. *Phys. Rev. A*, 71(3):033609, Mar 2005.

[26] D. Witthaut, S. Mossmann, and H. J. Korsch. Bound and resonance states of the nonlinear Schrödinger equation in simple model systems. *J. Phys. A: Math. Gen.*, 38:1777–1792, 2005.

[27] W. Schwalm. Elliptic functions sn, cn, dn, as trigonometry. University of North Dakota, 2002, http://www.und.nodak.edu/instruct/schwalm/MAA_Presentation_10-02/handout.pdf.

[28] L. D. Carr, M. A. Leung, and W. P. Reinhardt. Dynamics of the Bose-Einstein condensate: quasi-one-dimension and beyond. *J. Phys. B: At. Mol. Opt. Phys.*, 33:3983–4001, 2000.

[29] L. D. Carr, C. W. Clark, and W. P. Reinhardt. Stationary solutions of the nonlinear Schrödinger equation: I. Case of repulsive nonlinearity. *Phys. Rev. A*, 62:063610–1–10, 2000.

[30] K. Rapedius, D. Witthaut, and H. J. Korsch. Analytical study of resonant transport of Bose-Einstein condensates. *Phys. Rev. A*, 73(3):033608, 2006.

[31] L. D. Carr, C. W. Clark, and W. P. Reinhardt. Stationary solutions of the nonlinear Schrödinger equation: II. Case of attractive nonlinearity. *Phys. Rev. A*, 62:063611–1–10, 2000.

[32] L. D. Carr, K. W. Mahmud, and W. P. Reinhardt. Tunable tunneling: An application of stationary states of Bose-Einstein condensates in traps of finite depth. *Phys. Rev. A*, 64:033603, 2001.

[33] H. A. Ishkhanyan and V. P. Krainov. Multiple-scale analysis for resonance reflection by a one-dimensional barrier in the Gross-Pitaevskii problem. *Phys. Rev. A*, 80:045601, 2009.

[34] J. Denschlag, J. E. Simsarian, D. L. Feder, C. W. Clark, L. A. Collins, J. Cubizolles, L. Deng, E. W. Hagley, K. Helmerson, W. P. Reinhardt, S. L. Rolston, B. I. Schneider, and W. D. Phillips. Generating solitons by phase–engineering of a Bose-Einstein condensate. *Science*, 287:97–101, 2000.

[35] A. Weller, J. P. Ronzheimer, C. Gross, J. Esteve, M. K. Oberthaler, D. J. Frantzeskakis, G. Theocharis, and P. G. Kevrekidis. Experimental observation of oscillating and interacting matter wave dark solitons. *Phys. Rev. Lett.*, 101:130401, 2008.

[36] S. Burger, K. Bongs, S. Dettmer, W. Ertmer, K. Sengstock, A. Sanpera, G. V. Shlyapnikov, and M. Lewenstein. Dark solitons in Bose-Einstein condensates. *Phys. Rev. Lett.*, 83:5198–5201, 1999.

[37] L. Khaykovich, F. Schreck, F. Ferrari, T. Bourdel, J. Cubizolles, L. D. Carr, Y. Castin, and C. Salomon. Formation of a matter-wave bright soliton. *Science*, 296:1290–1293, 2002.

[38] W. P. Reinhardt and C. W. Clark. Soliton dynamics in the collisions of Bose-Einstein condensates: An analog of the Josephson effect. *J. Phys. B: At. Mol. Opt. Phys.*, 30:L785, 1997.

[39] S. Stellmer, C. Becker, P. Soltan-Panahi, E. M. Richter, S. Dörscher, M. Baumert, J. Kronjäger, K. Bongs, and K. Sengstock. Collisions of dark solitons in elongated Bose-Einstein condensates. *Phys. Rev. Lett.*, 101:120406, 2008.

[40] M. Abramowitz and I. A. Stegun, editors. *Handbook of Mathematical Functions*. Dover Publications, Inc., Mineola, New York, 1972.

[41] R. Haberman. *Applied Partial Differential Equations*. Prentice Hall, Upper Saddle River, New Jersey, fourth edition, 2003.

[42] F. Bowman. *Introduction to Elliptic Functions, With Applications*. Dover Publications, Inc., Mineola, New York, 1961.

[43] I. S. Gradshteyn and I. M. Ryzhik. *Table of Integrals, Series, and Products*. Academic Press, San Diego, California, sixth edition, 2000.

[44] E. T. Whittaker and G. N. Watson. *A Course of Modern Analysis: An Introduction to the General Theory of Infinite Processes and of Analytic Functions; With an Account of the Principal Transcendental Functions*. Cambridge University Press, Macmillan, New York, 1944.

[45] D. Park. *Introduction to the Quantum Theory*. Dover Publications, Inc., Mineola, New York, third edition, 2005.

[46] K. Gottfried and T. Yan. *Quantum Mechanics: Fundamentals*. Springer, New York, second edition, 2004.

[47] K. E. Strecker, G. B. Partridge, A. G. Truscott, and R. G. Hulet. Formation and propagation of matter wave soliton trains. *Nature*, 417:150–153, 2002.

[48] E. Weisstein. *CRC Concise Encyclopedia of Mathematics*. CRC Press, Boca Raton, Florida, second edition, 2003.

[49] A. Khare, A. Lakshminarayan, and U. Sukhatme. Local identities involving Jacobi elliptic functions. *Pramana Journal of Physics*, 62(6):1201–1229, 2004.

[50] H. E. Fettis. An Explicit Addition Formula for the Inverse Jacobian Elliptic Functions. *Mathematics of Computation*, 26(120):965–967, 1972.

[51] B. Dayton. *Theory of Equations*, chapter Analysis – Elliptic Functions. Oakton, 2002.

APPENDIX A

JACOBI ELLIPTIC FUNCTIONS

There are twelve Jacobi elliptic functions in all: sn, cn, dn, sc, nc, dc, cs, ds, ns [40]. Not all of these are independent. The Jacobi functions are doubly-periodic in the complex plane and they depend on two parameters: an independent variable u and the *elliptic parameter* m. For real parameter m, we may assume $0 \leq m \leq 1$. If m is outside of this range, transformations can be made to write the Jacobi function in terms of functions whose parameter is between 0 and 1 [40]. For $\mathrm{sn}(u|m)$, which appears in the density $\rho(x)$ of the BEC, these transformations are: for $m < 0$,

$$\mathrm{sn}(u|m) = \left(\frac{1}{1-m}\right)^{1/2} \mathrm{sd}\left[(1-m)^{1/2}u \middle| \left(\frac{-m}{1-m}\right)\right], \tag{A.1}$$

and for $m > 1$,

$$\mathrm{sn}(u|m) = m^{-1/2}\,\mathrm{sn}(um^{1/2}|m^{-1}). \tag{A.2}$$

When m lies between zero and unity, the Jacobi functions can be interpreted geometrically as the analog of the hyperbolic and trigonometric functions [27]. In this interpretation, the parameter m corresponds to the eccentricity of the ellipse. For $m = 0$, the Jacobi functions reduce to the trigonometric functions; for $m = 1$, to the hyperbolic functions.

The Jacobi functions are defined as inverse integrals [42], and by the locations of zeros and poles in the complex plane [40]. They may be related to one another by

various identities [49, 50, 51].

APPENDIX B

SUPPLEMENTAL RESULTS

B.1 Linear Independence of Powers of $\mathbf{sn}(u|m)$

Theorem 2. *The functions $sn^p(u|m)$ and $sn^q(u|m)$, $p, q \in \mathbb{Z}$, are linearly independent for $p \neq q$.*

Proof. Compute the Wronskian of the two functions:

$$W[\,\mathrm{sn}^p(u|m), sn^q(u|m)] = \begin{vmatrix} \mathrm{sn}^p(u|m) & \mathrm{sn}^q(u|m) \\ \frac{d}{du}[\,\mathrm{sn}^p(u|m)] & \frac{d}{du}[\,\mathrm{sn}^q(u|m)] \end{vmatrix} \tag{B.1}$$

$$= q\,\mathrm{sn}^p(u|m)\,\mathrm{sn}^{q-1}(u|m)\,\mathrm{cn}(u|m)\,\mathrm{dn}(u|m)$$

$$- p\,\mathrm{sn}^{p-1}(u|m)\,\mathrm{sn}^q(u|m)\,\mathrm{cn}(u|m)\,\mathrm{dn}(u|m) \tag{B.2}$$

$$= (q-p)\,\mathrm{cn}(u|m)\,\mathrm{dn}(u|m)\,\mathrm{sn}^{p+q-1}(u|m). \tag{B.3}$$

The product of Jacobi elliptic functions is nonvanishing except on a set of measure zero; therefore, for $p \neq q$ the functions are linearly independent. QED.

B.2 Linear Independence of Products of Powers of sn

Let

$$f_1(x) = \mathrm{sn}^p(a|m)\,\mathrm{sn}^q(u|m), \tag{B.4}$$

$$f_2(x) = \mathrm{sn}^r(a|m)\,\mathrm{sn}^s(u|m), \tag{B.5}$$

where p, q, r, s are integers, and assume without loss of generality that $a = u$. The case $a = u$ is analyzed in Section B.1. Computing the Wronskian of f_1, f_2, we find

$$W(f_1, f_2) = (r-p)\,\mathrm{cn}(a|m)\,\mathrm{dn}(a|m)\,\mathrm{sn}^{r+p-1}(a|m)\,\mathrm{sn}^{s+q}(u|m) + (q-s)\,\mathrm{cn}(u|m)\,\mathrm{dn}(u|m)\,\mathrm{sn}^{s+q-1}(u|m)\,\mathrm{sn}^{r+p}(a|m). \quad \text{(B.6)}$$

The Wronskian vanishes $\forall a, u$ only when $r = p$ and $q = s$; that is, when f_1 and f_2 are not distinct functions. In all other cases, f_1 and f_2 are linearly independent.

B.3 Continuity of $\partial_x \Psi(x,t)$ at Boundary

Let $\varepsilon > 0$. Integrate $\frac{\partial}{\partial x}\Psi(x,t)$ over a small interval on either side of the boundary a:

$$\int_{a-\varepsilon}^{a+\varepsilon} \frac{\partial}{\partial x}\Psi \, dx. \quad \text{(B.7)}$$

If $\Psi(x,t)$ is discontinuous at $x = a$, then this integral will be nonvanishing.
By the Fundamental Theorem of Calculus, we have

$$\int_{a-\varepsilon}^{a+\varepsilon} \frac{\partial}{\partial x}\Psi \, dx = \Psi(a+\varepsilon, t) - \Psi(a-\varepsilon, t). \quad \text{(B.8)}$$

If we take ε small enough such that the region $[a-\varepsilon, a+\varepsilon]$ does not include another boundary, then the right-hand side of Eq. (B.8) is 0, by continuity of the wave function; see Sec. 2.4. Since the potential $V(x)$ is piecewise-constant, and discontinuous at a finite number of boundaries, it is possible to choose such an ε. Therefore the first spatial derivative of $\Psi(x,t)$ must be continuous at the boundary.

APPENDIX C

MATHEMATICA CODE

The code used for computation of the transmission coefficient and resonances is given below. All comments are in italic.

Preliminary Setup

In order for parameter substitutions to work correctly, we must define things in terms of pure functions. Thus, convention: #1=A, #2=b, #3=x, #4=δ_0, #5=m, #6=B, #7=V(LHS or current region), #8=V(RHS), #9=g, #10=μ, #11=b^2

Clear everything. If the code has been run previously, then "i" is protected (see below); we need to "un-protect" it before we can clear its value.

```
Unprotect[i];
Clear["Global`*"];
```

Since "i" is used to represent the square root of -1, we need to protect it, to prevent it from taking on a numerical value later in the code.

```
Protect[i];
```

Miscellaneous Mathematica commands:

```
Off[General::spell, General::spell1];
```

Define which OS we're working on, because Windows and Linux have very different directory structures!

```
os = "LinuxA";
```

Define a subdirectory of the main transmission plots directory. This subdirectory is where the data output will be stored.

```
subDir = "set36/set36a";
```

Define operating systems. (Don't change these.) "LinuxF" and "WindowsF" refer to machines on Faraday; "LinuxL" and "WindowsL" refer to laptop; "LinuxA" is Alamode, and "WindowsA" is ADIT.

```
os1 = "LinuxF";
os2 = "WindowsF";
os3 = "LinuxL";
os4 = "WindowsL";
os5 = "LinuxA";
os6 = "WindowsA";
```

Define the main directory with the appropriate slash at the end

```
dir1main = "/home/ramiller/MastersWork/BarrierScattering/
TransmissionPlots/";
dir2main = "Y:\PH\Users\ramiller\MastersWork\BarrierScattering
\TransmissionPlots\";
dir3main = "/home/ramiller/AlamodeBackup/MastersWorkBackup/
BarrierScattering/transmissionplots/";
dir4main = "C:\MastersWork\BarrierScattering
TransmissionPlots";
dir5main = "/home/ramiller/Masters/BarrierScattering/
transmissionplots/";
dir6main = "Y:\MA\Users\ramiller\physics_stuff\MastersWorkBackup\
```

```
BarrierScattering\transmissionplots\";
```

Define full directory paths

```
dir1 = StringJoin[dir1main, subDir];
dir2 = StringJoin[dir2main, subDir];
dir3 = StringJoin[dir3main, subDir];
dir4 = StringJoin[dir4main, subDir];
dir5 = StringJoin[dir5main, subDir];
dir6 = StringJoin[dir6main, subDir];
```

Set local working directory

```
If[os == os6, SetDirectory[dir6], If[os == os5, SetDirectory[dir5],
If[os == os4, SetDirectory[dir4], If[os == os3, SetDirectory[dir3],
If[os == os2, SetDirectory[dir2], SetDirectory[dir1]]]]]];
```

Notebook Parameter Definitions

Precision and tolerance:

```
prec = 100;
tol = 10^-5;
disctol = 10^-5;
```

Linear cutoff value. If m or g is smaller than this value, we consider the linear limiting case.

```
linearCutoff = SetPrecision[10^-5, prec];
```

Bounds on μ for the transmission calculation loop.

```
μinit = SetPrecision[5, prec];
μfinal = SetPrecision[25, prec];
```

```
μstep = SetPrecision[1/100, prec];
```

Starting and ending file suffix for transmission and resonance data sets:

```
fileN = 1;
fileNfinal = 100;
```

General Definitions

Most of the functions with "Lin" appended to the name are used only to compute the exact linear case, when $g \equiv 0$. However, in some cases, such as the boundary condition equations, we run into problems with infinities if we use the nonlinear version of the expressions. Thus, in these cases we use the exact linear expression in the limit, when g is smaller than the value "linearCutoff" set above.

Replacement rules for $\sqrt{-1}$:

```
imRepRules = {i^2→-1, i^3→-i, i^4→1}
```

Define variables:

Eigenvalue (where V_0 is the potential in the region of interest).

```
μfNonLin = Chop[1/2 (#11 + (#1 + 3 #6) #9) + #7, tol] &;
μfLin = Chop[1/2 #11 + #7, tol] &;
μf = μfNonLin[#1, #2, #3, #4, #5, #6, #7, #8, #9, #10, #11] &;
```

One-boundary potential (step) function. The potentials V in each region and the boundary x_1 will be defined later.

```
V = If[x < x1, VI, VII];
```

Two-boundary potential (barrier) function:

```
Vb = If[x < x1, VI, If[x < x2, VII, VIII]]
```

Horizontal Scaling, squared:

```
bsqNonLin = Chop[2*(#10 - #7) - (#1 + 3*#6)*#9, tol] &;
bsqLin = Chop[2*(#10 - #7), tol] &;
bsq = bsqNonLin[#1, #2, #3, #4, #5, #6, #7, #8, #9, #10, #11] &;
```

Define real and imaginary parts of b:

```
Reb = If[bsq[#1, #2, #3, #4, #5, #6, #7, #8, #9, #10, #11] > 0, √#11,
SetPrecision[0, prec]] &;
Imb = If[bsq[#1, #2, #3, #4, #5, #6, #7, #8, #9, #10, #11] > 0,
SetPrecision[0, prec], √-#11]] &;
bf = Reb[#1, #2, #3, #4, #5, #6, #7, #8, #9, #10, #11] + i Imb[#1, #2,
#3, #4, #5, #6, #7, #8, #9, #10, #11] &;
```

Phase constant (squared); note that it is real for b pure real or pure imaginary.

```
αsqNonLin = Chop[#6 (#1 + #6) (#11 + #6 #9), tol] &;
αsqLin = Chop[#11 (#6^2 + #1 #6), tol] &;
αsq = αsqNonLin[#1, #2, #3, #4, #5, #6, #7, #8, #9, #10, #11] &;
```

Elliptic parameter. Note that $m \in \mathbb{R}$, by assumption.

** Irrelevant for linear case. However, since m is used as a parameter everywhere, we simply set it to 0 in the linear case (as it must be anyway). Note that for g = 0, mfNonLin = 0, but for g very small, mfNonLin will also be very small but nonzero.*

```
mfNonLin = Chop[(#1*#9)/#11, tol] &;
mfLin = SetPrecision[0, prec] &;
mf = mfNonLin[#1, #2, #3, #4, #5, #6, #7, #8, #9, #10, #11] &;
```

Note that when b is pure real or pure imaginary, then m is real. Specifically, for $A, B \in \mathbb{R}$, m is real. The Jacobi functions are always complex when m is complex, so we must have m real.

Density shift. (Used only when B is allowed to vary.) Since the expression for B blows up as $g \to 0$, we use the exact linear value in the limiting case.

```
BfNonLin = Chop[(2 (#10 - #7) - #11)/(3 #9) - #1/3, tol] &;
BfLin = SetPrecision[0, prec] &;
Bf = If[#5 < linearCutoff, BfLin[#1, #2, #3, #4, #5, #6, #7, #8, #9,
#10, #11] , BfNonLin[#1, #2, #3, #4, #5, #6, #7, #8, #9, #10, #11] ]
&;
```

Jacobi Function Definitions & Identities

For convenience, define Jacobi function shorthand

```
sn[y_, p_] := JacobiSN[y, p];
cn[y_, p_] := JacobiCN[y, p];
dn[y_, p_] := JacobiDN[y, p];
```

Pythagorean-type identities: (note that this will not work alone for powers other than 2, e.g., functions^4.)

```
pythIdentityRepRules = {JacobiCN[a_, b_]^2 → 1 - JacobiSN[a, b]^2,
JacobiDN[a_, b_]^2 → 1 - b JacobiSN[a, b]^2,
JacobiND[a_, b_]^2 → -b JacobiSD[a, b]^2 + 1,
JacobiCD[a_, b_]^2 → (b - 1) JacobiSD[a, b]^2 + 1};
```

We need to take account of the case where $m > 1$ (using reciprocal-parameter transformations) and where $m < 0$ (using negative-parameter transformations). Note that for $A, B \in \mathbb{R}$, m is pure real.

```
repRulesM = {JacobiSN[q_, m_] → If[m > 1, 1/m^1/2 sn[q*m^1/2, 1/m], If[m
< 0, (-m/(1 - m))^1/2 JacobiSD[q (1 - m)^1/2, -m/(1 - m)], JacobiSN[q,
```

```
m]]], JacobiCN[q_, m_] → If[m > 1, dn[q*m^(1/2), 1/m], If[m < 0,
JacobiCD[q (1 - m)^(1/2), -m/(1 - m)], JacobiCN[q, m]]], JacobiDN[q_,
m_] → If[m > 1, JacobiCN[q*m^(1/2), 1/m], If[m < 0, JacobiND[q (1 - m)^(1/2),
-m/(1 - m)], JacobiDN[q, m]]]};
```

Put all the rules together into one big replacement table:

```
jacobiRepRules = Flatten[Append[repRulesM, pythIdentityRepRules]]
```

Re and Im parts of Jacobi functions, used for computing derivatives:

```
Resn = (1/((cn[ Imb[#1, #2, #3, #4, #5, #6, #7, #8, #9, #10, #11] #3 +
Im[#4], 1 - #5] /.  jacobiRepRules)^2 + #5 (sn[ Reb[#1, #2, #3, #4, #5,
#6, #7, #8, #9, #10, #11] #3 +
Re[#4], #5] /.  jacobiRepRules)^2 (sn[ Imb[#1, #2, #3, #4, #5, #6, #7,
#8, #9, #10, #11] #3 +
Im[#4], 1 - #5] /.  jacobiRepRules)^2 /.  jacobiRepRules)^2 sn[ Reb[#1,
#2, #3, #4, #5, #6, #7, #8, #9, #10, #11] #3 +
Re[#4], #5] dn[ Imb[#1, #2, #3, #4, #5, #6, #7, #8, #9, #10, #11] #3 +
Im[#4], 1 - #5] /.  jacobiRepRules) &;
Imsn = (1/((cn[ Imb[#1, #2, #3, #4, #5, #6, #7, #8, #9, #10, #11] #3 +
Im[#4], 1 - #5] /.  jacobiRepRules)^2 + #5 (sn[ Reb[#1, #2, #3, #4, #5,
#6, #7, #8, #9, #10, #11] #3 +
Re[#4], #5] /.  jacobiRepRules)^2 (sn[ Imb[#1, #2, #3, #4, #5, #6, #7,
#8, #9, #10, #11] #3 +
Im[#4], 1 - #5] /.  jacobiRepRules)^2 /.  jacobiRepRules)^2 cn[ Reb[#1,
#2, #3, #4, #5, #6, #7, #8, #9, #10, #11] #3 +
Re[#4], #5] dn[ Reb[#1, #2, #3, #4, #5, #6, #7, #8, #9, #10, #11] #3 +
Re[#4], #5] sn[ Imb[#1, #2, #3, #4, #5, #6, #7, #8, #9, #10, #11] #3 +
```

```
Im[#4], 1 - #5] cn[ Imb[#1, #2, #3, #4, #5, #6, #7, #8, #9, #10, #11]
#3 + Im[#4], 1 - #5] /.  jacobiRepRules) &;
Recn = (1/((cn[ Imb[#1, #2, #3, #4, #5, #6, #7, #8, #9, #10, #11] #3 +
Im[#4], 1 - #5] /.  jacobiRepRules)^2 + #5 (sn[ Reb[#1, #2, #3, #4, #5,
#6, #7, #8, #9, #10, #11] #3 +
Re[#4], #5] /.  jacobiRepRules)^2 (sn[ Imb[#1, #2, #3, #4, #5, #6, #7,
#8, #9, #10, #11] #3 +
Im[#4], 1 - #5] /.  jacobiRepRules)^2 /.  jacobiRepRules)^2 cn[ Reb[#1,
#2, #3, #4, #5, #6, #7, #8, #9, #10, #11] #3 +
Re[#4], #5] cn[ Imb[#1, #2, #3, #4, #5, #6, #7, #8, #9, #10, #11] #3 +
Im[#4], 1 - #5] /.  jacobiRepRules) &;
Imcn = (-1/((cn[ Imb[#1, #2, #3, #4, #5, #6, #7, #8, #9, #10, #11] #3
+
Im[#4], 1 - #5] /.  jacobiRepRules)^2 + #5 (sn[ Reb[#1, #2, #3, #4, #5,
#6, #7, #8, #9, #10, #11] #3 +
Re[#4], #5] /.  jacobiRepRules)^2 (sn[ Imb[#1, #2, #3, #4, #5, #6, #7,
#8, #9, #10, #11] #3 +
Im[#4], 1 - #5] /.  jacobiRepRules)^2 /.  jacobiRepRules)^2 sn[ Reb[#1,
#2, #3, #4, #5, #6, #7, #8, #9, #10, #11] #3 +
Re[#4], #5] dn[ Reb[#1, #2, #3, #4, #5, #6, #7, #8, #9, #10, #11] #3 +
Re[#4], #5] sn[ Imb[#1, #2, #3, #4, #5, #6, #7, #8, #9, #10, #11] #3 +
Im[#4], 1 - #5] dn[ Imb[#1, #2, #3, #4, #5, #6, #7, #8, #9, #10, #11]
#3 + Im[#4], 1 - #5] /.  jacobiRepRules) &;
Redn = (1/((cn[ Imb[#1, #2, #3, #4, #5, #6, #7, #8, #9, #10, #11] #3 +
Im[#4], 1 - #5] /.  jacobiRepRules)^2 + #5 (sn[ Reb[#1, #2, #3, #4, #5,
```

```
#6, #7, #8, #9, #10, #11] #3 +
Re[#4], #5] /.  jacobiRepRules)^2 (sn[ Imb[#1, #2, #3, #4, #5, #6, #7,
#8, #9, #10, #11] #3 +
Im[#4], 1 - #5] /.  jacobiRepRules)^2 /.  jacobiRepRules)^2 dn[ Reb[#1,
#2, #3, #4, #5, #6, #7, #8, #9, #10, #11] #3 +
Re[#4], #5] cn[ Imb[#1, #2, #3, #4, #5, #6, #7, #8, #9, #10, #11] #3 +
Im[#4], 1 - #5] dn[ Imb[#1, #2, #3, #4, #5, #6, #7, #8, #9, #10, #11]
#3 + Im[#4], 1 - #5] /.  jacobiRepRules) &;
Imdn = (-1/((cn[ Imb[#1, #2, #3, #4, #5, #6, #7, #8, #9, #10, #11] #3
+
Im[#4], 1 - #5] /.  jacobiRepRules)^2 + #5 (sn[ Reb[#1, #2, #3, #4, #5,
#6, #7, #8, #9, #10, #11] #3 +
Re[#4], #5] /.  jacobiRepRules)^2 (sn[ Imb[#1, #2, #3, #4, #5, #6, #7,
#8, #9, #10, #11] #3 +
Im[#4], 1 - #5] /.  jacobiRepRules)^2 /.  jacobiRepRules)^2 #5 sn[
Reb[#1, #2, #3, #4, #5, #6, #7, #8, #9, #10, #11] #3 +
Re[#4], #5] cn[ Reb[#1, #2, #3, #4, #5, #6, #7, #8, #9, #10, #11] #3 +
Re[#4], #5] sn[ Imb[#1, #2, #3, #4, #5, #6, #7, #8, #9, #10, #11] #3 +
Im[#4], 1 - #5] /.  jacobiRepRules) &;
```

Horizontal offset, where ρ0 is the value of ρ at the boundary to the left of the region of interest. NOTE: to avoid defining another pure function (#) variable to be added _everywhere_, ρ0 must be substituted using the /. operator. Write one with positive square root and one with negative square root, and take the correct one when specific values are defined. The correct sign of the radical is determined by which one causes ρ to satisfy continuity conditions. The value of x, "#3", should be taken as the boundary

to the left of the region of interest. The argument of the square root is the same for linear and nonlinear cases. There are 2 relevant possibilities.

```
δ0f1NonLin = Chop[InverseJacobiSN[ Chop[Sqrt[(ρ0 - #6)/#1],
tol], #5] - #2*#3, tol] &;
δ0f2NonLin = Chop[InverseJacobiSN[ Chop[-Sqrt[((ρ0 - #6)/#1)],
tol], #5] - #2*#3, tol] &;
δ0f1Lin = Chop[ArcSin[Chop[Sqrt[(ρ0 - #6)/#1],
tol]] - #2*#3, tol] &;
δ0f2Lin = Chop[ArcSin[Chop[-Sqrt[((ρ0 - #6)/#1)],
tol]] - #2*#3, tol] &;
δ0f1 = If[#5 <= linearCutoff, δ0f1Lin[#1, #2, #3, #4, #5, #6,
#7, #8, #9,  #10, #11] , δ0f1NonLin[#1, #2, #3, #4, #5, #6,
#7, #8, #9,  #10, #11]] &;
δ0f2 = If[#5 <= linearCutoff, δ0f2Lin[#1, #2, #3, #4, #5, #6,
#7, #8, #9,  #10, #11] , δ0f2NonLin[#1, #2, #3, #4, #5, #6,
#7, #8, #9,  #10, #11]] &;
```

Density and its first spatial derivative (using complex-argument transformation, and simplifying for real A,B as found in analytical work)

```
Reρ = Chop[((#1/((cn[ Imb[#1, #2, #3, #4, #5, #6, #7, #8, #9,
#10, #11] #3 + Im[#4], 1 - #5] /.  jacobiRepRules)^2 + #5 (sn[
Reb[#1, #2, #3, #4, #5, #6, #7, #8, #9, #10, #11] #3 + Re[#4],
#5] /.  jacobiRepRules)^2 (sn[ Imb[#1, #2, #3, #4, #5, #6, #7, #8,
#9, #10, #11] #3 + Im[#4], 1 - #5] /.  jacobiRepRules)^2)^2 ((sn[
Reb[#1, #2, #3, #4, #5, #6, #7, #8, #9, #10, #11] #3 + Re[#4],
#5] /.  jacobiRepRules)^2 (dn[ Imb[#1, #2, #3, #4, #5, #6, #7, #8,
```

```
#9, #10, #11] #3 + Im[#4], 1 - #5] /.  jacobiRepRules)^2 - (cn[
Reb[#1, #2, #3, #4, #5, #6, #7, #8, #9, #10, #11] #3 + Re[#4],
#5] /.  jacobiRepRules)^2 (dn[ Reb[#1, #2, #3, #4, #5, #6, #7, #8,
#9, #10, #11] #3 + Re[#4], #5] /.  jacobiRepRules)^2 (sn[ Imb[#1,
#2, #3, #4, #5, #6, #7, #8, #9, #10, #11] #3 + Im[#4], 1 - #5] /.
jacobiRepRules)^2 (cn[ Imb[#1, #2, #3, #4, #5, #6, #7, #8, #9, #10,
#11] #3 + Im[#4], 1 - #5] /.  jacobiRepRules)^2)) /.  jacobiRepRules )
+ #6, tol] &;
Imρ NonLin = Chop[((2 #1)/((cn[ Imb[#1, #2, #3, #4, #5, #6, #7, #8,
#9, #10, #11] #3 + Im[#4], 1 - #5] /.  jacobiRepRules)^2 + #5 (sn[
Reb[#1, #2, #3, #4, #5, #6, #7, #8, #9, #10, #11] #3 + Re[#4], #5]
/.  jacobiRepRules)^2 (sn[ Imb[#1, #2, #3, #4, #5, #6, #7, #8, #9, #10,
#11] #3 + Im[#4], 1 - #5] /.  jacobiRepRules)^2)^2) (sn[ Reb[#1, #2, #3,
#4, #5, #6, #7, #8, #9, #10, #11] #3 + Re[#4], #5] cn[ Reb[#1, #2, #3,
#4, #5, #6, #7, #8, #9, #10, #11] #3 + Re[#4], #5] dn[ Reb[#1, #2, #3,
#4, #5, #6, #7, #8, #9, #10, #11] #3 + Re[#4], #5] sn[ Imb[#1, #2, #3,
#4, #5, #6, #7, #8, #9, #10, #11] #3 + Im[#4], 1 - #5] cn[ Imb[#1, #2,
#3, #4, #5, #6, #7, #8, #9, #10, #11] #3 + Im[#4], 1 - #5] dn[ Imb[#1,
#2, #3, #4, #5, #6, #7, #8, #9, #10, #11] #3 + Im[#4], 1 - #5]) /.
jacobiRepRules, tol] &;
Reρ Lin = #1 (Sin[ Reb[#1, #2, #3, #4, #5, #6, #7, #8, #9, #10, #11] #3
+ Re[#4]]^2 Cosh[ Imb[#1, #2, #3, #4, #5, #6, #7, #8, #9, #10, #11] #3
+ Im[#4]]^2 - Cos[Reb[#1, #2, #3, #4, #5, #6, #7, #8, #9, #10, #11] #3
+ Re[#4]]^2 Sinh[ Imb[#1, #2, #3, #4, #5, #6, #7, #8, #9, #10, #11] #3
+ Im[#4]]^2) + #6 &; Imρ Lin = 2 Sin[Reb[#1, #2, #3, #4, #5, #6, #7, #8,
```

```
#9, #10, #11] #3 + Re[#4]] Cos[ Reb[#1, #2, #3, #4, #5, #6, #7, #8,
#9, #10, #11] #3 + Re[#4]] Sinh[ Imb[#1, #2, #3, #4, #5, #6, #7, #8,
#9, #10, #11] #3 + Im[#4]] Cosh[ Imb[#1, #2, #3, #4, #5, #6, #7, #8,
#9, #10, #11] #3 + Im[#4]] &;
```

Linear density:

```
ρLin = ReρLin[#1, #2, #3, #4, #5, #6, #7, #8, #9, #10, #11] + i
ImρLin[#1, #2, #3, #4, #5, #6, #7, #8, #9, #10, #11] &;
```

Derivative of the density:

```
RedρNonLin = Chop[2 #1 ((Reb[#1, #2, #3, #4, #5, #6, #7, #8, #9, #10,
#11]  Resn[#1, #2, #3, #4, #5, #6, #7, #8, #9, #10, #11] - Imb[#1, #2,
#3, #4, #5, #6, #7, #8, #9, #10, #11] Imsn[#1,  #2, #3, #4, #5, #6,
#7, #8, #9, #10, #11]) (Recn[#1, #2, #3, #4, #5,  #6, #7, #8, #9, #10,
#11] Redn[#1, #2, #3, #4, #5, #6, #7, #8, #9,  #10, #11] - Imcn[#1,
#2, #3, #4, #5, #6, #7, #8, #9, #10, #11] Imdn[#1,  #2, #3, #4, #5,
#6, #7, #8, #9, #10, #11]) - (Reb[#1, #2, #3, #4, #5,  #6, #7, #8,
#9, #10, #11] Imsn[#1, #2, #3, #4, #5, #6, #7, #8, #9,  #10, #11] +
Imb[#1, #2, #3, #4, #5, #6, #7, #8, #9, #10, #11] Resn[#1,  #2, #3,
#4, #5, #6, #7, #8, #9, #10, #11]) (Recn[#1, #2, #3, #4, #5,  #6, #7,
#8, #9, #10, #11] Imdn[#1, #2, #3, #4, #5, #6, #7, #8, #9,  #10, #11]
+ Imcn[#1, #2, #3, #4, #5, #6, #7, #8, #9, #10, #11] Redn[#1,  #2, #3,
#4, #5, #6, #7, #8, #9, #10, #11])), tol] &;
ImdρNonLin = Chop[2 #1 ((Reb[#1, #2, #3, #4, #5, #6, #7, #8, #9, #10,
#11]  Imsn[#1, #2, #3, #4, #5, #6, #7, #8, #9, #10, #11] + Imb[#1, #2,
#3, #4, #5, #6, #7, #8, #9, #10, #11] Resn[#1,  #2, #3, #4, #5, #6,
#7, #8, #9, #10, #11]) (Recn[#1, #2, #3, #4, #5,  #6, #7, #8, #9, #10,
```

```
#11] Redn[#1, #2, #3, #4, #5, #6, #7, #8, #9,  #10, #11] - Imcn[#1,
#2, #3, #4, #5, #6, #7, #8, #9, #10, #11] Imdn[#1,  #2, #3, #4, #5,
#6, #7, #8, #9, #10, #11]) + (Reb[#1, #2, #3, #4, #5,  #6, #7, #8,
#9, #10, #11] Resn[#1, #2, #3, #4, #5, #6, #7, #8, #9,  #10, #11] -
Imb[#1, #2, #3, #4, #5, #6, #7, #8, #9, #10, #11] Imsn[#1,  #2, #3,
#4, #5, #6, #7, #8, #9, #10, #11]) (Recn[#1, #2, #3, #4, #5,  #6, #7,
#8, #9, #10, #11] Imdn[#1, #2, #3, #4, #5, #6, #7, #8, #9,  #10, #11]
+ Imcn[#1, #2, #3, #4, #5, #6, #7, #8, #9, #10, #11] Redn[#1,  #2, #3,
#4, #5, #6, #7, #8, #9, #10, #11])), tol] &;
Red$\rho$Lin = 2 #1 (Reb[#1, #2, #3, #4, #5, #6, #7, #8, #9, #10, #11] Sin[
Reb[#1, #2, #3, #4, #5, #6, #7, #8, #9, #10, #11] #3 + Re[#4]] Cos[
Reb[#1, #2, #3, #4, #5, #6, #7, #8, #9, #10, #11] #3 + Re[#4]] (Cosh[
Imb[#1, #2, #3, #4, #5, #6, #7, #8, #9, #10, #11] #3 + Im[#4]]^2 +
Sinh[Imb[#1, #2, #3, #4, #5, #6, #7, #8, #9, #10, #11] #3 + Im[#4]]^2)
- Imb[#1, #2, #3, #4, #5, #6, #7, #8, #9, #10, #11] Sinh[ Imb[#1, #2,
#3, #4, #5, #6, #7, #8, #9, #10, #11] #3 + Im[#4]] Cosh[ Imb[#1, #2,
#3, #4, #5, #6, #7, #8, #9, #10, #11] #3 + Im[#4]] (Cos[ Reb[#1, #2,
#3, #4, #5, #6, #7, #8, #9, #10, #11] #3 + Re[#4]]^2 - Sin[Reb[#1, #2,
#3, #4, #5, #6, #7, #8, #9, #10, #11] #3 + Re[#4]]^2)) &;
Imd$\rho$Lin = 2 #1 (Imb[#1, #2, #3, #4, #5, #6, #7, #8, #9, #10, #11]
Sin[Reb[#1, #2, #3, #4, #5, #6, #7, #8, #9, #10, #11] #3 + Re[#4]]
Cos[ Reb[#1, #2, #3, #4, #5, #6, #7, #8, #9, #10, #11] #3 + Re[#4]]
(Cosh[ Imb[#1, #2, #3, #4, #5, #6, #7, #8, #9, #10, #11] #3 +
Im[#4]]^2 + Sinh[Imb[#1, #2, #3, #4, #5, #6, #7, #8, #9, #10, #11] #3
+ Im[#4]]^2) + Reb[#1, #2, #3, #4, #5, #6, #7, #8, #9, #10, #11] Sinh[
```

```
Imb[#1, #2, #3, #4, #5, #6, #7, #8, #9, #10, #11] #3 + Im[#4]] Cosh[
Imb[#1, #2, #3, #4, #5, #6, #7, #8, #9, #10, #11] #3 + Im[#4]] (Cos[
Reb[#1, #2, #3, #4, #5, #6, #7, #8, #9, #10, #11] #3 + Re[#4]]^2 -
Sin[Reb[#1, #2, #3, #4, #5, #6, #7, #8, #9, #10, #11] #3 + Re[#4]]^2))
&;
dρ = If[#5 <= linearCutoff, RedρLin[#1, #2, #3, #4, #5, #6, #7, #8,
#9, #10, #11] + i ImdρLin[#1, #2, #3, #4, #5, #6, #7, #8, #9, #10,
#11], RedρNonLin[#1, #2, #3, #4, #5, #6, #7, #8, #9, #10, #11] + i
ImdρNonLin[#1, #2, #3, #4, #5, #6, #7, #8, #9, #10, #11]] &;
```

Equations (from boundary conditions) where V1 is V on the RHS of the boundary of interest, ρ0 and α0s represent ρ and α^2 respectively on the LHS, and A and B are the values on the RHS of the boundary of interest. V0 is the potential on the LHS of the boundary of interest. xb is the boundary of interest. We do not define the equations in terms of pure functions; rather, parameters such as μ, V1, and ρ0 will be substituted later using the /. operator. In the linear case, the equations can be solved analytically for A and B. We use these in the limit, since the solutions of the nonlinear versions result in infinities in Mathematica.

In the linear case, if the boundary happens to fall at a point where the density is zero, Mathematica can have problems with infinities. Therefore we simplify the expression for A explicitly in the linear case using the explicit formula for ρ. As a result, we must pass as parameters A,b, m, and δ_0 on the LHS of the boundary of interest.

```
eq1 = α0s == B (A + B) (2 μ - 2 V1 - A g - 2 B g);
eq2 = dρ0^2 == -4 (B - ρ0) (A + B - ρ0) (2 μ - 2 V1 - A g - 2 B g - ρ0
g);
```

```
solnNonLin = {A, B} /.  Solve[{eq1, eq2}, {A, B}];
linearSolnVals = {(AL bL^2 Cos[bL xb + δ0L]^2)/( 2 (μ - V1)) + ρ0, 0};
```

Since there are 6 nonlinear solutions, we define a list of six linear solutions (all the same, of course) for consistency with existing nonlinear code.

```
solnLin = {};
For[j = 1, j <= 6, ++j, AppendTo[solnLin, linearSolnVals]];
```

We take the linear expression in the limit:

```
Set[soln, If[Abs[mLHS] <= mLinear, solnLin, solnNonLin]];
```

Period of the density, using Jacobi's reciprocal transformation when $m > 1$. If b is imaginary, we must use the imaginary period, i K(1-m).

```
realperiod = If[#5 < 1, Chop[(2 EllipticK[#5])/#2, tol], Chop[(2
EllipticK[1/#5])/(#2 #5^(1/2)), tol]] &;
imperiod = 2 i Chop[EllipticK[1 - #5]/#2, tol] &;
period = If[Abs[Imb[#1, #2, #3, #4, #5, #6, #7, #8, #9, #10, #11]]
< tol, realperiod[#1, #2, #3, #4, #5, #6, #7, #8, #9, #10, #11],
imperiod[#1, #2, #3, #4, #5, #6, #7, #8, #9, #10, #11]] &;
```

Physical Parameter Definitions

Define global parameters, such as nonlinearity, and known parameters in region I

Define parameters on LHS of first boundary (region I)

**Make sure that $A_I + B_I >= 0$*

```
AI = SetPrecision[1, prec];
BI = SetPrecision[1, prec];
δ0I = SetPrecision[0, prec];
```

Boundary locations:

```
x1 = SetPrecision[ 2, prec];
x2 = SetPrecision[7, prec];
```

Potentials in regions I, II, III for barrier.

```
VI = SetPrecision[0, prec];
VII = SetPrecision[1, prec];
VIII = SetPrecision[0, prec];
```

Transmission Calculation

Numerically calculate the transmission coefficient and find resonances

Initialize data arrays:

```
transArr = {};
resArr = {};
```

Tolerance for resonances:

```
oneTol = SetPrecision[10^-4, prec];
```

Clear values that will be computed in transmission loop:

```
Clear[bI, AII, bII, δ0II, mII, BII, AIII, bIII, δ0III,  mIII, BIII,
μ0, x];
```

Number of subdivisions of integration region:

```
NumBoxes=25;
```

(This subdivides the region for Simpson's Rule. Each of these subdivisions will be further split into 4 equidistant points and Simpson's 3/8 Rule applied.)

Define substrings used in filenames:

```
transFileString = "transmission_";
resFileString = "resonance_";
```

Loop parameters:

```
glin = SetPrecision[10^-5, prec];
gstep = SetPrecision[1/100, prec];
ginit = SetPrecision[glin + (fileN - 1)*gstep, prec];
gfinal = SetPrecision[glin + (fileNfinal - 1)*gstep, prec];
```

Loop to compute the transmission coefficient, and export transmission data and resonance data to files.

```
For[g0=ginit,g0<=gfinal,g0=g0+gstep,
```

Initialize arrays for transmission and resonance data

```
transArr={};
resArr={};
```

Linear limits

```
If[g0<=mLinear,Set[BI,SetPrecision[0,prec]],Set[BI,
SetPrecision[1,prec]]];
```

Index for plot data files

```
μNum=1;
```

For each μ, compute the transmission...

```
For[μ0=μinit,μ0<=μfinal,μ0=μ0+μstep,
```

Initialize arrays for parameters, to be used later in the calculation

```
paramArr={};
generalParams={};
paramsI={};
paramsII={};
```

```
paramsIII={};
newParamsII={};
newParamsIII={};
```

Variables to hold values for numerical transmission integrals

```
intIII=SetPrecision[0,prec];
δxIII=SetPrecision[0,prec];
```

Put known parameters into arrays

```
generalParams=μ->μ0,g->g0;
paramsI=Flatten[Append[{A->AI,B->BI,δ0->δ0I,Vv->VI},generalParams]];
paramsII=Flatten[Append[{Vv->VII,V0->VI,V1->VII,xb->x1},generalParams]];
paramsIII=Flatten[Append[{xb->x2,A->AIII,B->BIII,b->bIII,V0->VII,
VI->VIII,δ0->δ0III,α->αIII,m->mIII},generalParams]];
```

Calculate remaining parameters in region I...

```
bIsquared=Chop[SetPrecision[bsq[AI,b,x,δ0,mI,BI,VI,VII,g0,μ0,bs],
prec],tol];
bI=Chop[SetPrecision[bf[AI,b,x,δ0I,mI,BI,VI,VII,g0,μ0,bIsquared],
prec],tol];
mI=Chop[SetPrecision[mf[AI,bI,x,δ0I,m,BI,VI,VII,g0,μ0,bIsquared],
prec],tol];
```

...and add their values to the array

```
paramsI=Flatten[Append[paramsI,m->mI]];
```

$\alpha_I{}^2$

```
αIs=Chop[SetPrecision[αsq[AI,bI,x,δ0I,mI,BI,VI,VII,g0,μ0,bIsquared],
prec],tol];
paramsI=Flatten[Append[paramsI,α0s->αIs]];
```

```
(*Density and its derivative in region I*)
ρI=Chop[SetPrecision[ρ[AI,bI,#3,δ0I,mI,BI,VI,VII,g0,μ0,bIsquared],
prec],tol]&;
dρI=Chop[SetPrecision[dρ[AI,bI,#3,δ0I,mI,BI,VI,VII,g0,μ0,bIsquared],
prec],tol]&;
(*Region I density and derivative at the first boundary, for use in equations*)
ρL=ρI[AI,bI,x1,δ0I,mI,BI,VI,VII,g0,μ0,bIsquared];
dρL=dρI[AI,bI,x1,δ0I,mI,BI,VI,VII,g0,μ0,bIsquared];
(*Parameter values needed for region II solutions*)
newParamsII={ρ0->ρL,dρ0->dρL,α0s->αIs,AL->AI,bL->bI,δ0L->δ0I,mLHS->mI};
paramsII=Flatten[Append[paramsII,newParamsII]];
(*Loop parameters*)
hasImPart=True;
index=1;
(*Loop through all algebraic solutions until a physically valid solution (real) is found*)
While[index<=6&&hasImPart,
AII=Chop[SetPrecision[Part[(soln/.paramsII),index,1]/.paramsII,
prec],tol];
BII=Chop[SetPrecision[Part[(soln/.paramsII),index,2]/.paramsII,
prec],tol];
If[Abs[Im[AII]]>tol||Abs[Im[BII]]>tol,hasImPart=True,hasImPart=False];
If[hasImPart,++index];
];
(*If no real solutions are found, print a message and abort*)
If[hasImPart,Print["Complex density solution encountered in region
```

```
II."]];
If[hasImPart,Print["AII = ",N[AII,5]]];
If[hasImPart,Print["BII = ",N[BII,5]]];
If[hasImPart,Print["g = ", N[g0,5]]];
If[hasImPart,Print["μ = ",N[μ0,5]]];
If[hasImPart,Abort[]];
```

Add known region II parameters to array

```
paramsII=Flatten[Append[paramsII,{A->AII,B->BII}]];
```

Calculate remaining parameters in region II...

```
bIIsquared=Chop[SetPrecision[bsq[AII,bII,x,δ0II,mII,BII,VII,VIII,
g0,μ0,bIIs],prec],tol];
bII=Chop[SetPrecision[bf[AII,bII,x,δ0II,mII,BII,VII,VIII,g0,μ0,
bIIsquared],prec],tol];
bII=bII/.i->I;
```

...and add their values to the array

```
paramsII=Flatten[Append[paramsII,b->bII]];
```

α_{II}^2

```
αIIs=Chop[SetPrecision[αsq[AII,bII,x,δ0II,mII,BII,VII,VIII,g0,
μ0,bIIsquared],prec],tol];
mII=Chop[SetPrecision[mf[AII,bII,x,δ0II,m,BII,VII,VIII,g0,μ0,
bIIsquared],prec],tol];
paramsII=Flatten[Append[paramsII,m->mII]];
δ0II=Chop[SetPrecision[δ0f1[AII,bII,x1,δ,mII,BII,VII,VIII,g0,μ0,
bIIsquared]/.paramsII,prec],tol];
paramsII=Flatten[Append[paramsII,δ0->δ0II]];
```

Density and its derivative in region II

```
ρII=Chop[SetPrecision[ρ[AII,bII,#3,δ0II,mII,BII,VII,VIII,g0,μ0,
bIIsquared],prec],tol]&;
dρII=Chop[SetPrecision[dρ[AII,bII,#3,δ0II,mII,BII,VII,VIII,g0,
μ0,bIIsquared],prec],tol]&;
```

Check boundary conditions

```
ρdisc1=Chop[Abs[ρII[AII,bII,x1,δ0II,mII,BII,VII,VIII,g0,μ0,
bIIsquared]-ρI[AI,bI,x1,δ0I,mI,BI,VI,VII,g0,μ0,bIsquared]],tol];
dρdisc1=Chop[Abs[dρII[AII,bII,x1,δ0II,mII,BII,VII,VIII,g0,μ0,
bIIsquared]-dρI[AI,bI,x1,δ0I,mI,BI,VI,VII,g0,μ0,bIsquared]],tol];
```

If the derivative is discontinuous, choose the other sign of the square root in the expression for δ_0

```
If[Abs[dρdisc1]<disctol,δ0II=Chop[SetPrecision[δ0f1[AII,bII,x1,δ
,mII,BII,VII,VIII,g0,μ0,bIIsquared]/.paramsII,prec],tol],
δ0II=Chop[SetPrecision[δ0f2[AII,bII,x1,δ,mII,BII,VII,VIII,g0,μ0,
bIIsquared]/.paramsII,prec],tol]];
```

Add δ_0 *to the array*

```
paramsII=Flatten[Append[paramsII,δ0->δ0II]];
```

Redefine density and derivative, using the (possibly) new value of δ_{0II}

```
ρII=Chop[SetPrecision[ρ[AII,bII,#3,δ0II,mII,BII,VII,VIII,g0,μ0,
bIIsquared],prec],tol]&;
dρII=Chop[SetPrecision[dρ[AII,bII,#3,δ0II,mII,BII,VII,VIII,g0,μ0,
bIIsquared],prec],tol]&;
```

Check boundary conditions with new values

```
ρdisc1=Chop[Abs[ρII[AII,bII,x1,δ0II,mII,BII,VII,VIII,g0,μ0,
```

```
bIIsquared]-ρI[AI,bI,x1,δ0I,mI,BI,VI,VII,g0,μ0,bIsquared]],tol];
dρdisc1=Chop[Abs[dρII[AII,bII,x1,δ0II,mII,BII,VII,VIII,g0,
μ0,bIIsquared]-dρI[AI,bI,x1,δ0I,mI,BI,VI,VII,g0,μ0,bIsquared]],tol];
(*If the derivative is still discontinuous (it shouldn't be!), print a message.*)
If[Abs[dρdisc1]>disctol,Print["Derivative discontinuity encountered
at x1"]];
If[Abs[dρdisc1]>disctol,Print["Discontinuity of ",dρdisc1]];
If[Abs[dρdisc1]>disctol,Print["g = ", N[g0,5]]];
If[Abs[dρdisc1]>disctol,Print["μ = ",N[μ0,5]]];
(*Add physical parameters to Region III array*)
paramsIII=Flatten[Append[{xb->x2,Vv->VIII,V0->VII,V1->VIII},
generalParams]];
(*Region II density and derivative at the second boundary, for use in equations*)
ρLL=ρII[AII,bII,x2,δ0II,mII,BII,VII,VIII,g0,μ0,bIIsquared];
dρLL=dρII[AII,bII,x2,δ0II,mII,BII,VII,VIII,g0,μ0,bIIsquared];
(*Parameter values needed for region III solutions*)
newParamsIII={ρ0->ρLL,dρ0->dρLL,α0s->αIIs,AL->AII,bL->bII,
δ0L->δ0II,mLHS->mII};
paramsIII=Flatten[Append[paramsIII,newParamsIII]];
(*Loop parameters*)
hasImPart2=True;
index2=1;
(*Loop through all algebraic solutions until a physically valid solution (real) is found*)
While[index2<=6&&hasImPart2,
AIII=Chop[SetPrecision[Part[(soln/.paramsIII),index2,1]
```

```
/.paramsIII,prec],tol];
BIII=Chop[SetPrecision[Part[(soln/.paramsIII),index2,2]
/.paramsIII,prec],tol];
If[Abs[Im[AIII]]>tol||Abs[Im[BIII]]>tol,hasImPart2=True,
hasImPart2=False];
If[hasImPart2,++index2];
];
```

If no real solutions are found, print a message and abort

```
If[hasImPart2,Print["Complex density solution encountered in region
III."]];
If[hasImPart2,Print["AIII = ",N[AIII,5]]];
If[hasImPart2,Print["BIII = ",N[BIII,5]]];
If[hasImPart2,Print["g = ", N[g0,5]]];
If[hasImPart2,Print["μ = ",N[μ0,5]]];
If[hasImPart2,Abort[]];
```

Add known region III parameters to array

```
paramsIII=Flatten[Append[paramsIII,{A->AIII,B->BIII}]];
```

Calculate remaining parameters in region III...

```
bIIIsquared=Chop[SetPrecision[bsq[AIII,bIII,x,δ0III,mIII,BIII,
VIII,VIII,g0,μ0,bIIIs],prec],tol];
bIII=Chop[SetPrecision[bf[AIII,b,x,δ0III,mIII,BIII,VIII,VIII,
g0,μ0,bIIIsquared],prec],tol];
bIII=bIII/.i->I;
```

...and add them to the array

```
paramsIII=Flatten[Append[paramsIII,b->bIII]];
```

α^2_{III}

```
αIIIs=Chop[SetPrecision[αsq[AIII,bIII,x,δ0III,mIII,BIII,
VIII,VIII,g0,μ0,bIIIsquared],prec],tol];
mIII=Chop[SetPrecision[mf[AIII,bIII,x,δ0III,m,BIII,VIII,
VIII,g0,μ0,bIIIsquared],prec],tol];
paramsIII=Flatten[Append[paramsIII,m->mIII]];
δ0III=Chop[SetPrecision[δ0f1[AIII,bIII,x2,δ,mIII,BIII,
VIII,VIII,g0,μ0,bIIIsquared]/.paramsIII,prec],tol];
paramsIII=Flatten[Append[paramsIII,δ0->δ0III]];
```

Density and its derivative in region III

```
ρIII=Chop[SetPrecision[ρ[AIII,bIII,#3,δ0III,mIII,BIII,VIII,
VIII,g0,μ0,bIIIsquared],prec],tol]&;
dρIII=Chop[SetPrecision[dρ[AIII,bIII,#3,δ0III,mIII,BIII,VIII,
VIII,g0,μ0,bIIIsquared],prec],tol]&;
```

Check boundary conditions

```
ρdisc2=Chop[Abs[ρIII[AIII,bIII,x2,δ0III,mIII,BIII,VIII,VIII,
g0,μ0,bIIIsquared]-ρII[AII,bII,x2,δ0II,mII,BII,VII,VIII,g0,
μ0,bIIsquared]],tol];
dρdisc2=Chop[Abs[dρIII[AIII,bIII,x2,δ0III,mIII,BIII,VIII,VIII,
g0,μ0,bIIIsquared]-dρII[AII,bII,x2,δ0II,mII,BII,VII,VIII,g0,
μ0,bIIsquared]],tol];
```

If the derivative is discontinuous, choose the other sign of the square root in the expression for δ_0

```
If[Abs[dρdisc2]<disctol,δ0III=Chop[SetPrecision[δ0f1[AIII,bIII,x2,δ,
mIII,BIII,VIII,VIII,g0,μ0,bIIIsquared]/.paramsIII,prec],tol],
```

```
δ0III=Chop[SetPrecision[δ0f2[AIII,bIII,x2,δ,mIII,BIII,VIII,VIII,
g0,μ0,bIIIsquared]/.paramsIII,prec],tol]];
```

Add δ_0 to the array

```
paramsIII=Flatten[Append[paramsIII,δ0->δ0III]];
```

Redefine density and derivative, using the (possibly) new value of δ_{0III}

```
ρIII=Chop[SetPrecision[ρ[AIII, bIII,#3,δ0III,mIII,BIII,VIII,VIII,
g0,μ0,bIIIsquared],prec],tol]&;
dρIII=Chop[SetPrecision[dρ[AIII,bIII,#3,δ0III,mIII,BIII,VIII,VIII
,g0,μ0,bIIIsquared],prec],tol]&;
```

Check boundary conditions with new values

```
ρdisc2=Chop[Abs[ρIII[AIII,bIII,x2,δ0III,mIII,BIII,VIII,VIII,g0,
μ0,bIIIsquared]-ρII[AII,bII,x2,δ0II,mII,BII,VII,VIII,g0,μ0,
bIIsquared]],tol];
dρdisc2=Chop[Abs[dρIII[AIII,bIII,x2,δ0III,mIII,BIII,VIII,VIII,g0,
μ0,bIIIsquared]-dρII[AII,bII,x2,δ0II,mII,BII,VII,VIII,g0,μ0,
bIIsquared]],tol];
```

If the derivative is still discontinuous (it shouldn't be!), print a message.

```
If[Abs[dρdisc2]>disctol,Print["Derivative discontinuity encountered
at x2"]];
If[Abs[dρdisc2]>disctol,Print["Discontinuity of ",dρdisc2]];
If[Abs[dρdisc2]>disctol,Print["g = ", N[g0,5]]];
If[Abs[dρdisc2]>disctol,Print["μ = ",N[μ0,5]]];
```

Export coefficients for plot

```
paramArr=Flatten[Append[paramArr,{AI,bI,δ0I,mI,BI,AII,bII,δ0II
,mII,BII,AIII,bIII,δ0III,mIII,BIII}]];
```

Calculate average density in region I.

```
ρavgI=1/period[AI,bI,x,δ0I,mI,BI,VI,VII,g0,μ0,bIsquared]*
Integrate[ρI[AI,bI,x,δ0I,mI,BI,VI,VII,g0,μ0,bIsquared],
{x,x1-period[AI,bI,x,δ0I,mI,BI,VI,VII,g0,μ0,bIsquared],x1}];
```

Simpson's Rule interval width for numerical integration

```
δxIII=1/numBoxes*period[AIII,bIII,x,δ0III,mIII,BIII,VIII,VIII,
g0,μ0,bIIIsquared];
```

Numerically integrate density in region III, over one period, using Simpson's 3/8 Rule. Note: NIntegrate leads to infinities.

```
For[j=0,j<numBoxes,++j,
xj=x2+#1 δxIII &;
δj=(xj[j+1]-xj[j])/3;
intIII=intIII+SetPrecision[3/8 δj (ρIII[AIII,bIII,xj[j],δ0III,mIII,
BIII,VIII,VIII,g0,μ0,bIIIsquared]+3 ρIII[AIII,bIII,xj[j]+δj,δ0III,
mIII,BIII,VIII,VIII,g0,μ0,bIIIsquared]+3 ρIII[AIII,bIII,
xj[j]+2*δj,δ0III,mIII,BIII,VIII,VIII,g0,μ0,bIIIsquared]
+ρIII[AIII,bIII,xj[j]+3*δj,δ0III,mIII,BIII,VIII,VIII,g0,μ0,
bIIIsquared]),prec];
];
```

Average density in region III

```
ρavgIII=SetPrecision[1/period[AIII,bIII,x,δ0III,mIII,BIII,VIII,VIII,
g0,μ0,bIIIsquared]*intIII,prec];
```

Transmission!

```
Tcoeff=SetPrecision[ρavgIII/ρavgI,prec];
```

Since densities are real, transmission also must be real. If not, print a message and

abort.

```
If[Abs[Im[Tcoeff]]>tol,Print["Complex transmission encountered.
Aborting."]];
If[Abs[Im[Tcoeff]]>tol,Print["g = ", N[g0,5]]];
If[Abs[Im[Tcoeff]]>tol,Print["μ = ",N[μ0,5]]];
If[Abs[Im[Tcoeff]]>tol,Print["mI = ",N[mI,5]]];
If[Abs[Im[Tcoeff]]>tol,Print["mIII = ",N[mIII,5]]];
If[Abs[Im[Tcoeff]]>tol,Abort[]];
```

Add (μ,T) pair to transmission array

```
transArr=Append[transArr,{μ0,Tcoeff}];
```

Check for resonance. If there is a resonance, add (μ,g) pair to resonance array.

```
If[Abs[Tcoeff-1]<=oneTol,AppendTo[resArr,{μ0,g0}]];
```

Export coefficient data for use in plotting density, if desired. See DensityPlotFrom-TransmissionNotebook_Nov11_2009.nb

```
plotFilename=StringJoin["rhoCoeffs_",ToString[fileN],"_",
ToString[μNum],".csv"];
Export[plotFilename,paramArr];
```

Increment μ-index

```
μNum=μNum+1;
];
```

Export transmission and resonance data

```
gstring=ToString[fileN];
finalTransFilename=StringJoin[transFileString,gstring,".csv"];
finalResFilename=StringJoin[resFileString,gstring,".csv"];
Export[finalTransFilename,transArr];
```

```
Export[finalResFilename,resArr];
```

Increment g-index

```
fileN=fileN+1;
];
```